Characteristic low friction and wear behaviors of CF-filled PTFE in dry gaseous hydrogen environment

陳, 乾

Kyushu University
Department of Mechanical Engineering
744 Motooka
Fukuoka, Japan

Characteristic low friction and wear behaviors of CF-filled PTFE in dry gaseous hydrogen environment

Qian Chen

January 2024

Declaration of Originality

I declare that the work presented in this thesis is my own and expressed in my own words except those declared otherwise. Any work used by any other authors in any form has been properly acknowledged where used. A list of all the references used has been included. This work has not already been submitted for any other degree and is not being submitted for any other degree.

Fukuoka, January 2024

Qian Chen

Copyright Declaration

Fukuoka, January 2024

Qian Chen

Related Publications

Journal Papers

- Q. Chen, T. Morita, Y. Sawae, K. Fukuda, J. Sugimura, Effects of trace moisture content on tribofilm formation, friction and wear of CF-filled PTFE in hydrogen. Tribology International 188 (2023) 108905.

Conference Proceedings

- Q. Chen, T. Morita, Y. Sawae, K. Fukuda, J. Sugimura, Effects of Trace Moisture Content on TriboFilm Formation, Friction and Wear of CF-filled PTFE in Hydrogen, 77th STLE Annual Meeting & Exhibition, 21-25 May. 2023, Long Beach, USA.

- Q. Chen, T. Morita, Y. Sawae, K. Fukuda, J. Sugimura, Friction and Wear of CF-filled PTFE in High-purity Hydrogen under Varying Trace Moisture Content, 9th International Tribology Conference, 25-30 Sep. 2023, Fukuoka, Japan.

All men by nature desire to know.

- Aristotle, Metaphysics (translated by W. D. Ross)

Contents

List of Figures

high pressure contact (left: at initial moisture content less than 0.25 ppm; right: at initial moisture content larger than 0.25 ppm)

Fig. 6. 7 SEM-EDX images of transfer films atop stainless steel specimens ((a) discontinued parts of brown patches with initial moisture content less than 0.25 ppm, (b) discontinued parts of purple patches with initial moisture content over 0.25 ppm.)

Abbreviations

ATR	Attenuated total reflection
BCC	Body centered cube
CF	Carbon fiber
COF	Coefficient of friction
DLC	Diamond like carbon
EDX	Energy-dispersive X-ray spectroscopy
FCC	Face centered cube
FCT	Face centered tetragon
FCV	Fuel cell vehicle
FTIR	Fourier-transform infrared spectroscopy
HHV	Higher heating value
PAN	Polyacrylonitrile
PEEK	Polyetheretherketone
PET	Polyethylene terephthalate
PPMv	Parts per million in volume
PTFE	Polytetrafluoroethylene
SEM-EDX	Scanning electron microscopy combined with energy dispersive X-ray spectroscopy
STP	Standard temperature and pressure
UHMWPE	Ultra-high molecular weight polyethylene
XPS	X-ray photoelectron spectroscopy

1. Introduction

1.1 General background

The concept “macromolecule”, sometimes also called “polymer”, was established by Staudinger in 1922 to distinguish the molecules of linear high polymers from the much smaller common low molecular weight molecules. Except the proteins and nucleic acids basic to the life process, the macromolecule contains structural materials as cellulose, textiles as nylon, elastomers as rubber and resins as phenolics [73-74]. Parameters like the monomer polymerized, reagents used to initiate the polymerization reaction or crosslink the polymer chains, environmental temperature and pressure can easily affect the linearity and average molecular weight of polymer, the tacticity of side chains on polymer backbone, which result in the changes to properties of polymer. Their ease in manufacturing and low unit cost, coupled with their potentially excellent tribological properties in engineered forms, make polymers play an important role in the materials and mechanical engineering [75]. Specifically, the advent of polytetrafluoroethylene (PTFE) composites in the 1950s, together with other materials such as polyamides and polyacetals, has undoubtedly led to their use in diverse applications include gears, bearings, artificial human joint bearing surfaces, coating and seals [65]. Polymer tribology has been studied and published as research articles and reports dealing with a variety of tribological phenomena on a considerably largen number of polymers in bulk, composites and hybrid forms for over 60 years.

Resource and environmental issues in modern society have become even more serious since the era when the word “tribology” was coined. Under these circumstances, fuel cells, which use hydrogen as an energy carrier, are attracting great attentions as a clean energy system that does not emit environment polluting gases such as carbon dioxide [76]. Moreover, fuel cell vehicles (FCVs) are desired for reducing fossil fuel consumption and greenhouse gas emissions in the transport and transportation fields, and technological development is being actively pursued to the popularization of FCVs. Machine elements such as bearings and seals in the hydrogen energy system are affected by the hydrogen environment through interactions between material surfaces and gaseous hydrogen.

Therefore, friction and wear characteristics of tribomaterials in the hydrogen environment should be appropriately understood to establish a design guideline for reliable hydrogen utilization systems.

1.2 Research goals

Hydrogen has the highest gravimetric energy density (higher heating value, HHV) of all known substances (142 MJ/kg), and it falls to 12 MJ/m3 (volumetric energy density HHV) at standard temperature and pressure (STP). Therefore, hydrogen gas used in FCVs is compressed up to 70 MPa, latest refueling station demands a hydrogen gas compressor operating at ~82 MPa to fill the high-pressure storage tanks. Such adiabatic compressing process of hydrogen gas abruptly increases the environmental temperature to 200 °C. Moreover, the electrode catalysts used in fuel cells are sensitive to contaminants such as water and oxygen; thus, no volatile lubricant can be used and the water content of the hydrogen gas used in FCVs is regulated to less than 5 ppm according to the ISO standard. Key elements such as piston rings operate under such condition must satisfy the tribological requirements, long friction and wear, along with high mechanical strength and sealing performance.

PTFE, which possesses excellent self-lubricating ability and a low friction coefficient owing to its extremely small size (~30 nm) of crystalline slice and low activation energy of slippage between bands [3], is considered as a representative polymeric sealing material for reciprocating gas compressors and regulator valves in fuel cell vehicles and related hydrogen infrastructures.

Conversely to the numerous studies on the tribological characteristics of PTFE and its composites in air or gases other than hydrogen [2-10, 28, 64, 74, 89, 100-108, 111-114, 127-134], studies in hydrogen gas are limited. Sawae et al. investigated the friction and wear behavior of unfilled PTFE and PTFE composites in gaseous hydrogen under standard pressure [80], and 40 MPa pressure [76, 81-82] to understand the intrinsic effect of hydrogen. They also elucidate the tribological function of filler materials used in PTFE composites in gaseous hydrogen at 100 °C [6].

Despite the investigations above, understanding of the friction, wear and tribofilm formation of PTFE composites in hydrogen gas at STP is insufficient. The effect of factors

other than atmospheric temperature and pressure on tribological properties of PTFE composites in hydrogen gas is not clear. The main motivation of this study is to improve the tribological properties of piston rings used in the oil-free reciprocating hydrogen gas compressor and to accumulate information for establishing a knowledge base for the logical material selection of piston rings.

As is known to all, operating conditions like contact pressure and sliding velocity can affect the tribological performance of polymer composites. Since trace moisture content has been reported to affect the friction and wear of iron in hydrogen gas [15], it was supposed to affect the tribological behaviors of PTFE composites in hydrogen gas as well. For this reason, this work focuses on understanding the tribological characteristics of CF-filled PTFE that performed well in previous study [6] with different contact pressure in dry hydrogen gas environment where moisture content is of a ppm level. Specifically, the transfer layer formation under different conditions was investigated, in order to correlate surface interactions and tribological behavior. The major contributions of this thesis to the field of PTFE composite tribology are:

- Information regarding the effect of gaseous hydrogen on the tribofilm formation, friction and wear of PTFE composites under 1 MPa normal load at STP and moisture content less than 1 ppm is limited. In Chapter 4, the propagation effect of hydrogen gas on carbon-based tribofilm formation, and its correlation to friction and wear decrease are revealed. Furthermore, an air exposure process is introduced to the sliding tests after a running-in stage of 10000 m to clarify the acceleration effect of water on the removal of tribofilm formed in gaseous hydrogen.
- The tribological behavior of CF-filled PTFE in gaseous hydrogen environments with trace moisture contents has so far not been reported. The effect of moisture content from 1 ppm to 40 ppm on carbon-based tribofilm and transfer film formation is investigated. The important role of the chemical composition of sliding counterface and its influence on the amount and structure of formed carbon films is demonstrated in Chapter 5.
- The friction, wear and tribofilm formation of CF-filled PTFE in hydrogen under high contact pressure of 7 MPa is explored in Chapter 6. The tribological performance of CF-filled PTFE has not been studied under such high contact pressure in hydrogen

gas. Extremely low initial moisture content level (less than 0.25 ppm) is considered to assist the formation of carbon film which induced the transition of friction and wear from high to ultralow value in hydrogen gas under high contact pressure.

- The findings presented in this work focus on the factors of carbon film formation of CF-filled PTFE at STP. Environmental factors like gaseous atmosphere, moisture content and operation factor such as contact pressure are revealed affecting the tribological response of CF-filled PTFE. Particularly, initial moisture content affects the carbon film formation of CF-filled PTFE. The increasement in contact pressure magnify the effects of water on the tribological response and shorten the running-in period for this composite.

1.3 Thesis outline

This thesis is structured as follows:

The materials used in this thesis are presented in Chapter 3. The different techniques, that used to measure the friction, wear and contact temperature, and that used to control the atmosphere water content of chamber, together with various surface characterization techniques are described in this section.

In Chapter 4, the effect of hydrogen gas on the friction and wear of CF-filled PTFE at STP under 1 MPa normal load with moisture content less than 1 ppm are studied. The formed tribofilm together with the tribochemical reaction are assessed. Moreover, the effect of water and oxygen on the tribofilm formed in hydrogen gas are studied.

In Chapter 5, the effect of trace moisture content on the tribofilm formation, friction and wear of CF-filled PTFE in hydrogen at STP under 1 MPa was investigated. On the basis of these results, mechanisms of for the tribofilm formation is proposed.

Chapter 6 compares performance of CF-filled PTFE under 1 MPa and 7 MPa normal load in hydrogen gas environment at STP with moisture content less than 1 ppm. Additionally, the influence of initial moisture content on carbon-based film formation under 7 MPa normal load is investigated.

In Chapter 7, the thesis is concluded and suggestions for future work are discussed.

2. Literature review

2.1. Hydrogen

Recognized as a decarbonized, sustainable, and non-polluting energy source, hydrogen energy is expected to serve an indispensable role in the provision of electricity, heat, industry, energy storage, and transport in the future.

Regarding the fact that hydrogen atom is the smallest one among the atoms of all elements, hydrogen gas can be easily diffused or dissolved in many materials. It also possesses high mobility at room temperature which can exceed the mobility of ions in aqueous solutions [138]. These properties of hydrogen induce the degradation of the mechanical properties of materials, which was first noted on the fracture properties of iron and steel by Johnson in 1874 and named as hydrogen embrittlement [139]. Since then, the deleterious effect of hydrogen on mechanical properties has been widely studied and been reported not only in iron and steel, but also many other materials [47-56, 140-149]. Zapffe demonstrated the pressure of hydrogen in bubbles provides the stress for the formation and propagation of cracks in steels [50]. Briscoe et al. and Stevenson et al. observed similar blister induced fractures in elastomers [47-49]. Gent et al. reported defect-initiated bubbles in rubbers grow to visible sizes after decompression of hydrogen gas [143-144]. Yamabe et al. conducted blister tests on various kinds of ethylene-propylene rubber (EPDM) and nitrile-butadiene rubber (NBR) composites in hydrogen gas and revealed that blister damage decreased with a decrease in hydrogen content which were proportional to hydrogen pressure [140-142]. Kazinczy and Petch indicated that the absorption of hydrogen at the crack tip or the surface imperfections will reduce the surface energy for crack propagation in metals and steels [51]. Morlet et al. and Troiano suggested that hydrogen can reduce the cohesive strength of the lattice [54-55]. Robertson reported the hydrogen enhancement of dislocation dynamics in stainless steel [56]. In addition to the reduction in ductility and fracture stress, the hydrogen embrittlement phenomenon was demonstrated to cause the change of fracture mode from ductile to brittle failure, the increase of slip localization, etc. [56, 145-149].

Besides the hydrogen embrittlement phenomenon stated above, hydrogen gas also has

been assumed imposing unique effects on friction and wear in many materials. It was believed that passivation of the carbon surface by adsorption of some species, including hydrogen and water, could eliminate the covalent bond interactions between carbons to yield lower friction. Donnet et al. concluded that hydrogen saturation on the carbon surfaces suppressed the carbon-carbon interaction which otherwise gave rise to higher friction [122]. Erdemir suggested that the super-low friction with highly hydrogenated DLC was provided by the elimination of the strong carbon-carbon interactions by hydrogen termination, in addition to the stronger shielding by di-hydration and repulsive electrostatic forces between hydrogen-terminated surfaces [124]. Fontaine et al, suggested that, while hydrogen loss from DLC surface occurred under sliding, hydrogen termination could be restored through introduction of hydrogen in surrounding gas [123]. Kurahashi et al. suggested H and/ or OH help the detachment of carbon from the DLC and chemical reactions for deposition on the counterface to enhance the transfer film formation whilst carbon-oxygen reaction retarded the formation of stable carbon film for low friction [41].

2.2. Polymer materials in hydrogen environment

The mainstream application of hydrogen technologies includes fuel cells that are widely used in vehicles and household heating systems, enabling the development of zero-greenhouse-gas-emission systems with reduced fossil fuel dependence [1,2].

For facilities in the hydrogen energy system such as hydrogen production plant, hydrogen refueling station, FCVs and residential fuel cells, tribological components like seals, bearings, valves are of widespread use [2, 6, 99, 140-142, 155, 157-159]. Specifically, typical hydrogen refueling station consists of storage tanks, compressors, hydrogen dispenser, pipes and valves.

With respect to the reciprocating gas compressors, piston rings and rod packing operated under extreme conditions including high gas pressure over 80 MPa, high sliding speed over 2 m/s, high gas temperature over 150 ℃ and water content less than 5 ppm [6, 99], are usually made of polymeric materials. These polymer composites usually possess excellent self-lubricating ability since no volatile lubricant can be used in hydrogen gas compressor to prevent gas contamination. For needle valves and ball valves for gas flow at pressure of 98 MPa, gland packings used as dynamic seals are typically made of

polymers [2]. Moreover, O-rings and U-packings used in pipes are made of rubbers [140-142, 155].

2.2.1 Properties pertaining to the tribological application of polymers

The ongoing pursuit of higher efficiencies and longer operating lifetime in modern industry have made the mechanisms behind friction and wear under extreme environmental conditions be of interest for decades. For this reason, tribological components must be able to function in dry conditions or incorporated a lubrication-for-life system. Bearing and seal materials must suffer little wear, yet tolerate abrasion, be inert to corrosive environments and accommodate shock loading or pressure differences to some extent. Such advances in industry have only been made possible by the development of components manufactured from polymeric composites. Polymers are widely used in industry applications due partly to their molecular structure and viscoelastic nature that made their potentially excellent tribological properties in engineered forms, and partly to their lighter in weight, more chemically inert and ease in manufacturing than metal components [65, 75].

The self-lubricating ability of polymers is frequently attributed to the formation of a so-called transfer layer or lubricant layer when soft phase such as polymers are rubbed against the hard phases such as steel countersurfaces [57, 121]. They are typically used to decrease friction and wear in industry applications involving severe sliding contacts, without the need for external lubrication [100].

The demand for developing novel lubricants generally arises in applications for automotive, power generation, metal forming and aerospace [87-88, 90-93], whose operating conditions always include high temperature, cryogenic temperature, vacuum pressure, high load, high speed and corrosive environments [94-98].

2.2.2. Polytetrafluoroethylene (PTFE)

PTFE is a semi-crystalline polymer, which represents complex crystalline phase behavior that includes four well-characterized phases, designated I-IV by Clark et al. [152-153].

These unusual crystal forms and substantial molecular motion of PTFE depends on atmospheric pressure and temperature [74, 100]. Three crystalline structures (phases II, IV and I) are observed at atmospheric pressure. When temperature is lower than 19 ℃, the molecular conformation of phase II is equivalent to a planar polyethylene type zig-zag which is given a 180° twist in 13 (CF_2) motifs. This is a 13/6 helix, which means the atoms are evenly spaced along a helix having six turns per 13 atoms to form the repeat unit. The structure is of a well-ordered triclinic form – one helix for the carbon and one for each fluorine. The first-order transition at 19 ℃ between phases II and IV is an unraveling in the helical conformation from a 13/6 conformation to a 15/7 conformation. Further rotational disordering and untwisting of the helices occurs above 30 ℃ to form a pseudohexagonal structure with dynamic conformational disorder and long-range positional and orientational order (phase I). In addition, the crystal form of PTFE is forced to a planar zig-zag conformation (phase III) at high atmospheric pressure (above 0.5 GPa). Brown et al. [151] demonstrated that crack propagation in PTFE is strongly phase dependent with a brittle to ductile transition associated with the three ambient pressure crystalline structures (phases II, IV and I). In this study, atmospheric temperature is higher than 25 ℃ and the molecular conformation of PTFE is phases IV and I. Increases in fracture toughness and local plastic deformation are suggested during the sliding tests.

Since the molecule has no branches and is not bulky, the molecular profile of PTFE is smooth and give rise to the low friction and easy formation of thin transfer film on the counterface in sliding [89]. Moreover, it has been pointed out that PTFE possesses low friction owing to its extremely small size (~30 nm) of crystalline slice and low activation energy of slippage between bands [3]. PTFE exhibits a very low friction and retains used mechanical properties at temperature from -260 to +260 ℃ for continues use. The crystalline melting points of PTFE is 327 ℃, much higher than that of other semicrystalline polymers. It is nearly chemically inert and does not absorb water, leading to excellent dimensional stability. Conversely, the dominant failure of PTFE under stress is indicated as cold flow and it reveals the highest wear among the semicrystalline polymers [100].

2.3. Friction of PTFE composites

2.3.1. General considerations

Definitions of friction from the glossary in the new ASME wear control handbook in 1980 [109]. Friction refers to the resisting force tangential to the common boundary between two bodies when, under the action of an external force, one body moves, or tend to move, relative to the surface of the other.

If two bodies are placed in contact under a normal load, F_N, a finite force is required to trigger or maintain sliding. This finite force is the friction force, F_F. In this situation, Amontons-Coulomb laws of dry sliding friction are used, the details of which are as follows:

- The friction force always acts in the direction opposite to that of the relative velocity of the surfaces.
- The friction force is proportional to the normal load.

$$F_F = f \cdot F_N$$

And the coefficient of friction can be calculated in the equation

$$f = F_F / F_N$$

- The friction force is independent of the apparent geometric area of contact.

Moreover, the friction coefficient is demonstrated as the combined effects of three parts: asperity deformation, ploughing by hard counterface asperities and wear debris and the adhesion between flat surfaces [110].

2.3.2. Effect of various fillers on friction coefficient

To overcome the inhibited weakness of PTFE, various fillers were used to develop composites for high wear resistance. Firstly, short fiber fillers, such as carbon, glass, and aramid fibers, and hard particles like bronze, aluminium oxide and polyetheretherketone (PEEK) have been successfully adapted to improve the strength and therefore the load-carrying capacity of PTFE composites under various wear modes [2, 5-10, 64]. Solid lubricants, such as graphite and MoS_2, have proved to be helpful even in reducing the low frictional coefficient of PTFE as well as the wear rate [106-108]. Moreover, nano-phased

materials, nanosized fillers such as nanoparticles and carbon nanotubes (CNTs) have shown the wear resistance of polymers even at very low filler content (~1–4 vol.%) [101-105].

The effect of various fillers on friction of PTFE composites has been reported in previous studies. Lancaster showed that glass fiber filled PTFE has higher friction than carbon fiber filled PTFE [111]. Tanaka et al. investigated the friction of 20 wt % glass fiber filled PTFE and 20 wt % CF-filled PTFE against steel and glass disk specimens at various sliding speed. They indicated the friction of CF-filled PTFE is greater than that of glass fiber filled PTFE [112-113]. Moreover, Tanaka et al. studied the friction behaviors of glass fiber, bronze, ZrO_2, TiO_2, MoS_2 and graphite filled PTFE [114]. They demonstrated that thin film of PTFE which exists at the interface between fillers and disk surface results in the similar friction behaviors of various types of filler filled PTFE. The only exception is ZrO_2-filled PTFE, in which condition there was not PTFE film formed. The absence of PTFE film gave rise to the friction of ZrO_2-filled PTFE higher than that of others.

2.3.3. Effect of sliding speed on friction coefficient

Shooter et al. and Bowden et al. studied the relationship between sliding speed, contact temperature and the friction of polymer sliding against steel [115-116]. From their results, the friction is neat independent of sliding speed when contact temperature remains constant. Conversely, at high sliding speed the friction coefficient is highly dependent on contact temperature. Since high sliding speed generates large amount of friction heat that always results in high contact temperature, it is difficult to investigate the effect of sliding speed without the influence of friction heat.

2.3.4. Effect of temperature on friction coefficient

Gardos digested self-lubricating materials such as PTFE and graphite composites operating in inert gases, air and vacuum at moderate temperature (to 540℃) and in high temperature air (to 640℃) [150]. He demonstrated chemical reaction from the interface such that, as exothermic oxidation, generated enough heat and various products to the friction couple. The dissipation of these heat, coupled with load-speed-induced flash

temperature, give rise to degradation of polymer matrix of the self-lubricating composites and increase the abrasive damage at the interface. According to the results obtained, he indicated the most important factor affects tribological behaviors is the effectiveness of preferentially accumulated, low shear strength layers on the composites. Sawae et al. conducted sliding tests using single-filler PTFE composites with four kinds of filler materials in gaseous hydrogen environments at 100 ℃ [6]. The results revealed that polyacrylonitrile (PAN)-based CF-filled PTFE exhibited the lowest friction and wear in hydrogen, and the tribological mechanisms of low friction and wear could be ascribed to the formation of carbon-based films on both the surfaces of the sliding couples.

2.3.5. Effect of water content on friction coefficient

Water content has long been known to affect the tribological characteristics of PTFE composites, especially the formation of PTFE transfer films. Based on the study of Lancaster, three effects of water were indicated being of great importance on the tribological behaviour of pure PTFE [11]. The absorbed water molecule or hydraulic effect induced cracking propagation on both PTFE and counterface material, tribochemical reactions with the sliding surfaces and prevention or propagation to the formation of three-body layers of aggregated wear debris. Additionally, regarding the influence of water on wear deterioration of PTFE, Mcnicol et al. performed valuable investigation on the degradation of transferred PTFE at high humidity (over 95% RH) [14], their results validated that adhesion between PTFE and stainless steel counterface was reduced by the increased amount of absorbed water on the metal surface.

Haidar et al. indicated that strong physical interactions between the PEEK filler particles and the counterface stabilized the PTFE transfer film, thereby exhibiting an ultralow wear rate and low friction coefficient in dry nitrogen (RH: 0.05%) [10].

Despite the aforementioned studies, the effects of trace moisture content in hydrogen gas on the tribological behaviors of carbon-filled PTFE, such as carbon film formation, remains unclear and has not yet been explained in the literature.

2.4 Wear of PTFE composites

Definitions of wear from the glossary in the new ASME wear control handbook in 1980 [109]. Wear is the progressive loss of substance from the operating surface of a body occurring as a result of relative motion at the surface. Similar to friction, the wear behavior of materials is also a very complicated phenomenon influenced by various factors and including varieties of wear mechanisms. Burwell demonstrated the wear mechanisms consists of four major parts [117]: abrasion, adhesion, surface fatigue and tribochemical processes.

For abrasive wear mechanism, Khrushov has built models base on comprehensive experimental work on abrasive wear of metallic and non-metallic. The details of which are as follows:

- Technically pure metals in an annealed state sliding against annealed steels show a direct proportionality between relatively wear resistance and pyramid hardness.
- For non-metallic hard materials and minerals, an approximately linear function between wear resistance and hardness is found.

As is known from the mechanical behavior of bulk materials under repeated mechanical stressing, microstructural changes in the material may occur which result in gross mechanical failure. These effects are mainly based on the action of stresses in or below the surfaces, and Lang indicated that surface fatigue occurs in journal bearings where the interacting surfaces are fully separated by a thick lubricant film [118].

The adhesive wear processes are initiated by the interfacial adhesive junctions which form if solid materials are in contact on an atomic scale. The wear resulting from adhesive processes has been described phenomenologically by the well-known Archard equation [119]. It depends on various properties of the materials in contact such as electronic structure of contacting partners, the crystal structure, crystal orientation, etc.

With respect to trobochemical wear, the environment and the dynamic interactions between the material components and the environment determine the wear process. The interaction of which can be expressed as cyclic stepwise processes.

2.4.1. Effect of water content on wear rate

Schubert carried out an extremely comprehensive series of wear tests to investigate the influence of humidity and type of gas on the wear of PTFE composites at 70 ℃, over a span of about 0.1-10000 ppm moisture content [12]. His results revealed the wear of any one PTFE composite was influenced by both the type of gas and its humidity. Fuchsluger et al. performed a similar series of wear tests of filled PTFE composites in air and in nitrogen [13]. They indicated moisture content had a direct effect on the ability of the material to develop a protective, wear-resistant lubricating film.

Furthermore, Campbell et al. suggested that tribochemically generated carboxylate end groups anchoring the polymer transfer films to the counterface can induce remarkably low wear rates of PTFE composites in humid air (RH: 50%) [7]. Similarly, Krick et al. and Harris et al. ascribed the ultralow wear behavior of PTFE/alumina composites in humid nitrogen (RH: 87%) to tribochemical degradation products such as carboxylates [8,9].

2.4.2. Effect of contact pressure on wear rate

The effects of load on the friction and wear performance of polymers and their composites have widely been reported [70]. Zhang et al investigated the tribological behaviors of PEEK under different contact pressure [62], they suggested a transition of wear mechanism from microcutting effect and elastic deformation under low contact pressure to the plastic flow and fracture with high contact pressure. Garrison extended the Khruschov's abrasive wear rule to the volume wear rates of ceramic materials as a non-linear function of applied load [63]. In addition, Anderson evaluated the wear behaviors of 15 % graphite filled polyimide and PTFE coated asbestos at a constrained temperature of 50 C under varying contact pressure [65], he indicated the increase in contact pressure gave rise to the increase in plastic deformation of both materials and finally resulted in the increase in wear rates. Similarly, Lancaster ascribed the increase in wear rates of bronze/PTFE/Pb bearings at high stress to the fracture of material and the additional surface damage induced by wear debris [67, 125]. Dowson et al demonstrated that higher applied load was critical for the disrupt of formed three-body layer which gave rise to the

increased wear rate of ultra-high molecular weight polyethylene (UHMWPE) [66]. Conversely, Voss et al declared that the effect of load on the wear of unfilled PEEK is reduced by added with glass fibers [64].

Moreover, high contact load may lead to the rise of temperature at sliding interface by the generation of friction heat. Since the mechanical properties of all polymers and composites decrease as the temperature is increase, the changes of wear rates induced by load may be partly due to temperature. Hanchi et al reported a sudden increase in both friction coefficient and wear rate of PEEK when contact temperature reaches glass transition [68]. Samyn et al indicated surface softening by increase of friction heat at higher contact pressure trigger the transition from mild to severe wear of PTFE filled polyethylene terephthalate (PET) [69].

Although previous studies have been carried out on the tribological characteristics of CF-filled PTFE in hydrogen with low contact pressure [6, 77, 80-82], information about that under high contact pressure conditions is limited.

2.5. Tribofilm

2.5.1 Definition

Polymers have increased in popularity for tribological applications for their so called “self-lubricating” property. This property is the results of polymeric materials being transferred from the polymeric component onto the countersurface (usually steel) and is called a transfer layer. Much has been written that polymer transfer to the counterface occurs during the sliding of polymers and that the effective transfer layers play an important role in their tribological characteristics [100, 126]. Briscoe [57] indicated that the processes of this formation as: 1. Produce a stable interface layer by mechanical work accompanied with subsurface damage. 2. Mobile additives migrate and provide a self-regenerating lubricant layer. He also described the effective transfer film as a “thin”, “uniform”, and “stable” layer of material that has been transferred from one surface to another by adhesive wear. In the scope of this work, the transfer layer is supposed as a polymeric material that adheres to a countersurface during rubbing, with no permanent state of adhesion required.

2.5.2 Formation in dry friction condition

When a polymer is rubbed against a metal countersurface, it experiences shear stresses and thermal softening as a result of frictional heating. The surface asperities of the polymer deform and yield leading to the removal of particles. In the absence of lubricants, the adhesion force between the two rubbing surfaces affects the transfer layer formation [57]. The pull-off force between the two surfaces may cause a large coefficient of friction and affects the amount wear. Within the first instance of contact, the softer material undergoes deformation and wear. The detached polymeric material can either form wear debris or attach onto the countersurface to create a transfer layer. It is a way for polymers to self-lubricate.

2.5.3 Factors on transfer film formation

For decades, mechanisms have been suggested to study the formation of transfer film and their role in friction and wear. J. Ye [127-128] indicated the driving force for PTFE transfer arises from surface energy reduction, where PTFE transfers to its counterpart with higher surface energy. Pooley et al. [129] observed the transfer of extremely thin PTFE film (2.5 nm), and ascribe the light transfer of PTFE that gave rise to the low friction to their smooth molecular profiles. Similarly, Tanaka et al. [130] revealed the transfer and low friction of PTFE sliding against glass surface. Makinson et al. [131] indicated the energetics of crack formation and propagation to form large PTFE fragments which will increase the overall wear rate are accelerated at higher lising speeds.

Moreover, the environmental sensitivity of the operating system has been investigated and tribochemical reactions was previously proposed mainly in cases of PTFE and its composites. The generation of carboxyl groups at humid environment was suggested to play a dominant effect on chelating polymer segments to metallic counterface, which resulted in low friction [7, 132-133]. Conversely, water was demonstrated to induce the adhesion of transfer film in the oxide-copper oxide-PTFE sliding system, as a result, accelerates the wear process [28]. Glaeser et al. [134] observed the transition of PTFE wear mechanism from the formation of flake-like debris and gross plastic deformation to

abrasive wear producing fine powdery debris in 77K. Sawae et al. [6] conducted sliding tests using single-filler PTFE composites with four kinds of filler materials in gaseous hydrogen environments at 100 ℃, revealed that formation of carbon-based films on sliding interfaces give rise to the lowest friction and wear in hydrogen. Chen et al. [120] investigated the tribological performance of CF-filled PTFE and indicated that carbon films formed on sliding counterface varied in structure and amount as disk surface chemical composition changes, resulting in different friction and wear behaviors.

2.6. Summary

Questions remain concerning the formation of a polymeric transfer layer onto the countersurface during dry sliding. Much of the work performed in this area to dates examines the formation of a transfer layer for PTFE and its composites at room temperature due to the poor performance of polymers under extreme conditions in hydrogen. There is therefore an interest in determining how the polymeric transfer layer formed under various harsh conditions. In this work, effects of hydrogen gas, trace moisture content and contact pressure on the tribofilm and transfer film formation of CF-filled PTFE are investigated in order to improve the tribological performance and life time of seals in the reciprocating gas compressors in hydrogen refueling station. Several surface analysis techniques such as optical microscopy and analytical techniques will be used to detect changes occurring at the transfer layer. This work will therefore add to current knowledge about the logical material selection of piston rings.

3. Materials and Methods

3.1 Materials

This study selected 20 wt% polyacrylonitrile (PAN)-based random-orientated CF-filled PTFE, a sealing ring material used in hydrogen gas compressors, owing to its adequate carbon film formation ability and low friction and wear behavior in a gaseous hydrogen environment [6]. The bar stock of the arranged PTFE composites was machined into pin-shaped specimens of dimensions 15 mm × 6 mm (length ×diameter).

Although austenitic stainless steel is used in hydrogen gas compressors, a harder martensitic stainless steel (SUS440C, JIS) with a Vickers hardness of 660 was used as the sliding counterface. Meanwhile, both austenitic (fcc-lattice) and martensitic (fct-lattice) steels are much less susceptible to hydrogen embrittlement than ferritic (bcc-lattice) steels [138]. Consequently, the wear of the counterface was limited, and most of the wear in the sliding tests occurred from the PTFE composites. In addition, disk-shaped specimens were fabricated using this material with an outer diameter, inner diameter, and thickness of 56 mm, 20 mm, and 3 mm, respectively. These specimens were finished with a lapping process using abrasive paper, yielding an average roughness of 0.05 μm.

All the pin and disk specimens were ultrasonicated in a mixture of acetone and hexane for 10 min. The cleaned samples were weighed using an electric balance to an accuracy of 0.01 mg after a vacuum process from 15 min to 2 hours and stored in a dry cabinet until the sliding test.

3.2 Methods

3.2.1 Friction and wear measurements

The sliding tests were performed on a pin-on-disk apparatus. High purity tribometer was used to measure coefficient of friction in this thesis.

3.2.1.1 High purity atmosphere control tribometer

The schematic of the high purity tribometer is shown in Fig. 1. The high-vacuum chamber was equipped with scroll and turbomolecular vacuum pumps. In addition, a custom-made tribometer revolved by a servomotor and a temperature sensor adjacent to the sliding interface were set in the chamber. The latter was used to collect temperature data near the sliding interface.

For the tribometer, the pin specimen, fixed in the pin holder, was loaded against the metal disk specimen through a lever arm with a dead weight. A biaxial load cell located between the pin holder and lever arm was used to measure the vertical contact force and tangential friction force exerted at the sliding interface. Subsequently, these data were used to calculate the friction coefficient as a quotient of the friction and vertical contact forces.

Baking processes of empty chamber were carried out at a temperature over 150 °C and environmental gas pressure magnitude of 10^{-4} Pa for at least 2 h to eliminate the effects of contaminants of residual air every time before the sliding test. After all the specimens settled in the tribometer, the chamber was sealed and evacuated until the atmospheric pressure was less than 5×10^{-4} Pa for the same reason. Hydrogen gas was subsequently supplied to the chamber through a moisture controller until the atmospheric pressure slightly exceeded the standard atmospheric pressure.

All pin and disk specimens are stored in desiccator before and after the sliding tests.

In chapter 4, sliding tests were conducted over two kinds of sliding distance in hydrogen and nitrogen. One was a total sliding distance of 40000 m, another was a sliding distance of 10000 m + 40000 m type, an air exposure process was carried out for at least 1 hour after the first 10000 m sliding. During the air exposure process, both pin and disk specimens were taken out from the chamber and exposed to the laboratory air at room temperature and standard atmosphere. Additionally, the contact pressure and sliding speed were set in accordance with the operating conditions of the PTFE seals in the reciprocating compressor at 1 MPa and 2 m/s, respectively [4]. The moisture content during the sliding tests was maintained at levels of less than 1 ppm. The sliding tests with the sliding distance of 10000 + 40000 m were conducted twice.

In chapter 5, all sliding tests were conducted over a total sliding distance of 40000 m, when the sliding couple was at a stable stage, according to a previous study [6]. In

addition, the contact pressure and sliding speed were set at 1 MPa and 2 m/s, respectively. The moisture content during the sliding tests was maintained at levels of less than 1, 10, 20, and 40 ppm because the water content in the hydrogen fuel was limited to less than 5 ppm, conforming to the ISO standard. The sliding tests were performed twice for each moisture content level.

In chapter 6, all sliding tests were conducted twice over the sliding distance of 40000 m. The contact pressure and the sliding speed was set as 7 MPa and 2 m/s , respectively. The moisture content during the sliding tests was maintained at levels from 200 ppb to 900 ppb.

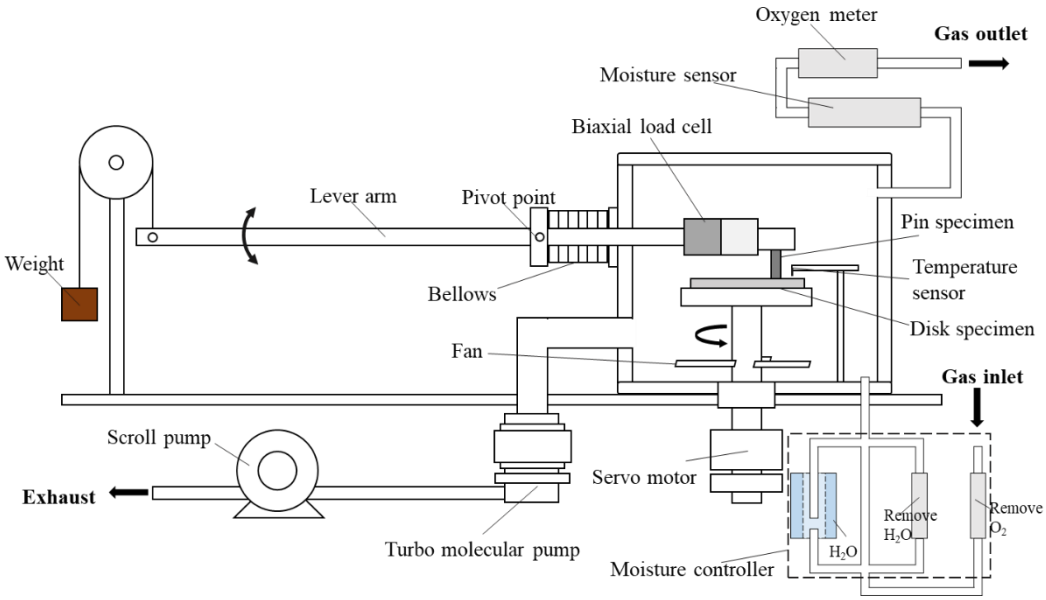

Fig. 3. 1. Schematic of Pin-on-Disk type tribometer installed in high-vacuum chamber

3.2.1.2 Moisture controller & analyzer

A moisture controller developed by Fukuda [15] coupled with a moisture analyzer (HALO, Tiger Optics, LLC, Warrington, PE, USA) was used to control and monitor the atmospheric environment. GE infrastructure sensing M-series thin-film aluminum oxide

sensors are used in the moisture analyzer, each sensor is individually computer-calibrated against known moisture concentrations. The measured dew point will be the real dew point of the system at the measurement location and at the time of measurement. The instrument has a very rapid response time and it is not affected by changes in fluid flow rate. The electronics output PPMv (parts per million in volume) in gases at constant pressure. Units of measure are commonly used in the gas industry to express the weight of water per unit volume of carrier gas. They all represent a vapor density and are derivable from the vapor pressure of water and the Perfect Gas Laws. Referenced to a temperature of 60 °F and a pressure of 14.7 psia, equation is as follow,

$$\frac{mg\ of\ water}{liter\ of\ gas} = 289 \times \frac{vapor\ pressure\ of\ water}{temperature\ (kelvin)}$$

The moisture controller consists of a contaminant remover and water charger. The contaminant remover is able to decrease the concentration of water and oxygen at a level of 10 ppb. The water charger with a permeation method to add aimed concentration of water from less than 100 ppb to 50000 ppb by changing the floating rate of the inlet gas and the height of permeation tip. The purified gas was directly led to the water charger and then introduced to the chamber without influencing the concentration of oxygen.

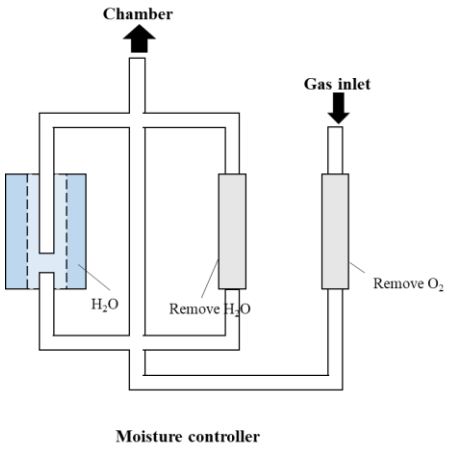

Fig. 3. 2. Schematic of moisture controller

3.2.1.3 Wear characterization

Every time before and after the sliding tests, the pin and disk specimens were weighed by the electronic balance to determine the gravimetric changes per test. These results were subsequently converted into volumetric changes and divided by the contact force and sliding distance to obtain the specific wear rate.

The final specific wear rate was calculated as equation

$$W_i = \frac{\Delta M_i \times SG_i}{N \times L}$$

Where W_i $(i = p: pin\ specimens,\ d: disk\ specimens)$ is the specific wear rate, ΔM_i $(i = p, d)$ is the amount of matter loss during the sliding test, SG_i $(i = p, d)$ is the relative density of specimens to water. N, L are the load and sliding distance, respectively.

3.2.2 Contact temperature

A temperature sensor adjacent to the sliding interface were set in the chamber. This sensor was used to collect temperature data near the sliding interface during the whole sliding test.

3.2.3 Surface characterization techniques

3.2.3.1 Confocal laser scanning microscopy

After the sliding test, the worn surfaces of both the pin and disk specimens were analyzed via optical microscopy at magnifications of 0.58, 1, 10, 20, and 50. The samples were then observed using a confocal microscope (VK-X, KENYENCE) at magnifications of 10 ×, 20 ×, 50 ×, and 150 × to obtain the surface area roughness and height distribution.

3.2.3.2 Laser Raman microscope

Raman spectroscopy is a standard nondestructive tool for the characterization of sp^2 carbon materials such as carbon black and pitch from graphite; sp^3 carbon material such as diamond; fullerene and sp carbon material such as carbine. It is a form of inelastic

scattering of photons, whose excitation puts the molecule into a virtual energy state before the photon is emitted. The energy difference between the initial and final energy state is typically used to determine the vibration modes of molecules. Since the magnitude of the Raman effect correlates with the polarizability of the electrons in the molecule and visible photons preferentially excite the π states, visual Raman spectroscopy is 50-230 times more sensitive to sp^2 sites.

A laser Raman microscope (DXR2xi, Thermo Fisher Scientific) was used to collect spectra from the tribofilms formed on the polymer composites and the transfer films formed on the disk specimens. Spectra of 15-20 points were analyzed from every specimen surface at magnifications of 50 × and 100 × using an excitation laser with a wavelength and power of 455 nm and 0.5 mw. Subsequently, carbon-based area intensity calculations and peak resolutions were performed to analyze the amount and structure of the self-formed carbon films on both specimen surfaces.

In chapter 5, the peak resolutions were conducted for the G and D bands of the transfer films. The intensities of the D_1, D_2, D_3 and G peaks were calculated [16,17] to analyze the structures of the formed carbon-based films.

3.2.3.3 Fourier transform infrared spectroscopy (FT-IR)

Fourier transform infrared spectroscopy is used to identify the chemical bonds and functional groups. The absorption of infrared radiation occurs at resonant frequencies which are affected by the modes of vibration, the strength of bonds and the mass of the atoms at either end of it.

The attenuated total reflection (ATR) analysis via Fourier-transform infrared spectroscopy (Nicolet iN10, Thermo Fisher Scientific) with a germanium tip at an angle of 0° was used to identify chemical compounds other than CF and PTFE in the tribofilms formed on the surfaces of the polymer composites. IR spectra were obtained from 256 scans between 675 to 4000 cm^{-1} at a wavenumber resolution of 4 cm^{-1}. The depth resolution of the FTIR is of the order of 1 μm. The resulting spectra were baseline corrected and the FTIR background was taken measurement with the germanium tip. The ATR pressure and the measurement aperture were 5 mN and $72 \times 72\ \mu m^2$, respectively. In Chapter 5, IR spectra obtained from the pin specimen surfaces were used to clarify the

existence of graphite structure and the oxidation of carbon radicals from PTFE.

3.2.3.4 X-ray photoelectron spectroscopy (XPS)

X-ray photoelectron spectroscopy (XPS) is a quantitative spectroscopic technique based on the photoemission process in high vacuum environment. The chemical states and the chemical bonds can be known from the measurement of the kinetic energy and the number of the ejected electrons. It is usually used to analyze the inorganic compounds and metal alloys.

An X-ray photoelectron spectrometry (JPS-9200KM, JEOL) with a monochromatic AlKa source of radiation at 1486.6ev was utilized to acquire the chemical composition inside the transfer films atop disk surfaces. After wide scanning of the uppermost surface of the sliding tracks, depth profiles of the chemical compositions at 8 and 46 nm beneath the worn surfaces were produced by argon ion beam etching. The accelerating voltage and current of the argon ion beam were 3 keV and 25.0 ma, respectively. The X-ray spot size is $2.5 \times 2.5\ mm^2$ and has a depth penetration of 1.1 mm.

3.2.3.5 Scanning electron microscope (SEM) and energy dispersive X-ray (EDX)

Energy-dispersive X-ray spectroscopy (EDX) is a technique used for chemical characterization. After the ejection of the electron in the inner shell of the atom by the electron beam excitation, an electron from the outer, higher energy shell falls to the inner position and the energy difference between the initial and final state of atom may be released in the form of X-ray. The number and energy of these X-rays are used to identify the atomic structure of the specimens.

A Scanning electron microscope combined with energy dispersive X-ray spectroscopy (SEM-EDX) (JSM-IT700HR, JEOL) was used to conduct the elemental mapping of the transfer films form atop disk surfaces. The EDX mode of the SEM was used with a typical accelerating voltage of 15 kV in high vacuum environment. Several areas corresponding to images with a magnification from 150 to 7000 were selected and have the depth

penetration of 1 μm.

4. Tribological properties of CF-filled PTFE in hydrogen

4.1. Introduction

For the realization of hydrogen society, more information about the effects of hydrogen on the mechanical and tribological properties machine elements used in hydrogen gas infrastructure are needed.

Although the PTFE transfer film can be facilely removed from the counterface, which yields a high wear rate of PTFE, the incorporation of fillers such as bronze, graphite, carbon fiber, and polyether ether ketone (PEEK) can improve the wear rates of PTFE composites by one to three orders of magnitude while maintaining a low coefficient of friction [4,5]. Therefore, PTFE composites have been commonly used as sealing ring materials in oil-free reciprocating gas compressors.

As mentioned in Chapter 2, the tribological behaviors of PTFE composites have been investigated under high temperature or high gaseous pressure conditions in hydrogen gas environment. However, information regarding the mechanism correlated with the tribological properties of PTFE composites in hydrogen environment at STP, especially the role of tribofilm formation, is still insufficient.

In this Chapter, the friction, wear and tribofilm formation of CF-filled PTFE which were used as sealing elements in hydrogen gas compressor were studied in hydrogen and nitrogen gas environments. An air exposure process was used to clarify the chemical stability of tribofilms formed in different gaseous atmosphere.

The overall aim of this chapter is to understand the effects of hydrogen on the formation of tribofilm of CF-filled PTFE at room temperature and standard atmosphere. The effect of air exposure on tribological properties of CF-filled PTFE was investigated. The chemical composition of tribofilm and transfer film formed atop the worn surfaces of sliding couple were analyzed.

4.2 Results and discussion

4.2.1 Effect of hydrogen on the friction and wear of CF-filled PTFE

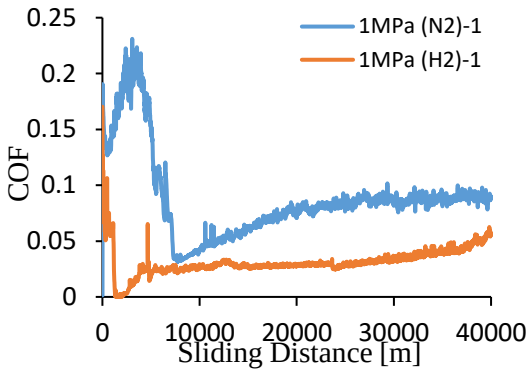

Fig. 4. 1. Variations of friction coefficient with sliding distance in different gaseous atmosphere (a) with total sliding distance of 40000 m

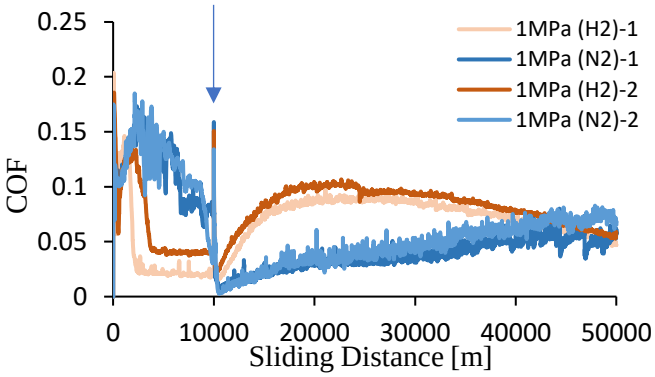

Fig. 4. 1. Variations of friction coefficient with sliding distance in different gaseous atmosphere (b) with total sliding distance of 50000 m, arrow in the graph means the air expose process

The variations in the friction coefficient with the sliding distance of 40000 m in hydrogen and nitrogen are shown in Fig. 4. 1 (a). The running-in stage in hydrogen ended after a sliding distance of approximately 1500 m from the start of the friction test. Then, it exhibited stable low-friction behavior with a friction coefficient of approximately 0.03 till the sliding distance of 40000 m. On the other hand, it took about 10000 m of sliding

distance in nitrogen for the running-in stage to come to an end. After that, the friction coefficient gradually increased as the sliding distance increased from 0.04 to 0.08.

The specific wear rate of the composites with the sliding distance of 40000 m in hydrogen and nitrogen are compared in Fig. 4. 2 (a). In all the sliding atmospheres, the magnitude of the specific wear rate was in the order of 10^{-7} mm^3/Nm. According to the acquired results, the wear rate of PTFE composite in nitrogen is more than twice of that in hydrogen.

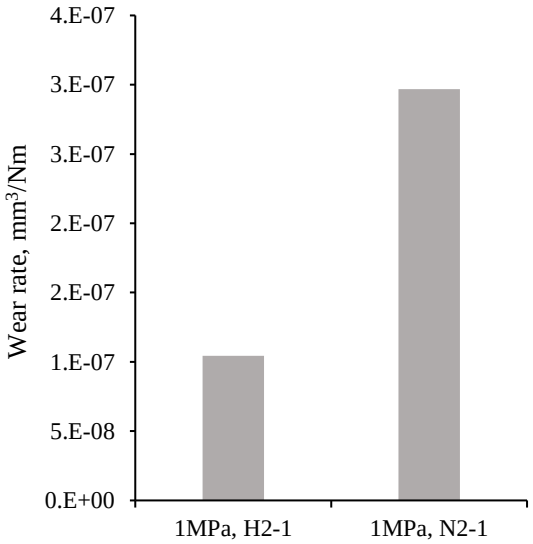

Fig. 4. 2. Plots of specific wear rates with sliding in different gaseous atmosphere (a) with total sliding distance of 40000 m

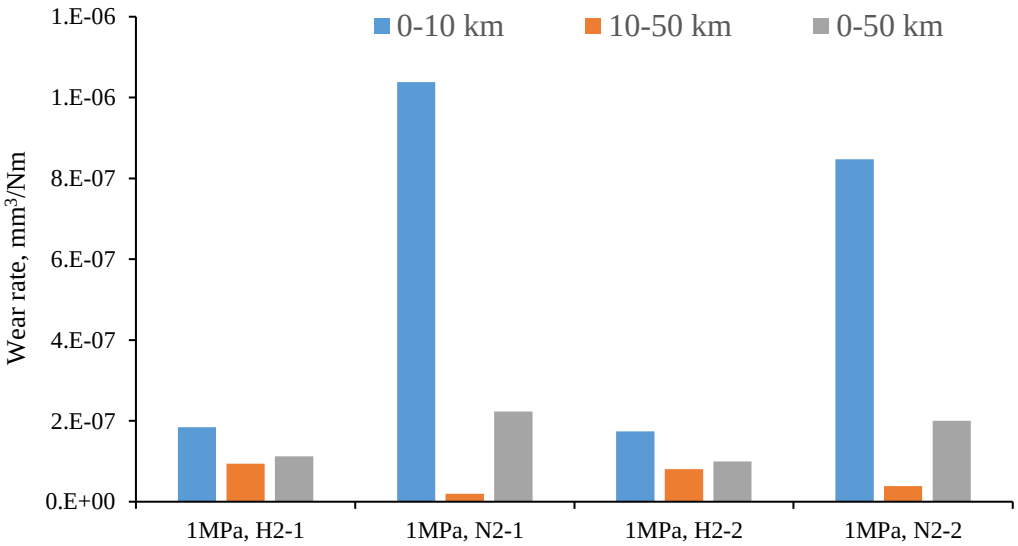

Fig. 4. 2. Plots of specific wear rates with sliding in different gaseous atmosphere (b) with total sliding distance of 50000 m

4.2.2 Effect of air exposure on the friction and wear of CF-filled PTFE

The variations in the friction coefficient with the total sliding distance of 50000 m in hydrogen and nitrogen are shown in Fig. 4. 1 (b). The friction coefficient obtained in every gaseous atmosphere corresponded well with each other, thus the experimental data were considered highly reliable. During the first 10000 m of running-in stage, both the friction coefficient in hydrogen and nitrogen corresponded with that shown in Fig. 4. 1 (left). After the air exposure process, the friction coefficient in hydrogen increased from less than 0.05 to 0.1 with the increase of sliding distance from 10000 m to 20000 m. It decreased to 0.05 as the sliding distance increased from 20000 m to 50000 m. Regarding the friction coefficient in nitrogen, a similar tendency to that of the total sliding distance of 40000 m was observed after the air exposure process. It increased from 0.01 to 0.07.

The specific wear rate of the composites with the total sliding distance of 50000 m are compared in Fig. 4. 2 (b). Similar reliability could be obtained from the small variation in the wear data in each gaseous atmosphere. Comparing to the wear rate in hydrogen, those in nitrogen were 5 times higher during the running-in stage whilst third less during the steady stage after air exposure process. Moreover, the average wear rates in both gaseous environment of the total sliding distance of 50000 m matched with those of the total sliding distance of 40000 m.

4.2.3 Characterization of the tribofilm and transfer film formed on the worn surfaces of sliding couple

4.2.3.1 Morphology of worn surfaces

Representative worn surface images of the PTFE composites are shown in Fig. 4. 3. The surfaces of the polymer composites specimens of both sliding distances in hydrogen were covered by a white tribofilm. In contrast, surfaces of both sliding distances in nitrogen exhibited discontinuous white tribofilm, more obvious filler tips and exposed resin parts.

More details regarding the height comparison between the CF filler and PTFE resin are shown in the corresponding 3D images (Fig. 4. 3). The colors in the 3D images illustrate the height of each component. The height differences between the CF fillers and the tribofilms as well as the area surface roughness of the PTFE composites specimens in nitrogen were obviously higher than those in hydrogen.

Similarly, Fig. 5 shows the optical and 3D images of the sliding tracks formed on the surfaces of the stainless steel specimens. For disk specimens of both sliding distances in hydrogen environment, characteristic brown (Fig. 4. 3 (c), marker (1)) and bluish (Fig. 4. 3 (c), marker (2)) patches were distributed along the sliding direction on the disk surface as transfer films. Regarding the surfaces of both sliding distances in nitrogen, similar brown and bluish patches were observed. Moreover, black patches of accumulated wear debris dispersed over the whole sliding tracks discontinuously, resulted in the higher area surface roughness of disk specimens in nitrogen environments than those in hydrogen environments.

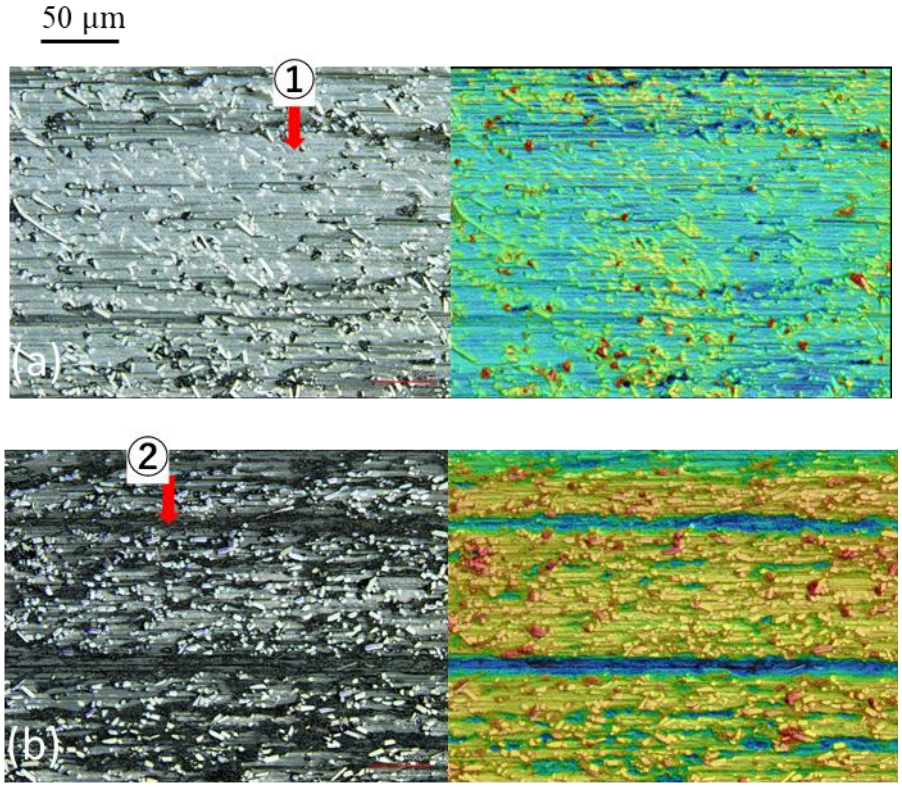

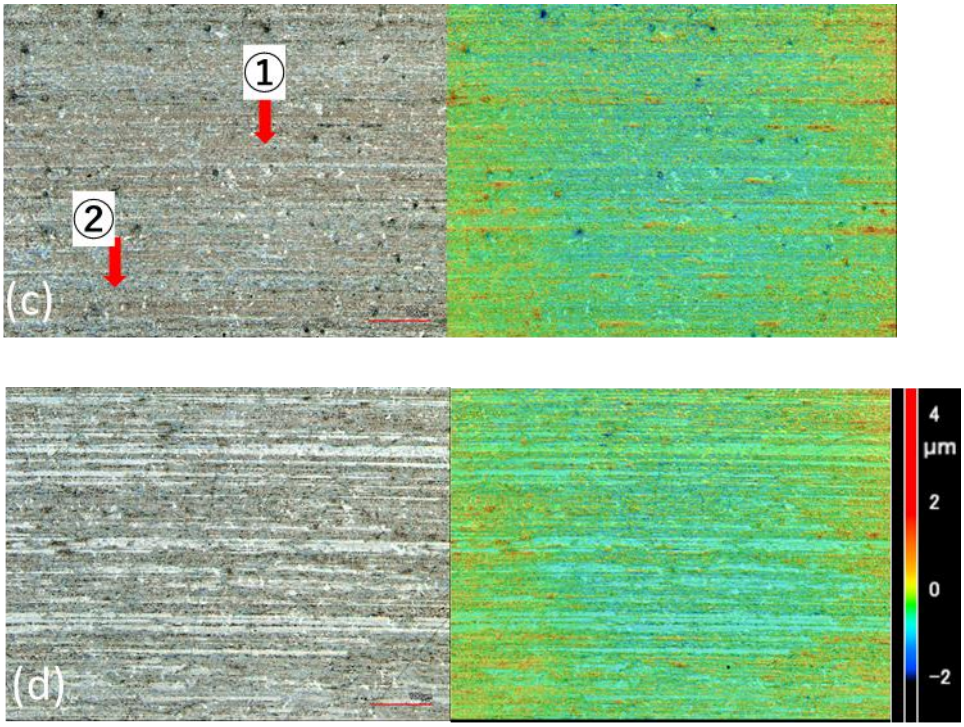

Fig. 4. 3. Optical and 3D images of worn surfaces of sliding couple in different gaseous atmosphere with total sliding distance of 40000 m: (a) pin specimen in hydrogen; (b) pin specimen in nitrogen; (c) disk specimen in hydrogen; (d) disk specimen in nitrogen

4.2.3.2 Microstructure and surface chemistry analysis

The white tribofilm observed atop the PTFE composites specimens of all sliding tests in both gaseous environments were analyzed using Raman spectroscopy. a G band (near 1580 cm^{-1}) corresponding to the graphite structure (sp^2 bond) and a D band (near 1350 cm^{-1}) corresponding to the disordered graphitic structure were observed (Fig. 4. 4 (a)). The characteristics of these spectra are similar to those of the carbon fiber, which is the filler of the polymer composite. Moreover, spectra acquired from the resin parts of pin surfaces in nitrogen environments (Fig. 4. 3. (b), marker (2)) show the typical spectra of pure PTFE at 1382, 1303, 1222, 735, 387, and 292 cm^{-1} (Fig. 4. 4 (b)). Similarly, typical G and D bands are observed in all brown, bluish and black patches of the transfer film formed on the disk surfaces, indicating the presence of carbon. However, the carbon

intensity obtained from the black patches were lower than those from brown and bluish patches. Since black patches were higher than others, the black patches were considered consist of both carbon and PTFE debris. These Raman spectra revealed the formation of a carbon-based film on both worn surfaces of the sliding couple. Furthermore, the ratios of intensities of D peaks to that of G peaks were calculated from the formed carbon films atop the worn surfaces of sliding couple for over 70 points, the results of which was shown in Fig. 4. 5. Not obvious differences could be found in the carbon structure of tribofilms atop pin specimen surfaces. however, the ratios from transfer films in nitrogen is evidently lower than that in hydrogen, which means that transfer films formed atop disk surfaces in nitrogen possesses higher ordered graphitic structure than that in hydrogen.

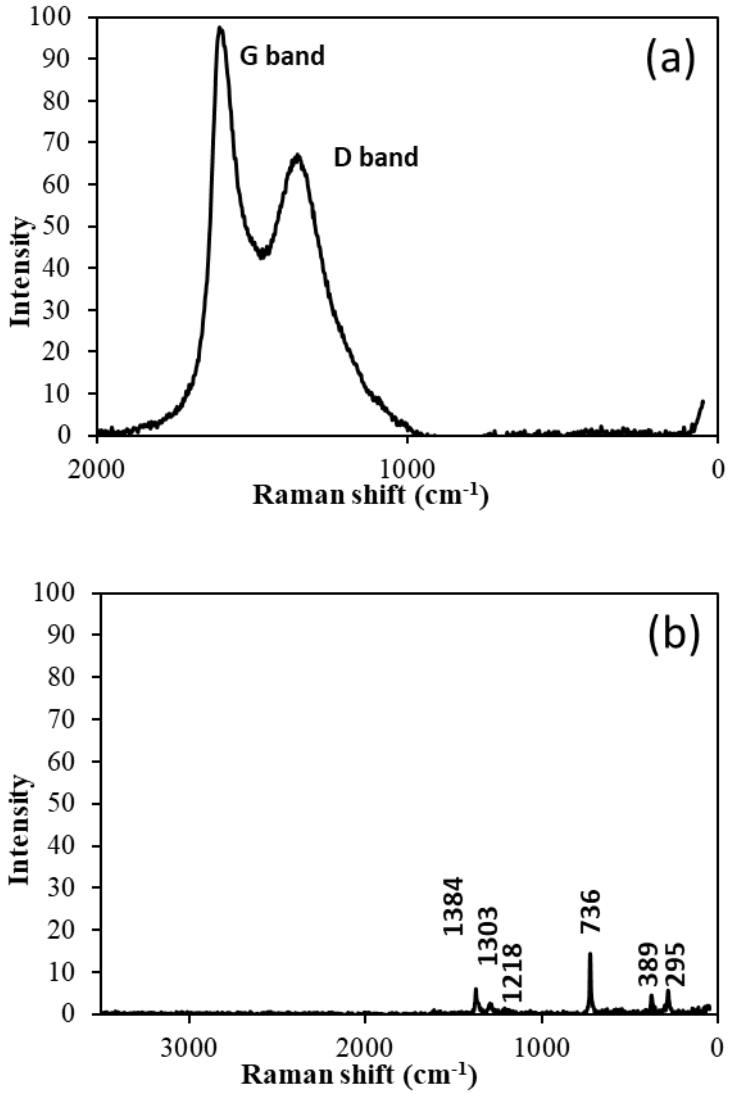

Fig. 4. 4. Representative Raman spectra obtained from worn surfaces of PTFE composites specimens (1) typical D and G bands obtained from tribofilm formed in hydrogen, (2) exposed resin surface in nitrogen

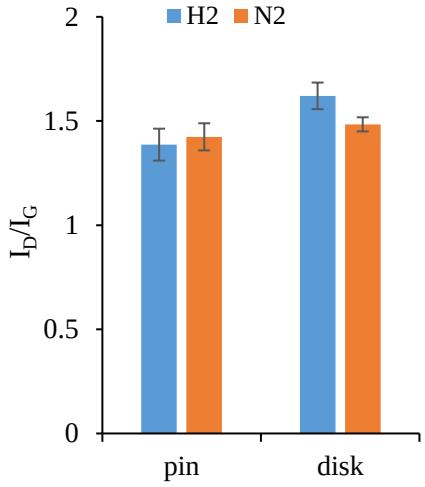

Fig. 4. 5. Ratios of peak Intensity of D bond to peak Intensity of G bond obtained from both worn surfaces in different gaseous atmosphere (n = 70)

All the XPS spectra were obtained three days after the sliding tests from the transfer films formed on the disk surfaces. All specimens were stored in desiccator after sliding tests. Specimens with the total sliding distance of 50000 m in both hydrogen and nitrogen were analyzed according to the friction and wear results. Spectra in the fluorine (F 1s), carbon (C 1s), oxygen (O 1s), iron (Fe $2p_{3/2}$), and chromium (Cr $2p_{3/2}$) regions were obtained from the brown and black patches. The average atomic ratios of these five elements were calculated, and the relationships at a depth of 0 to 46 nm with gaseous atmospheres are shown in Fig. 4. 6. The atomic ratios of iron, chromium and carbon are almost the same from the transfer films in hydrogen and in nitrogen. In addition, the atomic ratio of carbon decreased with the increase of depth of the transfer films whilst those of iron and chromium increased. However, the atomic ratios of fluorine and oxygen differed in hydrogen and in nitrogen. The ratios of fluorine are higher in nitrogen while that of oxygen are higher in hydrogen. Both atomic ratios of fluorine and oxygen

increased in the deeper sides of the transfer films.

Spectra of transfer films in hydrogen and nitrogen at different depths are shown in Fig, 4. 6. For Fe 2p3/2, peaks at 706.8±0.2 eV, 711.3±0.1 eV, 714.2±0.8 eV, 710.9±0.1 eV, and 714.9 eV were identified as pure iron, iron (II) fluoride, iron (III) fluoride, iron (III) oxide and ferrous carbonate [30–33]. Both transfer films in hydrogen and in nitrogen consisted of iron oxides and iron fluorides. However, spectrum of pure iron was only observed from the transfer film in nitrogen. Similarly, pure chromium was identified from transfer films in nitrogen. Although in little amount, such pure chromium was also found in transfer films under hydrogen environments. Regarding the F 1s, peaks at 684–685.5 and 685.7 eV were subscribed to iron fluorides [26,28–30]. Obvious increase in the intensity of metal fluorides in the deeper sides of transfer films in nitrogen revealed larger amount of that in the subsurface layers of transfer films in nitrogen, which matched with the atomic ratios shown in Fig. 4. 6. Spectra of metal fluorides in F 1s with stronger intensity were also found in the surface of transfer films in nitrogen. With respect to the O 1s, peaks at 529.7±0.3 eV, 531.3–532 eV, and 533 eV corresponded to Iron (III) oxide (metal oxides), C=O bonds from metal carbonates and organic compounds or O–H bonds from hydroxyl groups, organic C–O bonds [28,30]. Although both transfer films in hydrogen and nitrogen contained metal oxides and organic compounds or hydroxyl groups, higher ratio of metal oxides was identified from the surface of transfer films in hydrogen. Moreover, for C 1s spectra, peaks at 284.3±0.1 eV, 285.2±0.1 eV and 286.4±0.4 eV were related to the sp^2 and sp^3 hybrids forms of carbon, and C–O bonds [26–29]. Since the C-F bonds are not observed in C 1s spectra (290~293 eV, [26]), PTFE was considered do not exist in the transfer film. Moreover, as revealed by Takahagi et al. [154], peaks near 285 eV in C1s comes from the -C- species after removal of all fluorine atoms. Clearly, decrease in the amount of carbon in the subsurface layers of transfer films in hydrogen could be seen from the results above.

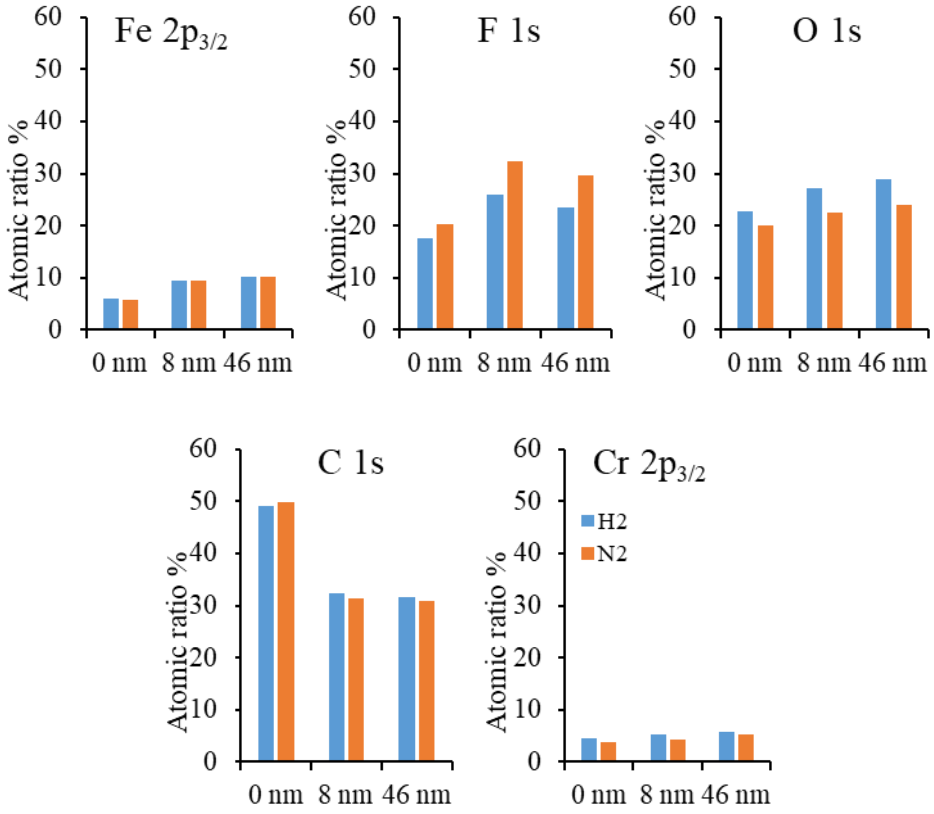

Fig. 4. 6. Correlation between atomic ratios of transfer films formed atop disk surfaces and gaseous atmosphere

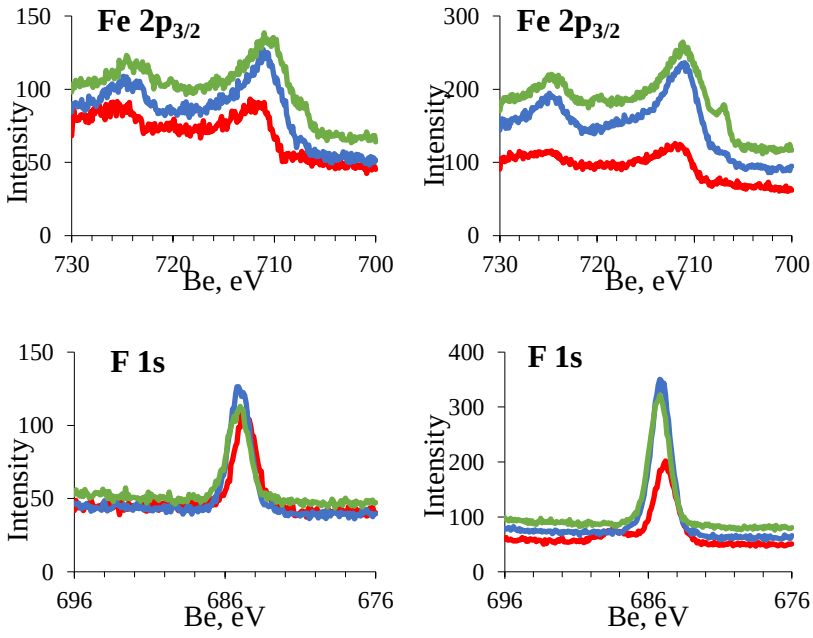

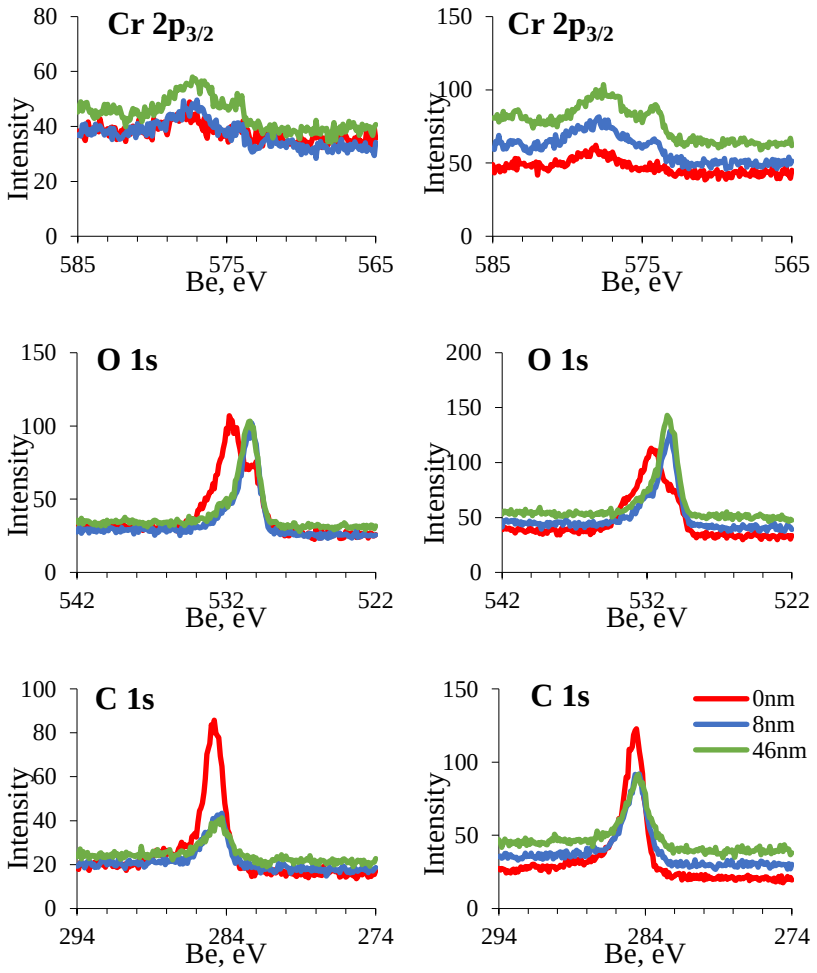

Fig. 4. 7. XPS spectra at 5 element regions from disk surfaces in different gaseous atmosphere (left: in hydrogen; right: in nitrogen)

4.2.4 Tribofilm formation and their role on friction and wear mechanisms

All the results of the present experiments indicate that the gaseous atmosphere and air contaminants play important roles in the formation of carbon-based films, friction, and wear. Varieties in the chemical compositions of transfer films as well as that in the amount of formed carbon films were thought to result in the different friction and wear behaviors of the CF-filled PTFE under hydrogen and nitrogen environments.

For sliding tests under hydrogen environments, carbon-based tribofilm and transfer film

formed atop both PTFE composites and stainless steel worn surfaces. It is considered that the removal and transfer of PTFE and CFs debris within the interfaces give birth to this formation. In addition, as suggested by Erdemir [124], the strong carbon-carbon interactions within the carbon-based film can be eliminated by hydrogen termination. Sliding between these carbon-based films resulted in the low friction and most stable wear behavior after running-in stage in the total 40000 m sliding and the sliding before air contaminant under hydrogen environments.

Although in little amount, the presence of pure metals at the depth of 46 nm of the transfer film (Fig. 4. 7.) is thought partly due to the removal of passive layers which consisted of metal oxides or metal hydroxides [36] on the surfaces of disk specimens and has been demonstrated to decrease significantly in such environments [37], and partly due to the reduction reaction between metal oxides and hydrogen. These pure transition metals are considered to catalyze the formation of the carbon-based transfer film, as reported in previous studies [39,40], in which the iron particles function as a carbon nanotube reactor. Moreover, metal fluorides and part of the C-C bonds found in the transfer films are also regarded as the reaction products from the tribochemcial reaction between PTFE and metal oxides which has been demonstrated by Onodera et al. [34,35].

After the air exposure process, contaminant such as water and oxygen are absorbed in the surfaces of both pin and disk specimens. Oxidations of pure metals and tribochemical reaction between carbon, water and oxygen are suggested occurring in the interface at the beginning of sliding, resulting in the higher atomic ratios of oxygen and intensity of metal oxides that are observed from transfer films in hydrogen. Moreover, the adsorption of water vapor, as investigated by Andersson et al. [42], is suggested to attenuate the strong covalent bond interactions between carbon atoms on DLC films, thus promoting the detachment of formed carbon-base films. Consequently, both wear rate and the friction coefficient increased after the air exposure process. Moreover, from the mere differences between wear rates before and after the air exposure process, the formed carbon films are thought detachable and transfer wear processes became the dominant wear mechanism as the depleted films is repeated replenished [57]. This wear mechanism resulted in the decrease of friction coefficient with the increase of sliding distance.

With respect to the sliding tests in nitrogen, severe wear (Fig. 4. 2. (right)) occurred

during the running-in stage of sliding, the wear and transfer of PTFE and CF debris give rise to the formation of thick and rough carbon-based films with highly ordered graphitic structure (Fig. 4. 5.) atop both worn surfaces of sliding couple. Sliding between these carbon films resulted in the characteristic drop in friction, the lowest friction coefficient and the lowest wear during steady stage.

Furthermore, the presence of pure iron on the deep side of the transfer film (Fig. 4.7. right) was thought due to the removal of the metal oxide film on the disk surfaces during the running-in stage. As stated above, these pure transition metals are considered to catalyze the formation of the thick carbon-based transfer film with highly ordered graphitic structure. Similarly, tribochemical reaction between PTFE and metal oxides is considered occurring at the interfaces during running-in stage as well. These tribochemically generated metal fluorides, in a large amount (Fig. 4. 7. right), are thought to hold stronger van der Waals forces with the delocalized electrons of graphitic debris because of the strong electronegativity of fluorine atoms. This is considered to give rise to the formation of a carbon-based transfer film with a higher-order graphitic structure. However, these thick carbon films are considered to be mechanically unstable [57, 120] and removed as sliding continued, resulted in the increase of friction after running-in stage.

Differed with the tribological performance after the air exposure process in hydrogen, small variations can be found from the friction and wear of CF-filled PTFE in the sliding tests with or without air contaminants. It is suggested that the large amount of metal fluorides functioned as the protect layers of both pure metals and part of carbon films.

Therefore, the direct effects of hydrogen in this sliding process are summarized as follows: (1) The strong carbon-carbon interactions within the carbon-based film can be eliminated by hydrogen termination. (2) Reduction reaction between metal oxides and hydrogen.

4.3 Conclusion

Tribological characteristics of CF-filled PTFE were sensitive to the gaseous atmosphere, the lowest friction and wear coupled with the most stable behavior were observed in hydrogen.

Transfer films formed on stainless steel surfaces varied in chemical composition as gaseous atmosphere changes, resulting in different friction and wear behaviors. This changes of tribological behaviors are summarized as follows:

1. In hydrogen, the surfaces of wear couple were covered by carbon-based tribofilms. Sliding contact between those films led to the lowest average friction coefficient and wear rate. Transfer wear processes is the dominant wear mechanism.

2. Carbon-based tribofilm formed in hydrogen gas were sensitive to contaminants such as water and oxygen, the air expose process giving way to the discontinuous and thinner carbon films and resulted in an increased friction and wear.

3. In nitrogen, direct contact between PTFE and steel led to the high friction and severe wear during the running-in stage. Thick carbon-based films with highly ordered graphitic structure formed during this period led to the drop in friction and lowest wear after running-in stage. Tribochemically generated metal fluorides layers made the tribofilms in nitrogen insensitive to air contaminants. Friction increased with the remove of carbon-based tribofilms.

5. The effect of trace moisture on the tribological behavior of CF-filled PTFE in hydrogen

The content of this section has in part been published in:

[120] Q. Chen, T. Morita, Y. Sawae, K. Fukuda, J. Sugimura, Effects of trace moisture content on tribofilm formation, friction and wear of CF-filled PTFE in hydrogen. Tribology International 188 (2023) 108905.

5.1 Introduction

As the latest FCV contains hydrogen gas at 70 MPa, the refueling station demands a hydrogen gas compressor operating at ~82 MPa to fill the high-pressure storage tanks. Such adiabatic compressing process of hydrogen gas abruptly increases the environmental temperature to 200 °C. The electrode catalysts used in fuel cells are sensitive to contaminants such as water and oxygen; thus, the water content of the hydrogen gas used in FCVs is regulated to less than 5 ppm according to the ISO standard. Therefore, sealing elements in FC systems are expected to exhibit suitable tribological behaviors in high-pressure, high-temperature, and trace-moisture environments.

The majority of the hydrogen gas is produced via the centralized reformation of natural gas as well as the deployment of clean alternatives such as electrolysis in hydrogen generation [1]. Furthermore, alternative emerging approaches include thermochemical water splitting, photoelectrochemical cells, and biological pathways. Thus, the moisture content of the hydrogen used in reciprocating gas compressors varies.

As discussed in Chapter 4, the chemical composition of tribofilms formed on worn surface of sliding couple differed in hydrogen and nitrogen, the carbon film formed in hydrogen were sensitive to water in the air. However, the effect of trace moisture content on the tribological behaviors of CF-filled PTFE in hydrogen gas has never been discussed.

The overall aim of this chapter is to explore the effects of trace moisture on the tribological characteristics of CF-filled PTFE in a high-purity hydrogen environment. In addition, experimental data are provided to establish the material selection criteria for the

sealing elements of gas compressors in hydrogen fueling stations.

In this chapter, a series of pin-on-disk sliding tests were conducted to clarify the relationship between the trace moisture content and the friction and wear of PTFE composites in hydrogen. After the sliding tests, both surfaces of the wear couple were analyzed to understand the physical and chemical phenomena occurring at the sliding interface.

5.2 Results and discussion

5.2.1 Effect of moisture content on friction and wear of CF-filled PTFE

The variations in the friction coefficient and moisture content with the sliding distance are shown in Fig. 5. 1. The moisture content in the sliding tests was well-maintained at each content level, and the friction coefficients obtained at every moisture content level corresponded well with each other. Hence, the experimental data were considered highly reliable. In addition, the friction coefficient remained approximately constant with increasing distance over a wide range of distances for moisture contents less than 1 ppm and approximately 40 ppm. However, the friction coefficients around 10 and 20 ppm were easily influenced by changes in moisture content.

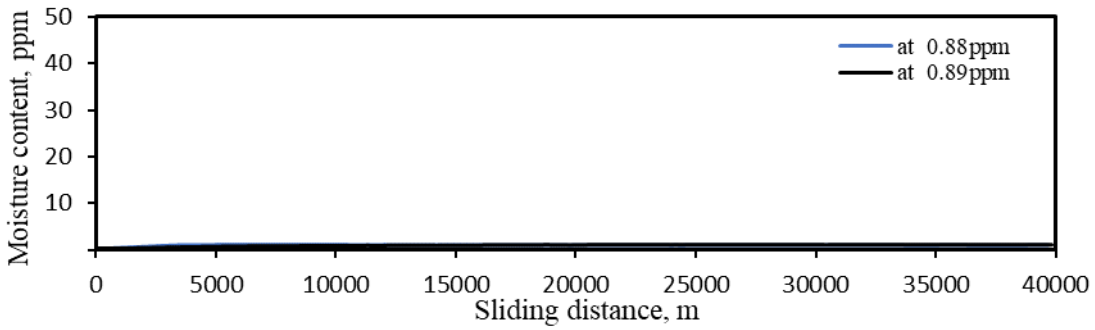

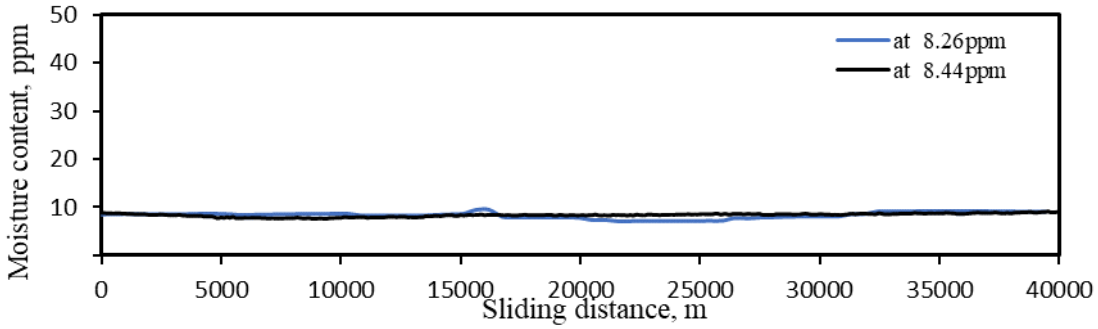
Moisture content, ppm
50
40
30
20
10
0
5000
10000
15000
20000
25000
30000
35000
40000
Sliding distance, m
at 8.26ppm
at 8.44ppm

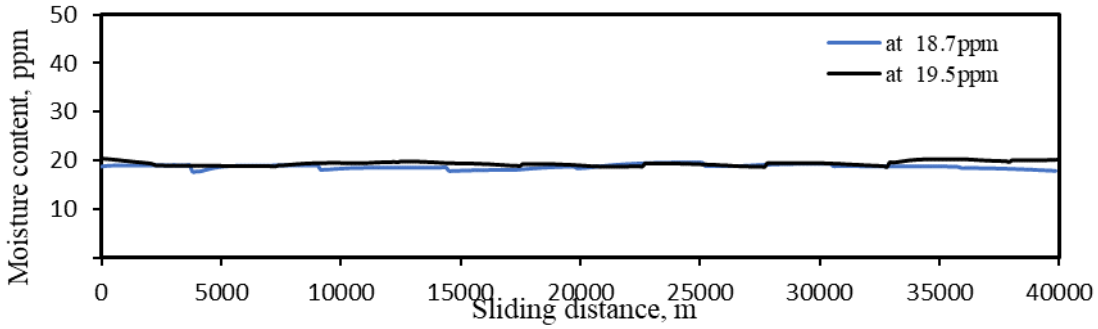
Moisture content, ppm
50
40
30
20
10
0
5000
10000
15000
20000
25000
30000
35000
40000
Sliding distance, m
at 18.7ppm
at 19.5ppm

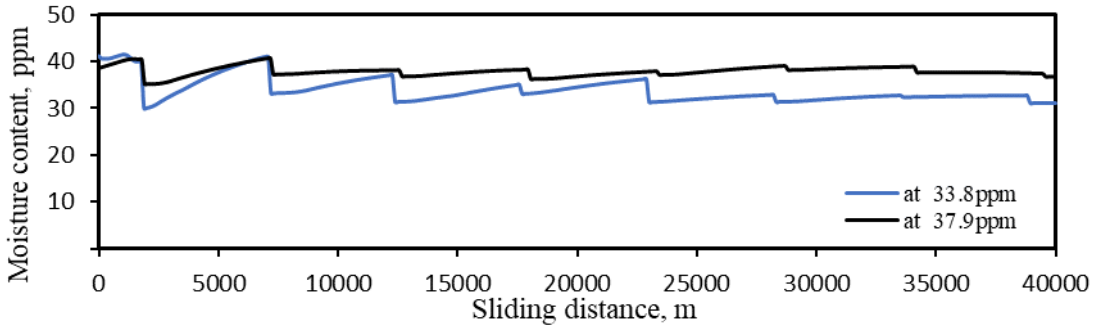
Moisture content, ppm
50
40
30
20
10
0
5000
10000
15000
20000
25000
30000
35000
40000
Sliding distance, m
at 33.8ppm
at 37.9ppm

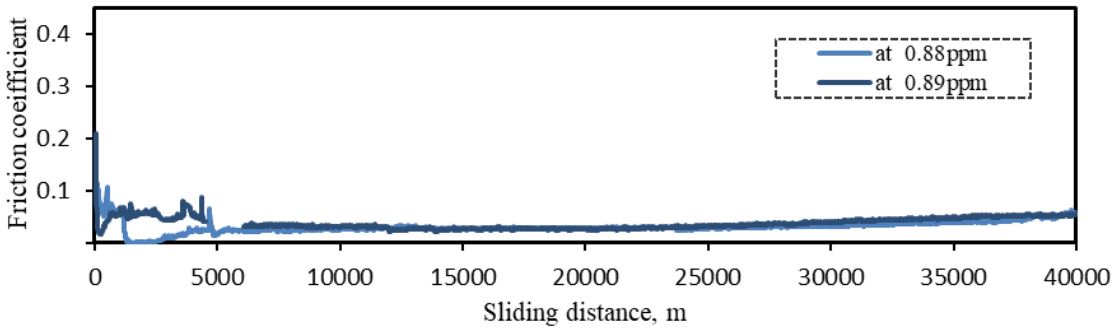
Friction coeifficient
0.4
0.3
0.2
0.1
0
5000
10000
15000
20000
25000
30000
35000
40000
Sliding distance, m
at 0.88ppm
at 0.89ppm

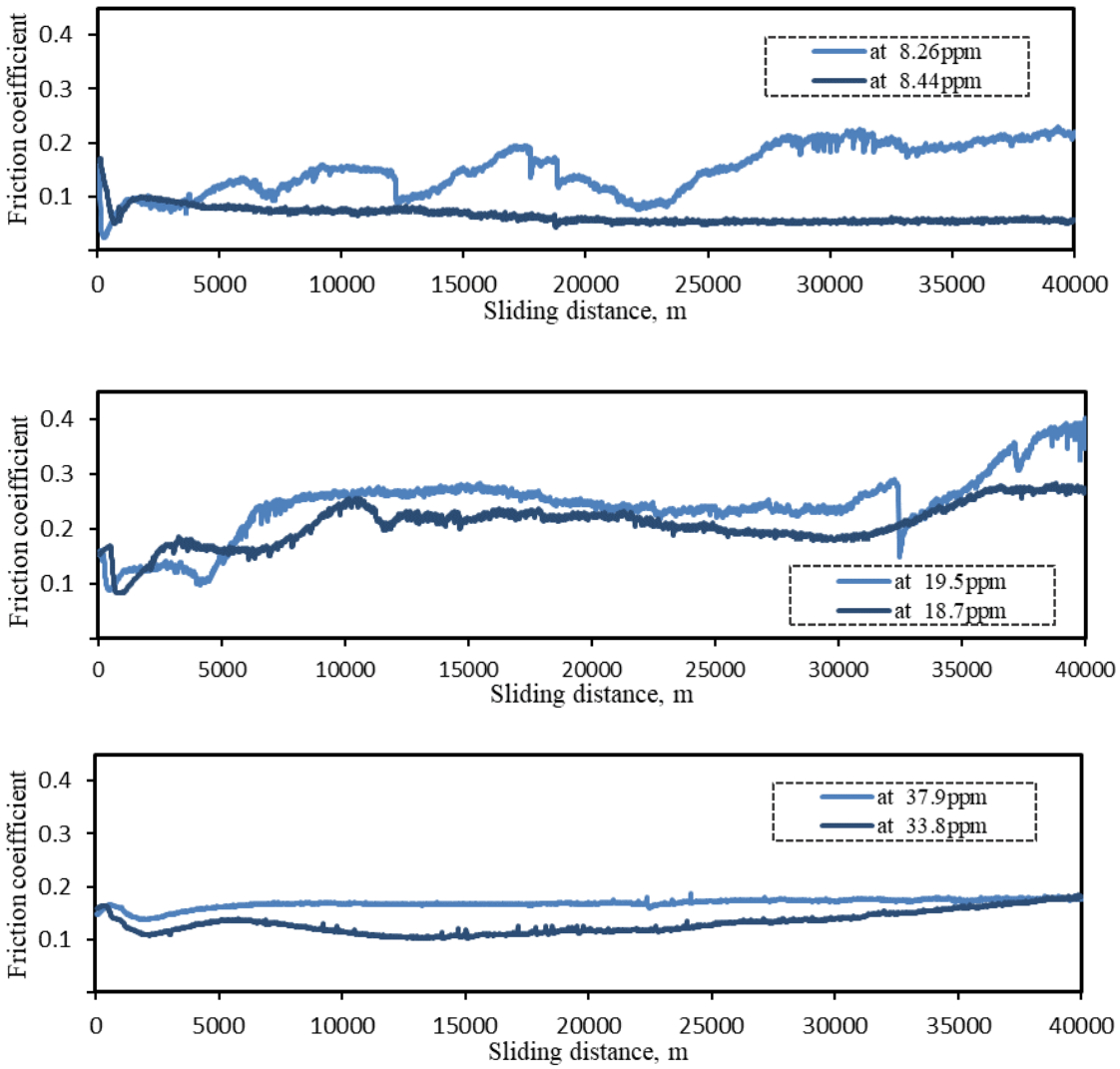

Fig. 5. 1. Variations of friction coefficient and moisture content with sliding distance

Plots of the specific wear rates and average friction coefficients against the moisture content are shown in Fig. 5. 2. (a) and (b), respectively. The average value of the friction coefficient during the last 100 m of the sliding test was used. According to the obtained results, the specific wear rates of the PTFE composite specimens tended to increase as the moisture content increased from 1 to 20 ppm and remained approximately constant after 20 ppm. In all the sliding tests, the magnitude of the specific wear rate was in the order of 10-7 mm3/Nm. Regarding the average coefficient of friction, a similar tendency to that of the specific wear rate was observed when the moisture content was between 1 and 20 ppm, and the average friction coefficient increased from 0.05 to 0.38. However,

when the moisture content exceeded 20 ppm, the average friction coefficient decreased from 0.38 to 0.17.

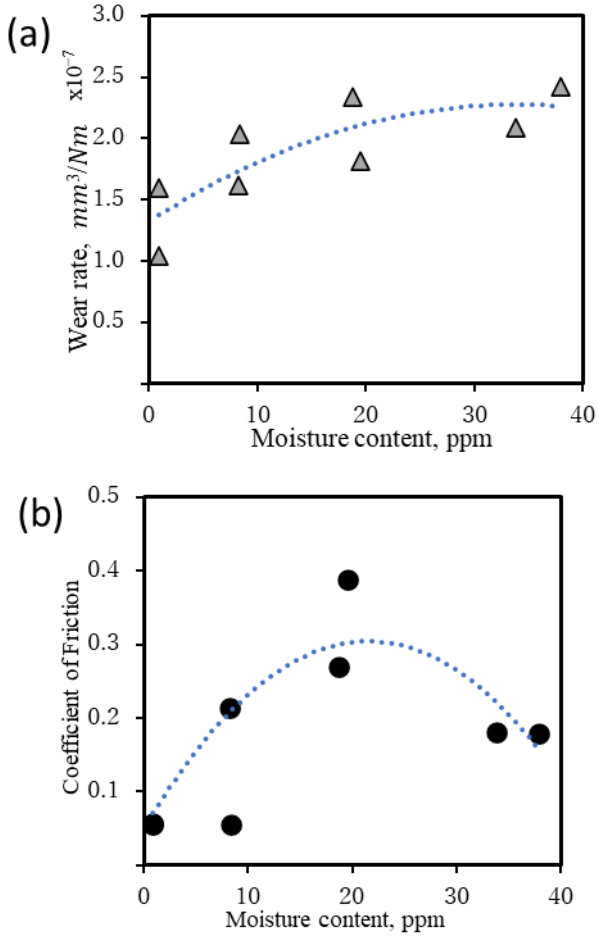

Fig. 5. 2. Plots of specific wear rates and average friction coefficient against moisture content

5.2.2 Characterization of the tribofilm and transfer film formed on the worn surfaces of sliding couple

5.2.2.1 Morphology of worn surfaces

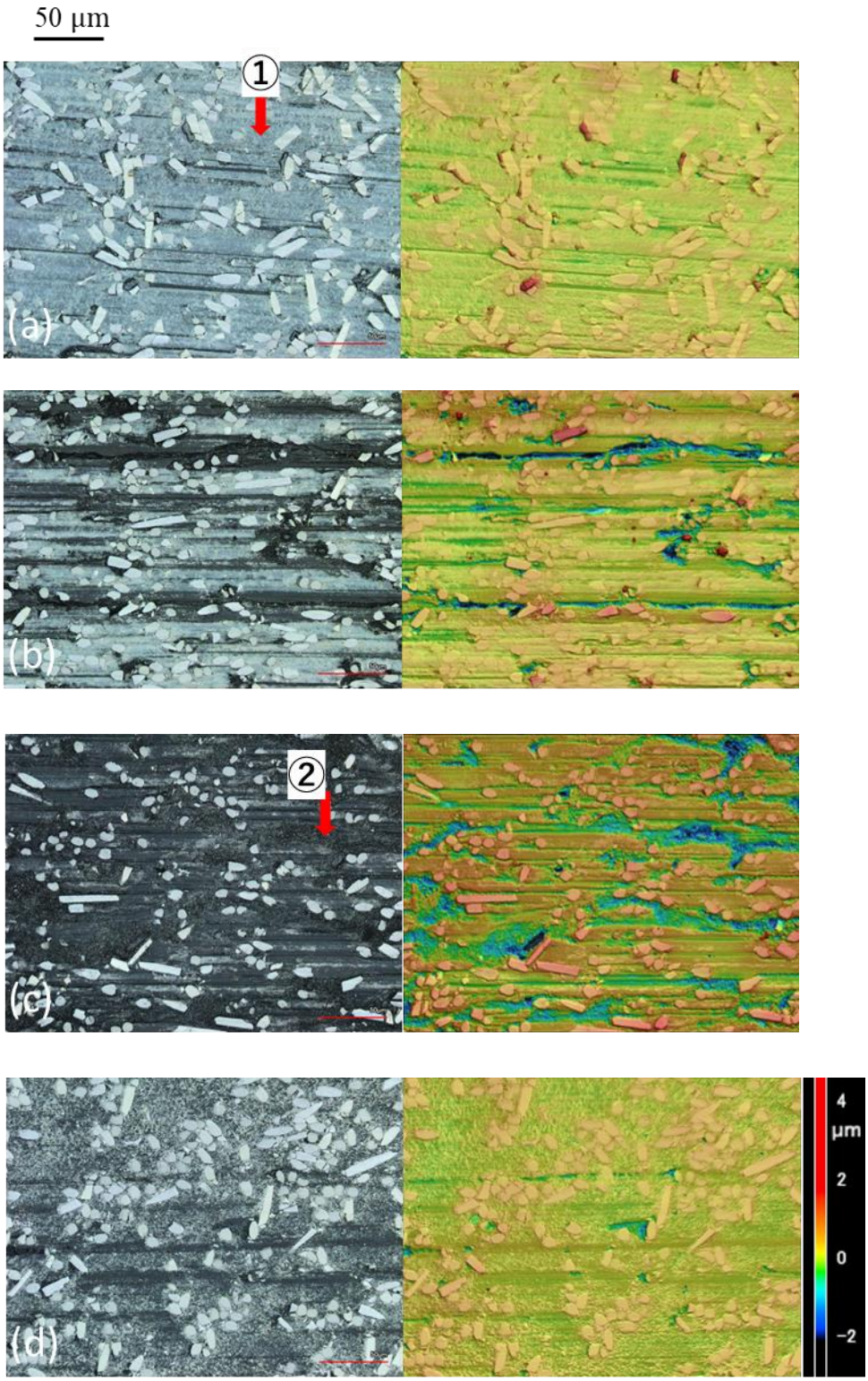

Fig. 5. 3. Optical and 3D images of worn surfaces of PTFE composite specimens with moisture content: (a) 0.89 ppm; (b) 8.26 pp; (c) 18.7 ppm; (d) 33.8 ppm

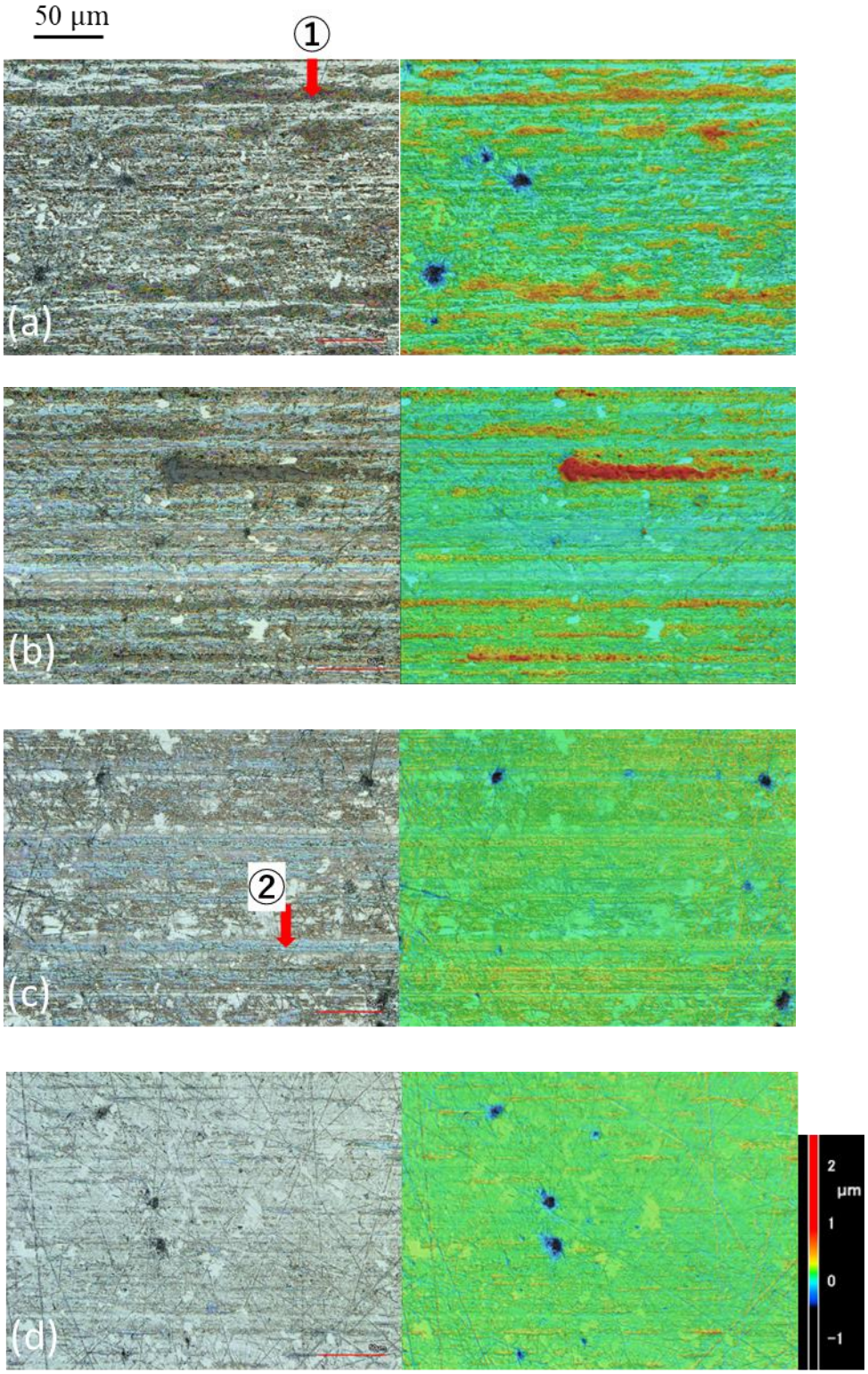

Fig. 5. 4. Optical and 3D images of worn surfaced of stainless-steel specimens with moisture content: (a) 0.89 ppm; (b) 8.26 pp; (c) 18.7 ppm; (d) 33.8 ppm

Representative images of the worn surfaces of the PTFE composites are shown in Fig. 4. The surfaces of the polymer composite specimens with moisture contents of less than 1 ppm (Fig. 5. 3. (a)) were covered by a white tribofilm, and a similar white tribofilm was observed atop the specimen surfaces at a moisture content of approximately 40 ppm (Fig. 5. 3. (d)). In contrast, surfaces with moisture contents of approximately 10 and 20 ppm (Fig. 5. 3. (b–c)) exhibited discontinuous white tribofilms, more obvious filler tips, and exposed resin parts.

More details regarding the height comparison between the CF filler and PTFE resin are shown in the corresponding 3D images (Fig. 5. 3.). The colors in the 3D images illustrate the height of each component. The height differences between the CF fillers and the tribofilms developed as the moisture content increased from 1 to 20 ppm. In particular, the CFs at a moisture content of approximately 20 ppm were obviously higher than those at other parts of the surface. However, the fillers were at almost the same height or buried in the tribofilms in environments where the moisture content was less than 1 ppm or approximately 40 ppm.

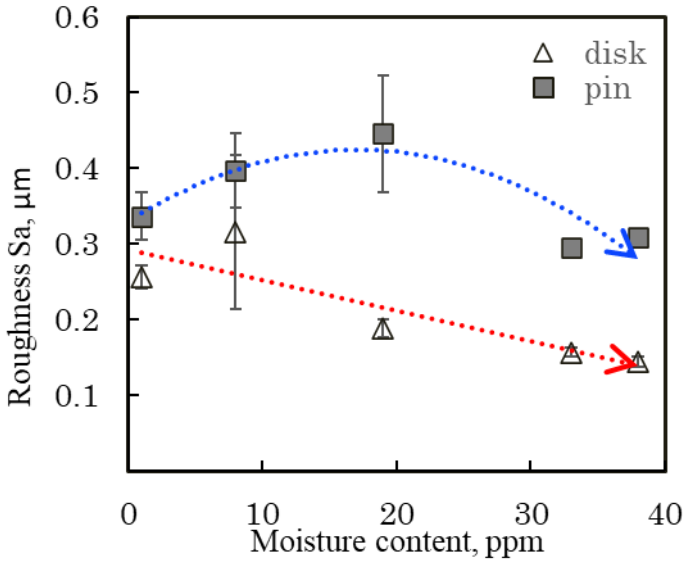

Fig. 5. 5. Plots of area roughness of PTFE composite and stainless-steel worn surfaces against moisture content (n = 40)

Similarly, Fig. 5 shows the optical and 3D images of the sliding tracks formed on the

surfaces of the stainless steel specimens. Characteristic brown (Fig. 5. 4. (a), marker (1)) and bluish (Fig. 5. 4. (c), marker (2)) patches were distributed discontinuously on the disk surface as transfer films. These bluish patches expanded most of the counterface atop the disk specimens as the moisture content increased from 1 to 20 ppm, while the accumulated brown patches gradually disappeared. When the moisture content exceeds 20 ppm, the surface is covered with a thin brown transfer film.

5.2.2.2 Microstructure and surface chemistry analysis

When the white tribofilms on the pin specimens (e.g., Fig. 5. 4., marker (1)) were analyzed using Raman spectroscopy, spectra similar to that of carbon fiber filler were observed (Fig. 5. 6. (1)). Additionally, the spectra of the pin surfaces with a moisture content of approximately 20 ppm (Fig. 5. 4., marker (2)) show the typical spectra of pure PTFE (Fig. 5. 6. (2)). Spectra obtained from both surfaces of sliding couple indicated the presence of carbon and the formation of a carbon-based film.

The carbon area intensity (900-1900 cm^{-1}) was calculated from the Raman spectra obtained from both tribofilms and transfer films formed on the worn surfaces, and the results are depicted in Fig. 5. 7. The area intensities of the transfer films decreased with increasing moisture content, indicating that the formation of carbon-based transfer films decreased or was prevented. Compared with the area intensity of the transfer film, that of the tribofilm on the PTFE composite surface remained almost constant. These values indicate that the tribofilms formed at all moisture content levels had similar carbon amounts.

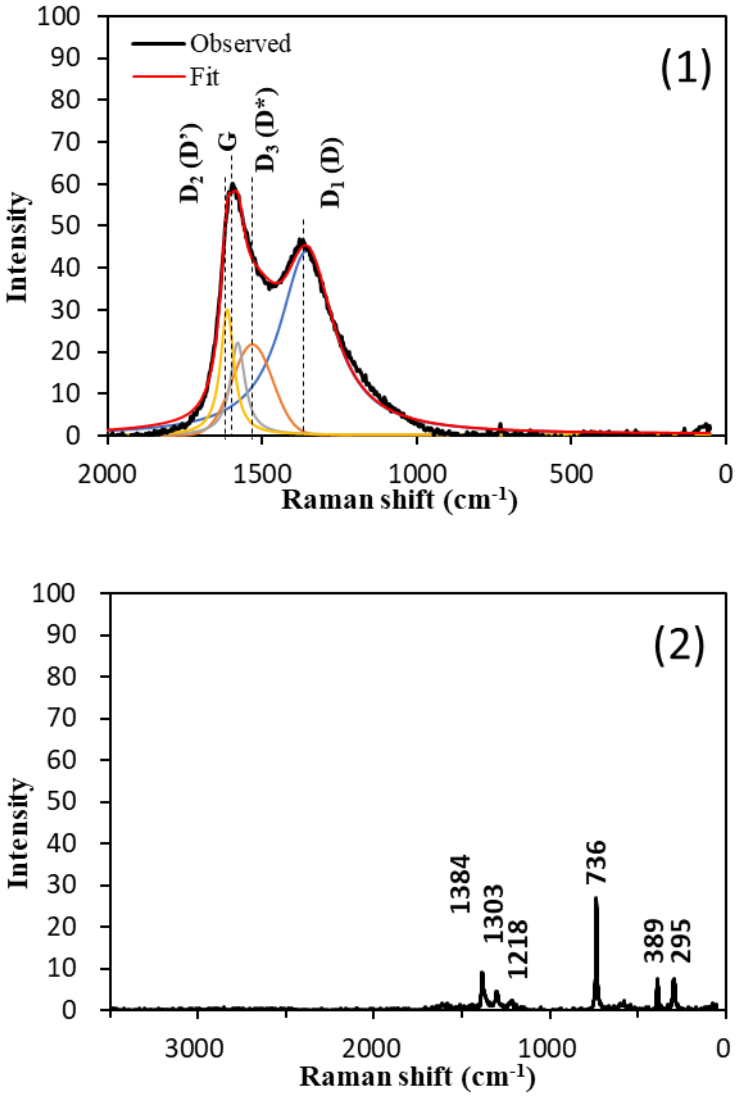

Fig. 5. 6. Representative Raman spectra obtained from worn surfaces of PTFE composites specimens (1) multiple peak-fit for D and G bands in the spectra obtained from tribofilm formed in 0.89 ppm, (2) exposed resin surface in 18.7 ppm

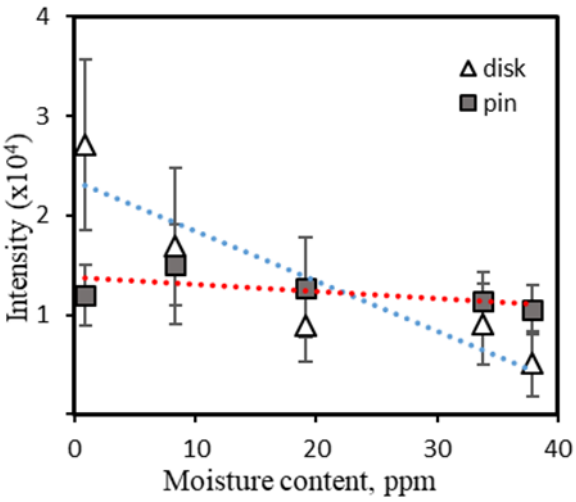

Fig. 5. 7. Variation of carbon area intensity calculated from Raman spectra obtained from both tribofilm and transfer film formed atop worn surfaces with moisture content (n = 200)

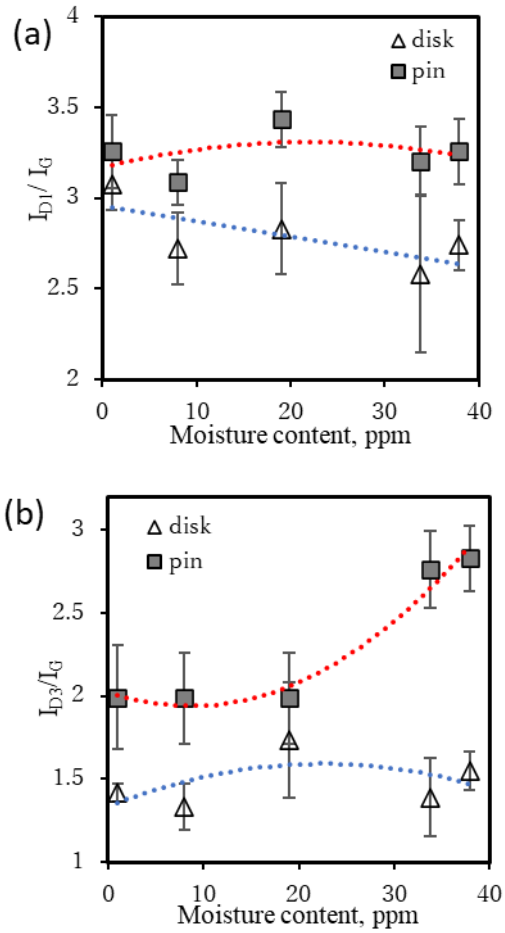

Fig. 5. 8. Plots of ratio of peak Intensity of D_1 and D_3 to peak Intensity of G peak obtained from both worn surfaces against moisture content. (a) Ratio of peak Intensity of D_1 to that of G peak; (b) ratio of peak intensity of D_3 to that of G peak (n = 200)

Moreover, the peak resolutions were obtained for the G and D bands of the transfer films (Fig. 5. 6 (1)). The intensities of the D_1, D_2, D_3 and G peaks were calculated [16,17] to analyze the structures of the formed carbon-based films. The ratio of the peak intensity of D_1 to that of G was calculated to evaluate the relationship between the amount of disordered graphitic lattice and ideal graphitic lattice (Fig. 5. 8. (a)). This ratio from transfer films decreases as the moisture content increases, indicating the formation of a more graphitic structure in the transfer film. In contrast, the ratio of the tribofilms remained almost constant; only a slight increase was observed at approximately 20 ppm, which suggests an increase in defects in the graphitic structure of the tribofilms. Additionally, the ratios of the peak intensities of D_3 and G were used to evaluate the fraction of amorphous carbon in the ideal graphitic lattice (Fig. 5. 8. (b)). Above 20 ppm, the ratio of the tribofilms increased with increasing moisture content, revealing an increase in the amorphous carbon in the tribofilms. Moreover, this increase indicates the weakening of the formed carbon-based tribofilm because the peak intensity of the D band relative to that of the G band showed a negative correlation with the hardness of the carbon-based film and the mechanical strength of the CFs [18,19]. In addition, the ratio of the transfer films exhibited a similar trend to that of the tribofilm in Fig. 5. 8. (a), with only a slight increase observed at approximately 20 ppm. This result indicated an increase of amorphous carbon in the transfer films approximately 20 ppm.

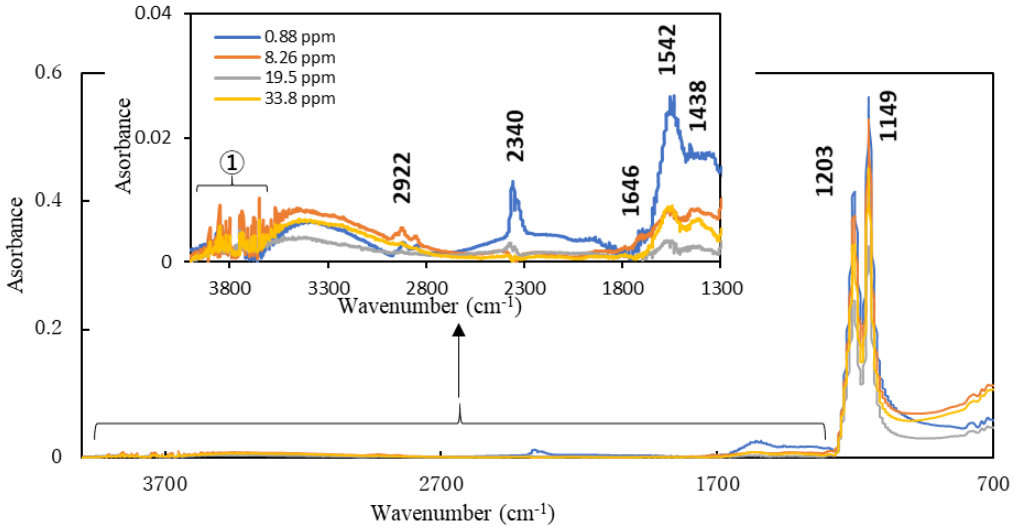

Fig. 5. 9. IR spectra obtained from tribofilms formed atop PTFE composites surfaces

To further clarify the changes in the structure of the carbon-based films and the chemical reactions on the PTFE composite surface that may occur with an increase in moisture content, IR spectra were acquired from the tribofilms formed on the polymer surfaces. As shown in Fig. 5. 9, weak absorption bands were observed in the 1542 cm-1 region, which can be identified as C = C bonds (sp^2) usually found in aromatic rings in graphene materials and carbon skeletons in CNT and DLC samples, respectively [20–22]. Moreover, the bands at 2340 cm^{-1}, 2922 cm^{-1} and 3600–3900 cm^{-1} region (Fig. 5. 9, marker (1)) were ascribed to CO_2, C-H, and -OH stretching vibrations, respectively. In addition, the CF_2 and CC bonds of PTFE and CF showed strong absorption bands in the 1206 cm^{-1} region [23]. An intense absorption band was observed in the 1150 cm^{-1} region, corresponding to the CF_2 bond of PTFE and the C–O bond of the carboxyl group [24,25]. The intensity of the C = C bonds decreases as the moisture content increases from 1 to 20 ppm. This was observed when the moisture content exceeded 20 ppm.

XPS spectra were obtained within one week of the sliding tests from the transfer films formed on the disk surfaces. All specimens were stored in desiccator after the sliding tests. Specimens with moisture contents of less than 1, 20, and 40 ppm were analyzed. First, a comparison has been made between XPS signals acquired from a wide scan of the bluish and brown patches were compared. As a result, the bluish patches revealed stronger

intensities of Fe 2p3/2 and F 1s together with a much weaker intensity of C 1s than those from brown patches, at 707, 685, and 284.5 eV, respectively [26]. The bluish patches consisted of more PTFE, iron fluorides, and less carbon than the black patches.

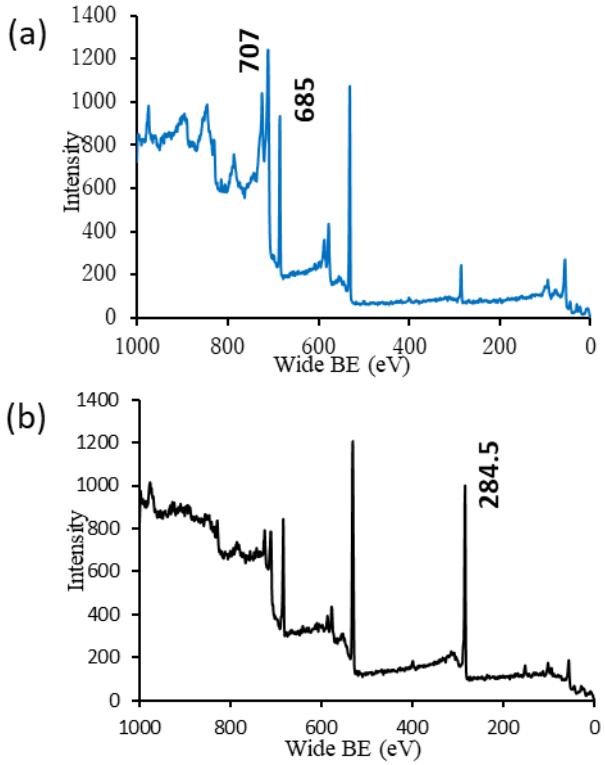

Fig. 5. 10. XPS spectra obtained from transfer film formed atop stainless steel surfaces ((a) bluish patch, (b) brown patch)

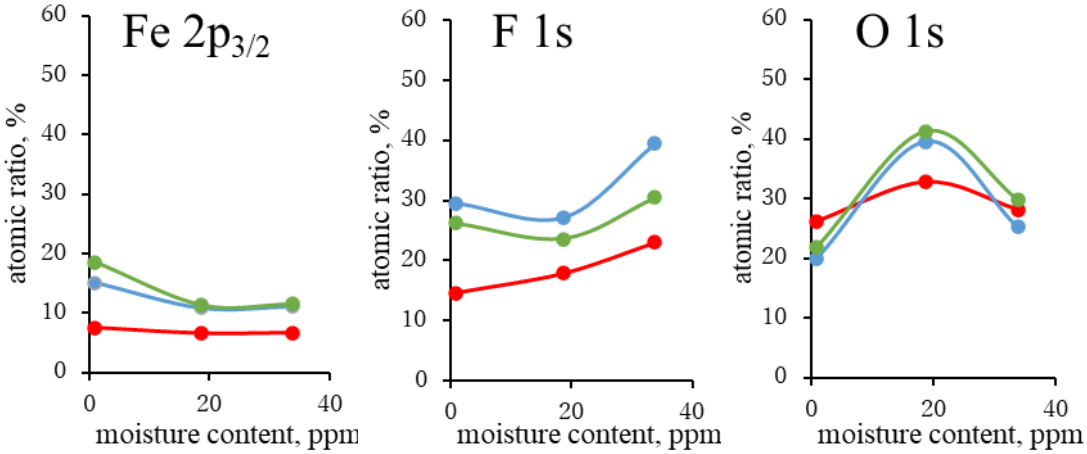

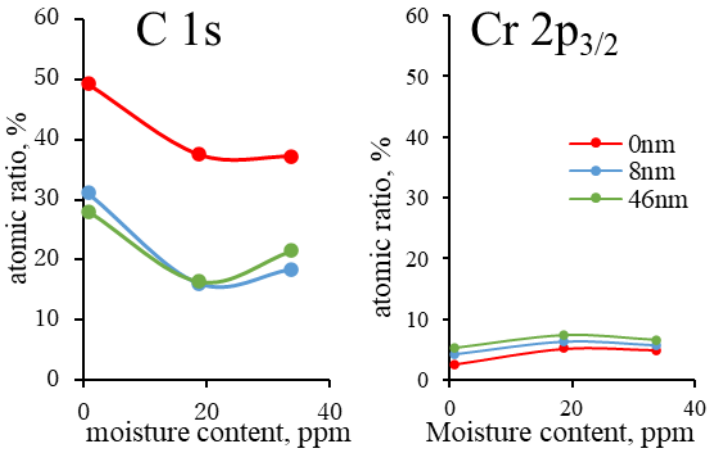

Fig. 5. 11. Correlation between atomic ratios of transfer films formed atop disk surfaces and moisture content

Spectra in the fluorine (F 1s), carbon (C 1s), oxygen (O 1s), iron (Fe $2p_{3/2}$), and chromium (Cr $2p_{3/2}$) regions were obtained from the brown patches. The atomic ratios of these five elements were calculated, and the relationships at a depth of 0–46 nm with the moisture content are shown in Fig. 5. 11. On the surface of the transfer film, the atomic ratio of carbon decreased with increasing moisture content, whereas the atomic ratio of fluorine increased with increasing moisture content. The atomic ratio of oxygen increased with an increase in the moisture content up to 20 ppm and decreased when the moisture content exceeded 20 ppm. At depths of 8 and 46 nm of transfer film, the atomic ratios of iron and carbon decreased as the moisture content increased to 20 ppm. After exceeding 20 ppm, the atomic ratio of fluorine and carbon increased.

Furthermore, peak resolutions were performed on the spectra obtained from the disk surfaces based on the typical spectra shown in Fig. 5. 12. With respect to the C 1s spectra, peaks at 284.3±0.1 eV, 285.2±0.1 eV, 286.4±0.4 eV, 288.6±0.6 eV, 287.3 eV and 292.5 eV were related to the sp^2 and sp^3 hybrids forms of carbon, C–O bonds, C=O bonds from ester and C–F bonds from graphite fluorides and PTFE [26–29]. The C 1s peak appeared at 288 eV could be the one shifted 4.30 eV from the -C- species, indicating the chemical structure of CF_2-C*F-CF_2, which also comes from the PTFE after removal of some fluorine atoms [154]. For Fe $2p_{3/2}$, peaks at 706.8±0.2 eV, 711.3±0.1 eV, 714.2±0.8 eV, 710.9±0.1 eV, and 714.9 eV were identified as pure iron, iron (II) fluoride, iron (III) fluoride, iron (III) oxide and ferrous carbonate [30–33]. For O 1s, peaks at 529.7±0.3 eV,

531.3–532 eV, and 533 eV corresponded to Iron (III) oxide (metal oxides), C=O bonds from metal carbonates and organic compounds or O–H bonds from hydroxyl groups, organic C–O bonds [28,30]. For F 1s, peaks at 684–685.5, 685.7, and 689.2±0.4 eV were subscribed to iron fluorides, C–F bonds from graphite fluorides, and PTFE [26,28–30].

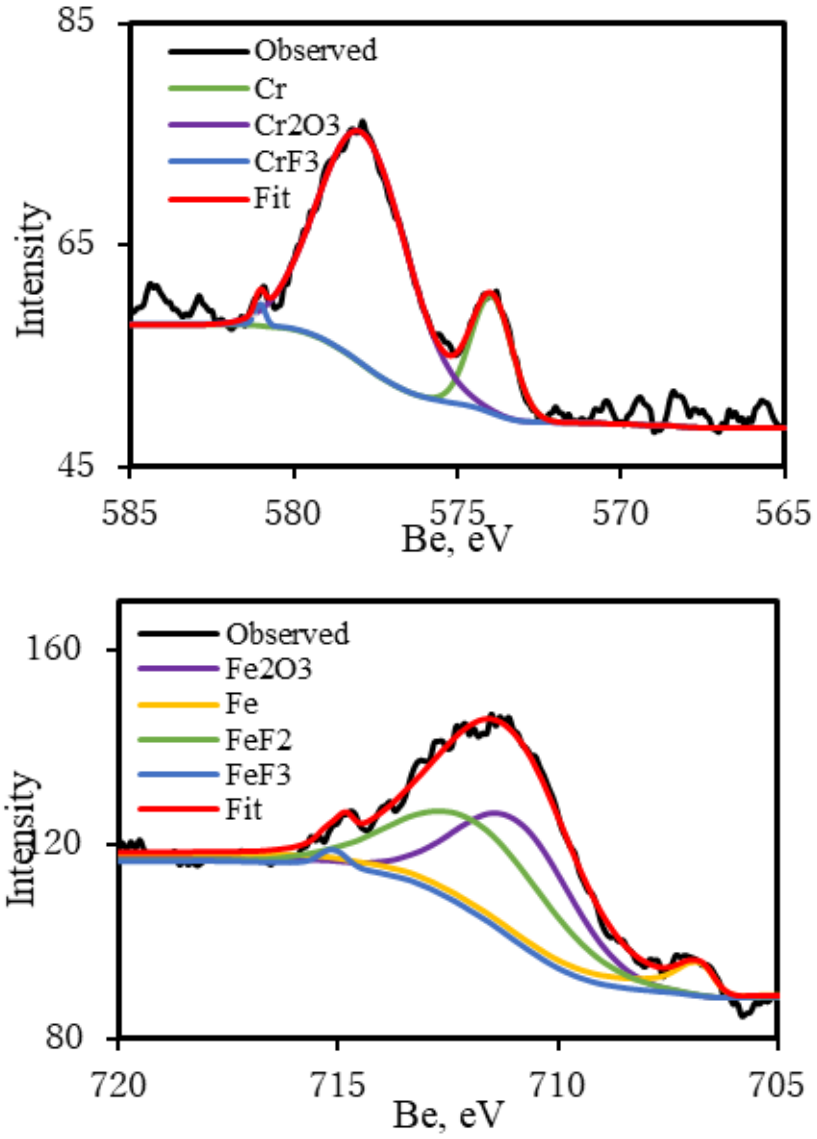

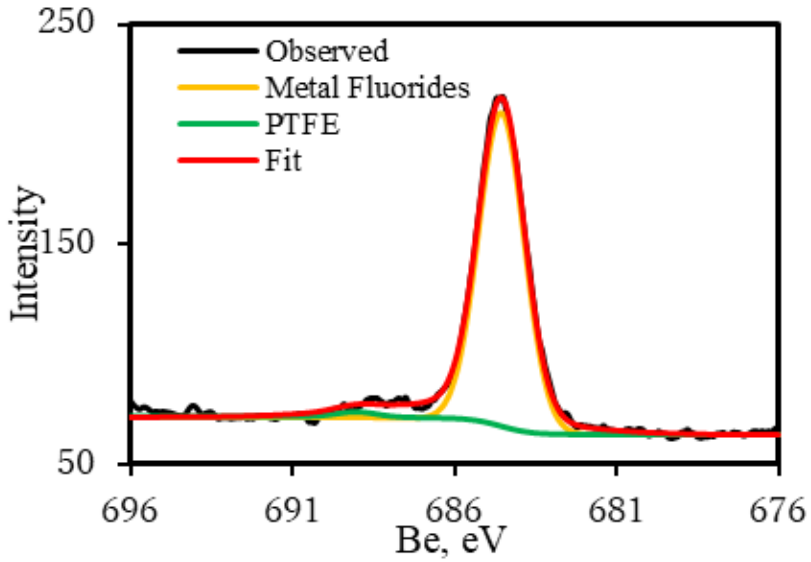
250
150
50
Intensity
Observed
Metal Fluorides
PTFE
Fit
696
691
686
681
676
Be, eV

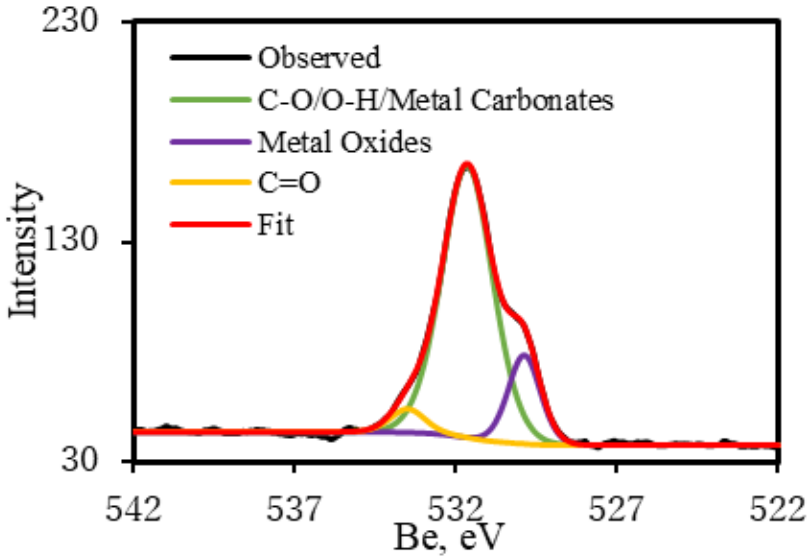
230
130
30
Intensity
Observed
C-O/O-H/Metal Carbonates
Metal Oxides
C=O
Fit
542
537
532
527
522
Be, eV

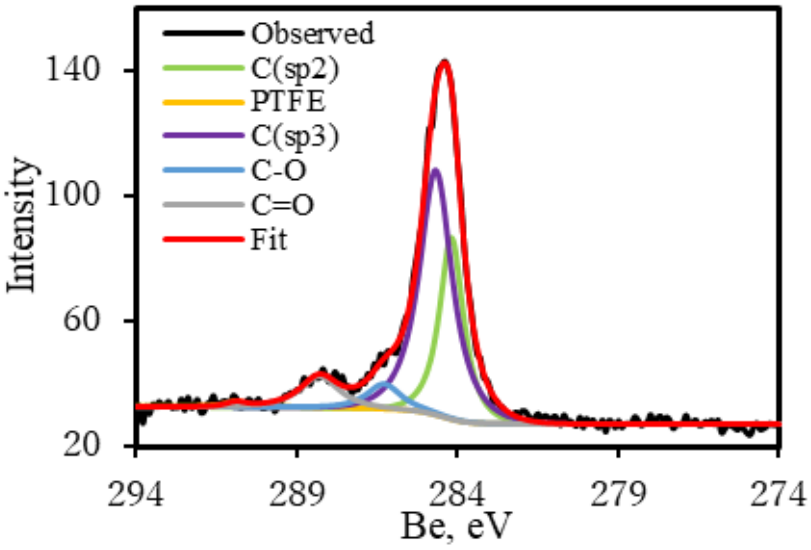
140
100
60
20
Intensity
Observed
C(sp2)
PTFE
C(sp3)
C-O
C=O
Fit
294
289
284
279
274
Be, eV

Fig. 5. 12. Representative multiple peak-fits for XPS spectra at 5 element regions from disk surfaces (0 nm, 0.89 ppm)

Consequently, the typical compounds observed in every elemental region were selected, as illustrated in Fig. 5. 12. With respect to the compounds derived from stainless steel, pure iron was identified only at a depth of 46 nm under a moisture content of less than 1 ppm and approximately 40 ppm in the transfer films. The atomic ratio of iron oxides increased as the moisture content increased from 1 to 20 ppm, indicating that iron reacted with water at these moisture content levels. Above 20 ppm, the proportion of iron oxides decreased, whereas that of iron fluorides increased. The chromium compounds showed similar tendencies to the iron compounds. The presence of pure iron with a moisture content of approximately 40 ppm was attributed to the shelter effect of the increased iron fluorides.

For the compounds transferred from the PTFE composites, the atomic ratio of carbon decreased as the moisture content increased from 1 ppm to 20 ppm. After the moisture content exceeded 20 ppm, this ratio remained constant at the transfer film surface, whereas it increased at the deeper sides of the transfer films. This trend for carbon corresponds well with the Raman analysis results (Fig. 5. 7.). Moreover, Carboxyl groups were observed in the transfer film (Fig. 5. 13.); these groups are considered to be the reaction products of PTFE and water, with a maximum moisture content of approximately 20 ppm. A similar tendency for PTFE was observed at the surface of the transfer film, the maximum value of which was found at a depth of 46 nm, with a moisture content of less than 1 ppm. This suggests a reaction between the PTFE and iron under these conditions [34,35].

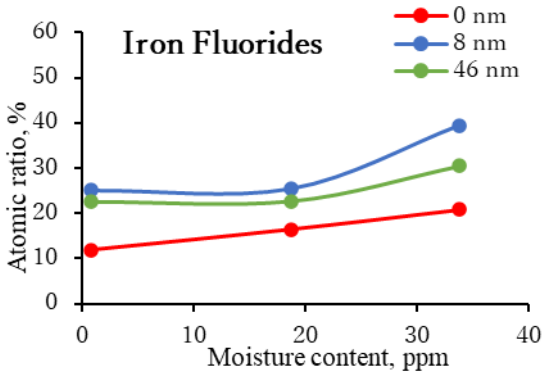

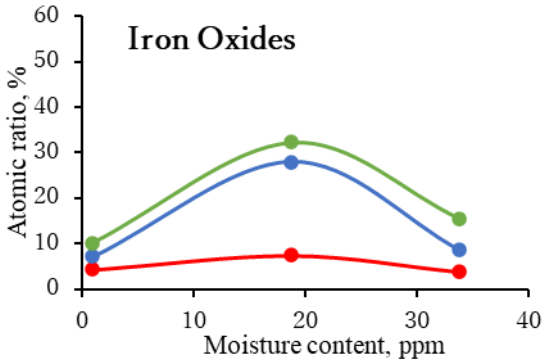
Iron Oxides
Atomic ratio, %
60
50
40
30
20
10
0
0
10
20
30
40
Moisture content, ppm

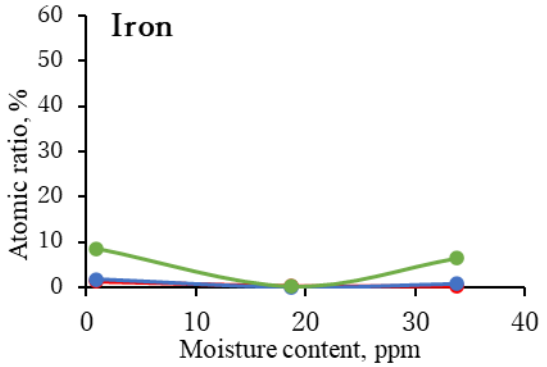
Iron
Atomic ratio, %
60
50
40
30
20
10
0
0
10
20
30
40
Moisture content, ppm

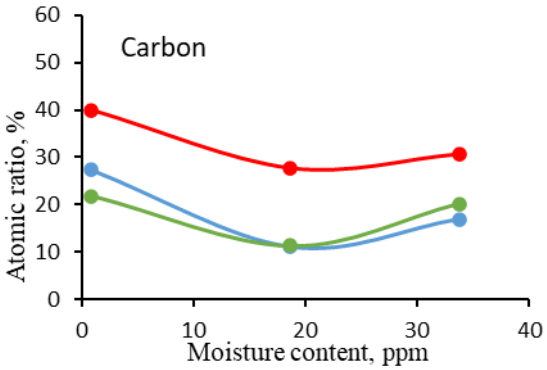
Carbon
Atomic ratio, %
60
50
40
30
20
10
0
0
10
20
30
40
Moisture content, ppm

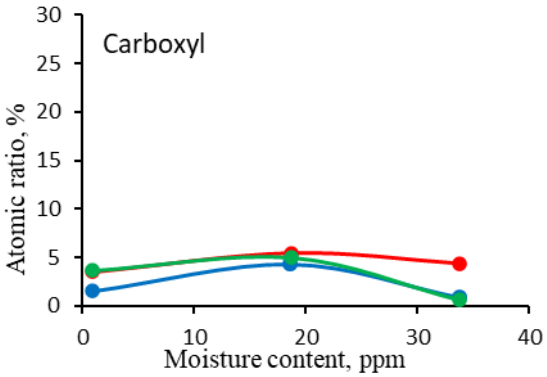
Carboxyl
Atomic ratio, %
30
25
20
15
10
5
0
0
10
20
30
40
Moisture content, ppm

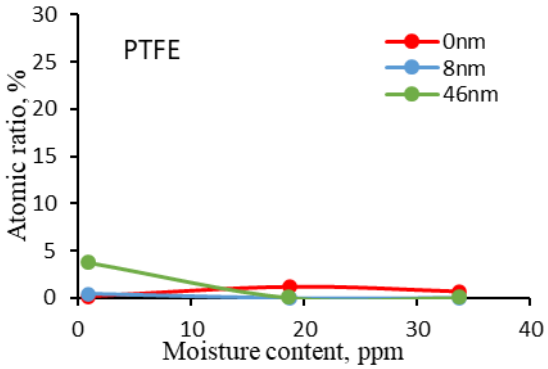

Fig. 5. 13. Correlation between chemical composition of transfer films and moisture content

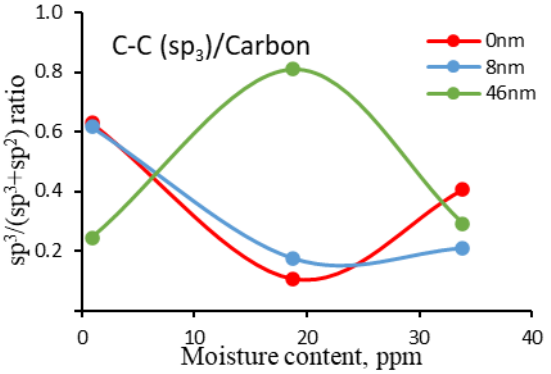

Fig. 5. 14. Plots of ratio of atomic amount of C–C sp^3 band to that of carbon from transfer films against moisture content

Furthermore, the ratio of the atomic amount of the C–C sp^3 band to that of carbon was calculated, as illustrated in Fig. 5. 14. This ratio decreased with increasing moisture content at depths ranging from 0 to 8 nm, which corresponded with the Raman analyses (Fig. 5. 8. (a)). However, this ratio attained its maximum at a depth of 46 nm, with a moisture content of approximately 20 ppm. This value can be partly ascribed to the removal and transfer of the water-molecule-saturated CFs and carbon-based tribofilms.

5.2.3 Tribofilm formation and their role on friction and wear mechanisms

All the results of the present experiments indicate that the trace moisture content in a

high-purity hydrogen gas environment plays an important role in the formation of carbon-based films, friction, and wear. Varieties in the formed carbon structure and the amount of such films were thought to give rise to the characteristic friction and wear behaviors of the PAN-based CF-filled PTFE composites under different moisture content environments.

The surface conditions based on previously obtained results are shown in Fig. 5. 15. Prior to the sliding test (Fig. 5. 15 (a)), the surface of the stainless steel was covered with a protective film of metal oxides or metal hydroxides [36] and the CFs were buried in the PTFE resin.

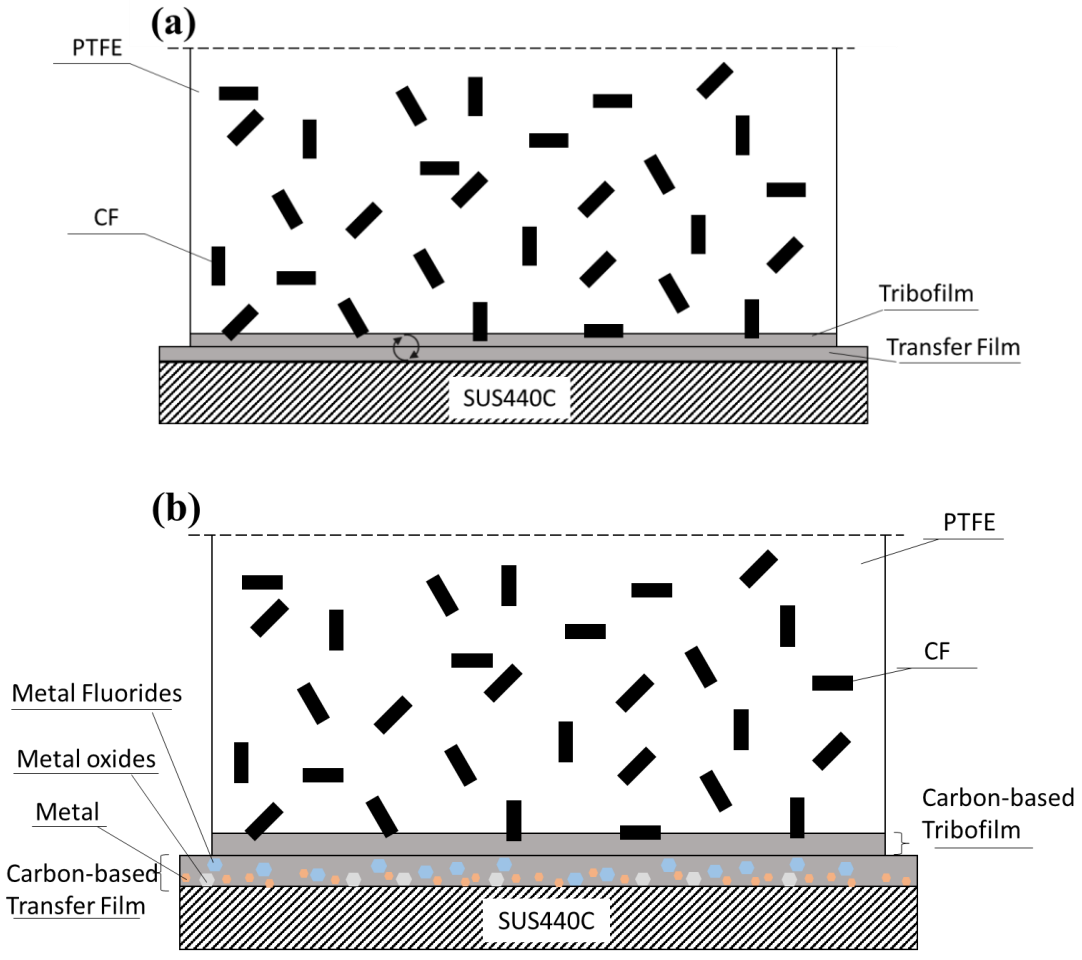

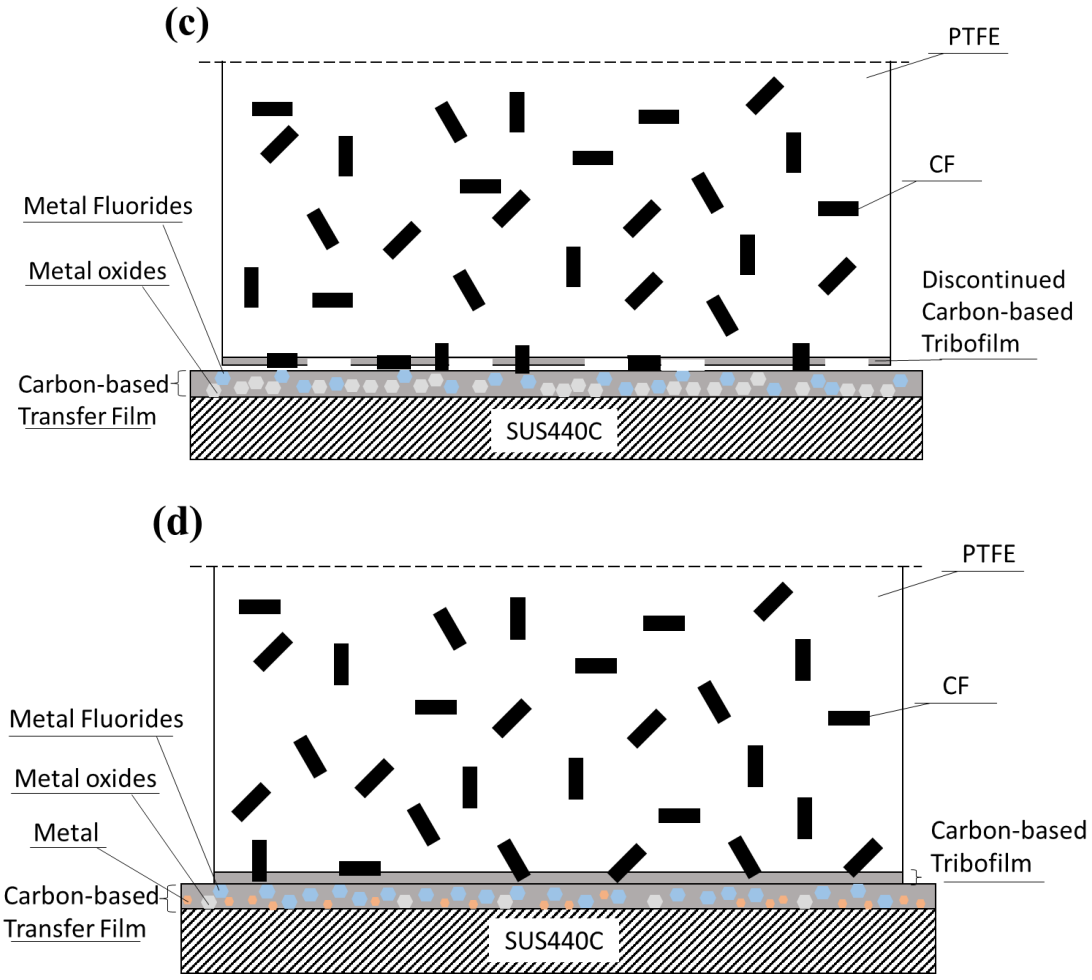

Fig. 5. 15. Schematic of surface condition of both worn surfaces. (a) Before the sliding test; (b) moisture content < 1 ppm, (c) moisture content ~20 ppm, (d) moisture content ~40 ppm

5.2.3.1 Tribofilm formation and CF-filled PTFE tribology in moisture content less than 1 ppm

After sliding in the moisture content less than 1 ppm (Fig. 5. 15. (b)), a carbon-based tribofilm formed atop the PTFE composites worn surface with the surface area roughness of 0.3 μm (Fig. 5. 5–6). The C–C bond (sp2) observed in Fig. 5. 11 is attributed to the debris of CFs, and the presence of carboxyl groups (Figs. 5. 9. and 13.) indicated a tribochemical reaction between PTFE and water, albeit in small amounts. Such reaction has always been seen in the sliding of PTFE composites in a humid environment [7–10].

Meanwhile, it is considered that removal and transfer of PTFE and CFs debris formed the thick transfer film on the sliding tracks of stainless-steel surface with a surface area roughness of 0.3 μm (Fig. 5. 5.-6.). The sliding between the carbon-based films resulted in the lowest friction and wear with stable sliding behavior at this moisture content.

Moreover, the presence of pure iron on the deep side of the transfer film (Fig. 5. 13.) was partly due to the removal of the metal oxide film on the disk surface, which has been demonstrated to decrease significantly in such environments [37], and partly due to the reduction reaction of metal oxides. Furthermore, as demonstrated by Onodera et al. [34,35], a tribochemical reaction between the PTFE and metal oxides may occur at this interface. One of the reaction products was the C-C bond of the chain scission of the PTFE backbone. Kavan et al. reported carbynoid species as electrochemical products of PTFE and alkali metal amalgams [38]. Similar species are found in the carbon-based transfer film. In addition, the pure iron particles found on the deep side of the transfer film are considered to catalyze the formation of the graphitic structure of the carbon-based transfer film, as reported in previous studies [39,40], in which the iron particles function as a carbon nanotube reactor.

5.2.3.2 Tribofilm formation and CF-filled PTFE tribology in moisture content of approximately 20 ppm

For the surfaces of the sliding couple which slid in a moisture content of approximately 20 ppm (Fig. 5. 15. (c)), the tribofilms on the surface of the PTFE composite specimens became discontinuous and rough, whereas the carbon fiber fillers protruded from the surfaces to support the load (Fig. 5. 2. and 5.). Meanwhile, thinner but smoother transfer films formed on top of the disk surfaces owing to the polishing effect of the protruded carbon fibers (Fig. 4 and 6). Direct contact between the PTFE resin and passivated layer of metal oxides resulted in high friction and wear.

As illustrated in Fig. 5. 13, the PTFE and carboxyl groups were identified, and the iron fluorides gradually increased on the surface of the transfer film. Kurahashi et al. [41] demonstrated the retardation effects of carboxyl groups on the formation of carbon-based films; a similar mechanism is considered to cause a large decrease in the carbon-based

transfer film. The adsorption of water vapor, as investigated by Andersson et al. [42], is suggested to attenuate the strong covalent bond interactions between carbon atoms on DLC films, thus promoting the detachment of carbon during the sliding of the DLC film. Such effects of carboxyl groups and water were thought to not only accelerate the reduction in carbon-based film formation but also reduce the filler-resin bonding, as reported by Kalantar et al. of PTFE composites [43]. In addition, the amount of metal oxides increased, corresponding to the reaction between the metal and water on the deeper side of the transfer film (Fig. 5. 13).

Similarly, the Raman and IR spectra revealed a decrease in graphite in the tribofilms of both carbon-based films (Fig. 5. 7. and 9.). Since the electronegativity of oxygen molecule is strong, the chemical generated iron oxides surface was thought to hold together with graphitic wear debris through the delocalized π electrons by van der Waals forces, thus exhibited a higher ordered graphitic structure in the formed carbon-based transfer films (Fig. 5. 14.).

5.2.3.3 Tribofilm formation and CF-filled PTFE tribology in moisture content of approximately 40 ppm

When the moisture content of the sliding environment was approximately 40 ppm, as depicted in Fig. 5. 15. (d), the PTFE composite surfaces were fully covered by a smooth carbon-based tribofilm (Fig. 5. 3., 5., and 7.), whereas the transfer film formed on the disk surfaces exhibited a higher-order graphitic structure (Fig. 5. 8.). Sliding between these carbon-based films resulted in a decrease in friction.

Furthermore, hydrated fluoride products from the water-PTFE reaction were suggested to react with metal oxides and induce an increase in metal fluorides in the transfer film. The passivated layers of iron fluorides formed in the transfer film resulted in the presence of pure iron on the deeper side of the transfer film (Fig. 5. 13.). In addition, the IR spectra illustrate the presence of graphite in the tribofilm (Fig. 5. 9.). Moreover, iron fluorides are thought to hold stronger van der Waals forces with the delocalized electrons of graphitic debris because of the strong electronegativity of fluorine molecules. This is considered to give rise to the formation of a carbon-based transfer film with a higher-order graphitic

structure.

However, according to previous studies [18,19] and the Raman peak resolution results (Fig. 5. 8.), the hardness and strength of the carbon-based transfer film increased with increasing moisture content, whereas those of the tribofilm formed on the PTFE composite surfaces decreased when the moisture content exceeded 20 ppm. Based on the principle of Khruschov [44], these changes in the hardness of thinner carbon-based films could contribute to a high wear rate at this moisture content level. Moreover, the reduction in the hardness of the tribofilms was attributed to the permeation of water molecules in both the PTFE composites and tribofilms; such plasticization of PTFE under water lubrication has also been observed in previous studies [45,46]. This plasticization promoted the wear of the PTFE composites and was thought to give rise to the exposure of fresh CFs and the newly formed tribofilm (Fig. 5. 3.). In addition, it was suggested that sliding between hard-carbon-based tribofilms contributed to a decrease in friction when the moisture content exceeded 20 ppm.

5.2.3.4 Linking applied trace moisture contents with CF-filled PTFE friction and wear

Therefore, the direct effects of moisture content in this sliding process are summarized as follows: (1) Increased moisture content changed the reactions between PTFE and metal to reactions between PTFE and water, metal and water. (2) Water molecules not only permeated both carbon-based tribofilms and PTFE composites also accelerated the detachment of carbon.

5.3 Conclusion

Tribological characteristics of CF-filled PTFE were sensitive to the trace moisture content in high-purity hydrogen gas environment, the lowest friction and wear coupled with the most stable behavior were observed at moisture content less than 1 ppm.

Carbon films formed on sliding counterface varied in structure and amount as disk surface chemical composition changes, resulting in different friction and wear behaviors. This changes of tribological behaviors are summarized as follows:

1. when the moisture content of the sliding environment was less than 1 ppm, both surfaces of wear couple were covered by thick carbon-based tribofilms, sliding contact between those films led to the low and stable friction.
2. As moisture content increased, tribofilms became discontinued and got thinner while carbon fiber fillers protruded from the surfaces to support load, direct contact between PTFE and steel increased friction and wear.
3. After moisture content exceeded 20 ppm, worn surfaces were fully covered again by thinner but smoother carbon-based tribofilms with highly ordered graphitic structure, contact between these films resulted in the decrease of friction.

6. The tribological performance of CF-filled PTFE in hydrogen under high contact pressure

6.1 Introduction

PTFE, with many advantages over other traditional materials [100], has been proven of considerable benefit in the reciprocating compressor systems [4]. Maximum pressure differential across the piston for single-acting cylinder is one of the important pressure considerations in the case of piston ring seals. For non-lubricated service, conventional PTFE composites seals are available for pressures up to 10 MPa to 18 MPa [4]. On the contrary, the seal elements in oil-free reciprocating hydrogen gas compressors in the hydrogen refueling station are operated with contact pressure of 1 MPa [6]. For higher efficiency of the hydrogen gas compressor, tribological behavior of sealing materials under higher contact pressure should be evaluated.

As stated in Chapter 2, various factors have been reported to influence the friction and wear of polymer composites, among which the contact pressure or load and the sliding speed are the most frequent ones since the PV factors related not only to the wear rate but also to the temperature rise at the sliding interfaces [125].

However, the friction and wear mechanism associated with contact pressure of CF-filled PTFE in hydrogen gas environment is not clear.

The first aim of this chapter is to investigate the effects of contact pressure on the tribological characteristics of CF-filled PTFE in a high-purity hydrogen environment. Secondly, from the work of Chapter 4 and 5, trace moisture is supposed to affect the formation of carbon-based tribofilm under high contact pressure condition in hydrogen gas.

In this chapter, a series of pin-on-disk sliding tests were conducted with average contact pressure of 7 MPa in hydrogen. Friction and wear behavior under different contact pressure and those under 7 MPa contact pressure with different initial moisture content were analyzed. After the sliding tests, both surfaces of the wear couple were analyzed to understand the physical and chemical phenomena occurring at the sliding interface.

6.2 Results and discussion

6.2.1 Effect of contact pressure on tribology of CF-filled PTFE

The variations in the friction coefficient and moisture content with the sliding distance are shown in Fig. 6. 1. (a). Comparing to the low friction coefficient gained under low contact pressure, those under high contact pressure represents unstable friction behaviors. The friction characteristics under high contact pressure seems sensitive to the moisture content less than 1 ppm. Moreover, sliding tests with similar initial moisture contact (about 0.23 ppm) under different contact pressure showed relatively low friction coefficient.

With respect to the specific wear rates calculated under different contact pressure conditions, similar tendency to that of friction are observed. Under the contact pressure of 7 MPa, sliding test with average moisture content of 0.22 ppm revealed fairly low wear rate at the magnitude of 10^{-8} whilst those with average moisture content of 1.1 ppm exhibited high wear rate about $5x10^{-7}$ mm^3/Nm.

From these results, initial moisture content was thought to affect the friction and wear of CF-filled PTFE under different contact pressure.

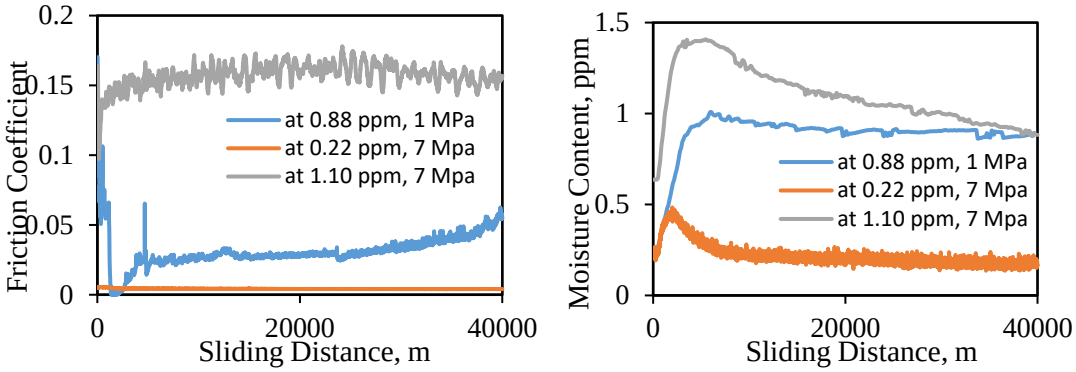

Fig. 6. 1. (a) Variations of friction coefficient and moisture content with sliding distance under different contact pressure

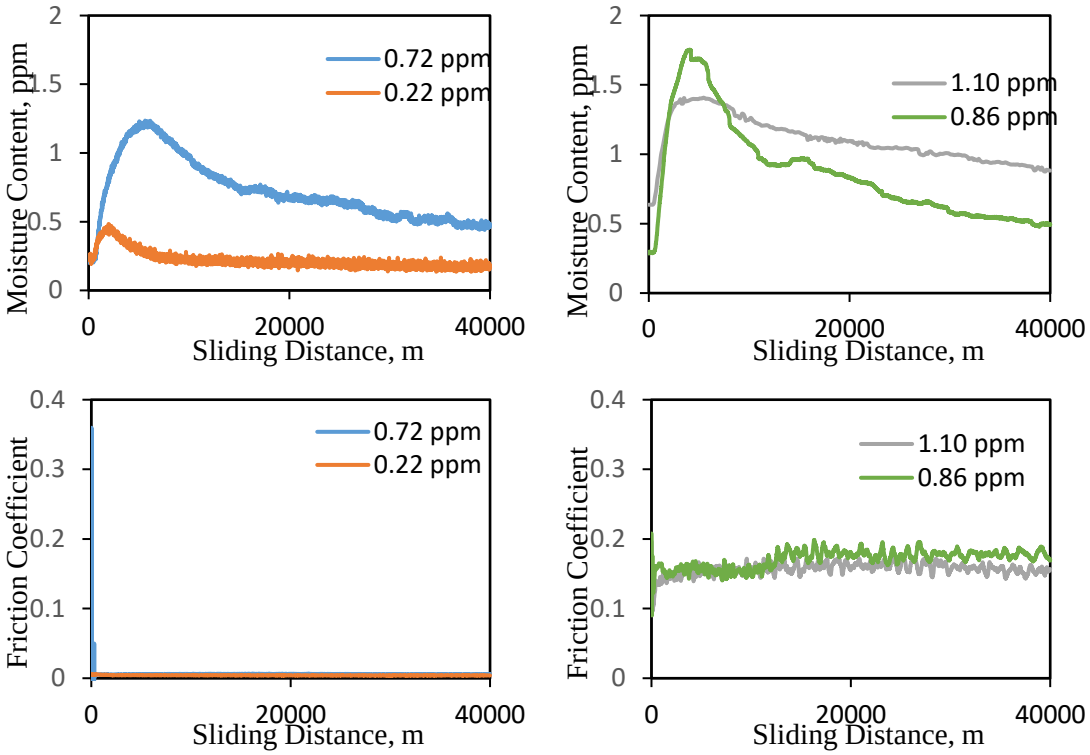

Fig. 6. 1. (b) Variations of friction coefficient and moisture content with sliding distance in high pressure contact

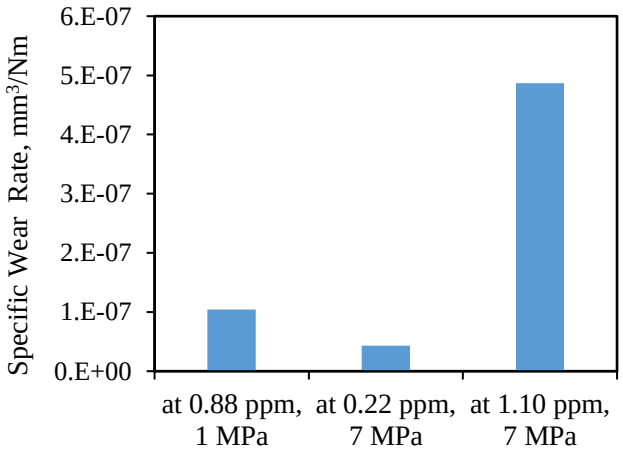

Fig. 6. 2. (a) Specific wear rates under different contact pressure

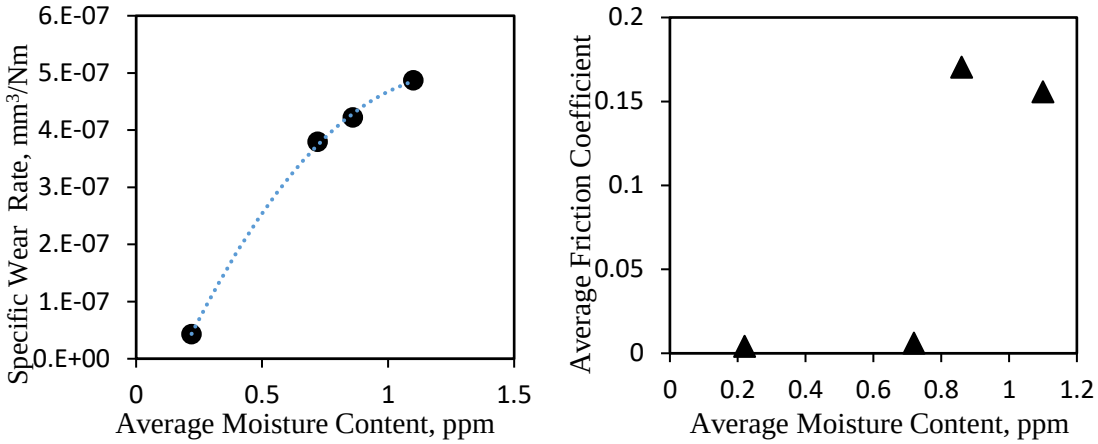

Fig. 6. 2. (b) Plots of specific wear rates and average friction coefficient against average moisture content

6.2.2 Effect of initial moisture content on tribology of CF-filled PTFE under high contact pressure

The variations in the friction coefficient and moisture content with the sliding distance are shown in Fig. 6. 1. (b). The friction coefficients obtained at every moisture content level corresponded well with each other, and the experimental data were considered highly reliable. In addition, from the variations in moisture content with sliding distance shown above, transition of initial moisture content at 0.25 ppm induced the friction coefficient in high pressure contact in hydrogen from low to high. Moreover, the friction coefficient remained approximately constant after the first sliding distance of 500 m, which may be the running-in stage of the CF-filled PTFE in high pressure contact in hydrogen.

Plots of the specific wear rates and average friction coefficient against the average moisture content are shown in Fig. 6. 2. (b). (left) and (right), respectively. The average value of friction coefficient was calculated during the last 100 m of the sliding test. According to the obtained results, the specific wear rates of the PTFE composites specimens increased as the average moisture content increase. Regarding the average friction coefficient, a similar transition at the average moisture content of approximately 0.8 was observed. The average friction coefficient shifted from 0.005 to 0.15 after average

moisture content exceeded approximately 0.8 ppm.

6.2.3. Characterization of the tribofilm and transfer film

6.2.3.1. Morphology of worn surfaces

Representative optical and corresponding 3D images of worn surfaces of the PTFE composites and stainless steel are shown in Fig. 6. 3. The colors in these images represent the height of each component. Surfaces of the polymer composites with initial moisture content less than 0.25 ppm (Fig. 6. 3. (a)) were covered by white tribofilm with an area surface roughness of 0.76 μm. In contrast, hardly white tribofilm can be seen atop the surfaces with initial moisture content over 0.25 ppm (Fig. 6. 3. (b)), whose area roughness is 2.84 μm, carbon fiber fillers protruded from the surfaces and dark PTFE resin exposed as well.

For the sliding tracks formed on the surfaces of the stainless steel specimens, characteristic brown (Fig. 6. 3. (c), marker (1)), bluish (Fig. 6. 3. (c), marker (2)) and purple (Fig. 6. 3. (d), marker (3)) patches were distributed along the sliding direction on the disk surfaces as transfer films. The brown and bluish patches dispersed the whole surfaces of disk specimens while those purple ones only existed in the transfer films formed at initial moisture content higher than 0.25 ppm.

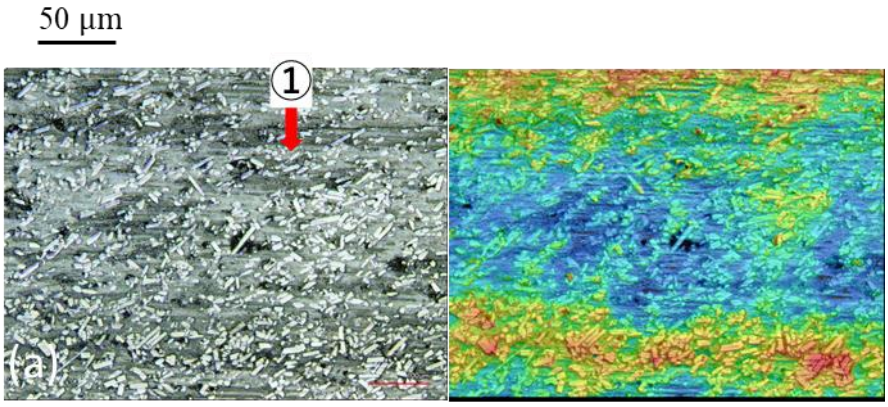

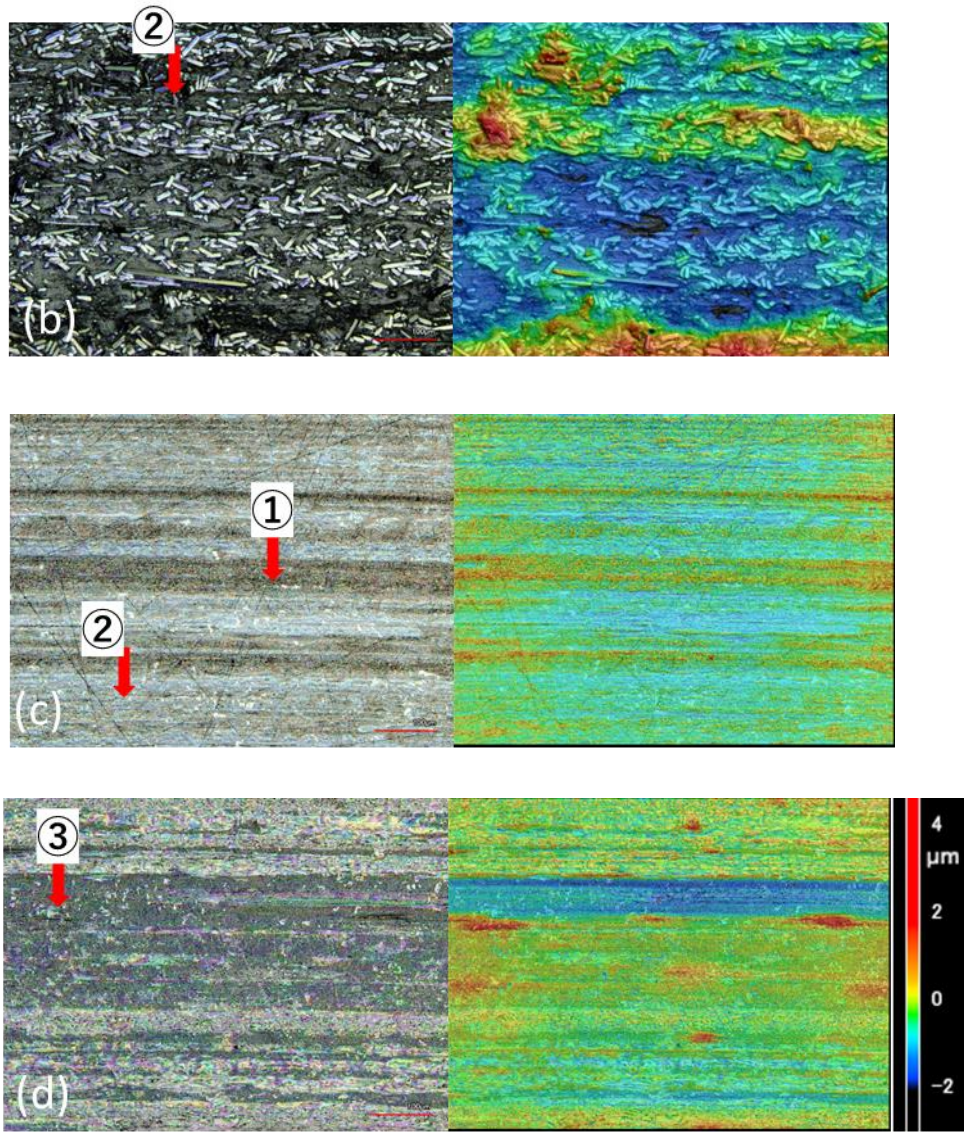

Fig. 6. 3. Optical and 3D images of worn surfaces of sliding couple with different initial moisture content level in high pressure contact: (a) pin specimen at initial moisture content less than 0.25 ppm; (b) pin specimen at initial moisture content larger than 0.25 ppm; (c) disk specimen at initial moisture content less than 0.25 ppm; (d) disk specimen at initial moisture content larger than 0.25 ppm

6.2.3.2. Microstructure and surface chemistry analysis

A G band (near 1580 cm^{-1}) corresponding to the graphite structure (sp^2 bond) and a D band (near 1350 $cm^{-1)}$ corresponding to the disordered graphitic structure were observed in the Raman spectra acquired from white tribofilms on the pin specimens (Fig. 6. 4.). Although seen as dark PTFE resins in the optical images of pin specimens (Fig. 6. 3. (b)), the Raman spectra from these surfaces also exhibited carbon spectra. Similarly, typical G and D bands are observed in all brown, bluish and purple patches formed on the disk surfaces, indicating the presence of carbon. However, the carbon intensity obtained from the purple patches were significantly lower than those from brown and bluish patches. Since the purple patches were higher than others (Fig. 6. 3. (d)), the purple patches were considered contained carbon debris and other compounds. These Raman spectra revealed the formation of a carbon-based film on both worn surfaces of the sliding couple.

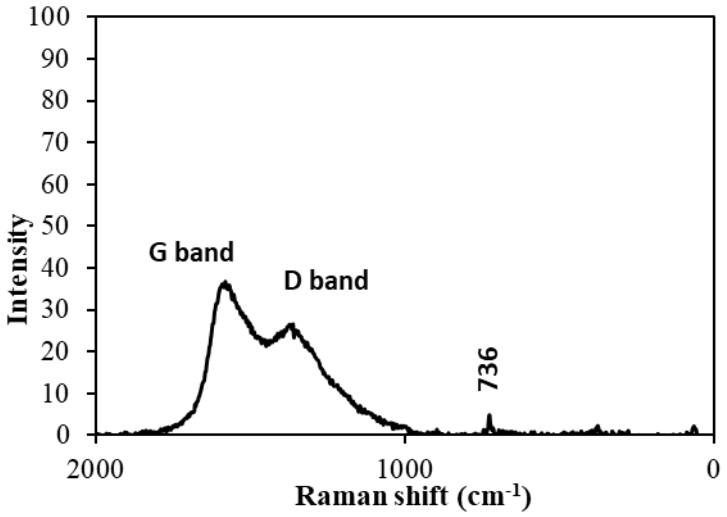

Fig. 6. 4. Representative Raman spectra obtained from worn surfaces of PTFE composites specimens, multiple peak-fit for D and G bands in the spectra obtained from tribofilm formed in hydrogen

All the XPS spectra were obtained three days after the sliding tests from the transfer films formed on the disk specimen surfaces. All specimens were stored in desiccator after the sliding tests. Spectra in the fluorine (F 1s), carbon (C 1s), oxygen (O 1s), iron (Fe $2p_{3/2}$), and chromium (Cr $2p_{3/2}$) regions were obtained from the brown and purple patches. The average atomic ratios of these five elements were calculated, and the correlation to the moisture content at a depth of 0 to 46 nm are shown in Fig. 6. 5. Most of all, the atomic ratio of carbon from transfer film at initial moisture content less than 0.25 ppm is nearly

twice than that at initial moisture content level higher than 0.25 ppm. In addition, ratios of metals increased at the deeper sides of transfer films with both moisture content levels, and the ratios acquired from higher moisture content level is higher than that from the lower level one. Regarding the ratios of fluorides, similar tendency was observed to that of metals and the ratios in higher moisture content level are higher than that in the lower one.

Typical spectra obtained from the disk surfaces are shown in Fig. 6. 6. For Fe $2p_{3/2}$, peaks at 706.8±0.2 eV, 711.3±0.1 eV, 714.2±0.8 eV, 710.9±0.1 eV, and 714.9 eV were identified as pure iron, iron (II) fluoride, iron (III) fluoride, iron (III) oxide and ferrous carbonate [30–33]. The pure iron as well as the pure chromium were only observed at the depth of 46 nm in the transfer film formed on the surface of disk specimens at moisture content level less than 0.25 ppm. Peak position at higher moisture content level shifted to the high bonding energy sides near 581 eV in Cr $2p_{3/2}$ indicated the increase in chromium (IV) oxides and hydroxides [135]. For F 1s, peaks at 684–685.5, 685.7, and 689.2±0.4 eV were subscribed to iron fluorides, C–F bonds from graphite fluorides, and PTFE [26,28–30]. Only on the surface of transfer films in high moisture content level was the PTFE debris existed. With respect to the C 1s spectra, peaks at 284.3±0.1 eV, 285.2±0.1 eV, 286.4±0.4 eV, 288.6±0.6 eV, 287.3 eV and 292.5 eV were related to the sp2 and sp3 hybrids forms of carbon, C–O bonds, C=O bonds from ester and C–F bonds from graphite fluorides and PTFE [26–29]. The carbon spectra of C-F bonds matched with that from fluorine. Similarly, the presence of C-O bonds was also only observed on the surface of transfer film at high moisture content level. For O 1s, peaks at 529.7±0.3 eV, 531.3–532 eV, and 533 eV corresponded to Iron (III) oxide (metal oxides), C=O bonds from metal carbonates and organic compounds or O–H bonds from hydroxyl groups, organic C–O bonds [28,30]. Spectra of organic C-O bonds corresponded well with that from carbon.

Moreover, SEM-EDX analyses were carried out to the discontinued parts of purple patches (Fig. 6. 7 (b)) with an initial moisture content higher than 0.25 ppm and that of carbon films formed in the environment where initial moisture content is less than 0.25 ppm (Fig. 6. 7. (a)). As shown in Fig. 6. 7. (a), at the circle parts where the carbon films were discontinued and Raman spectra of metal oxides were identified, the existence of chromium was observed. This result corresponded to the XPS spectra shown in Fig. 6. 6.

And carbon did not adhere to the chromium surface. On the other hand, for carbon films that were not covered by purple patches in Fig. 6. 7. (b), chromium oxides were found.

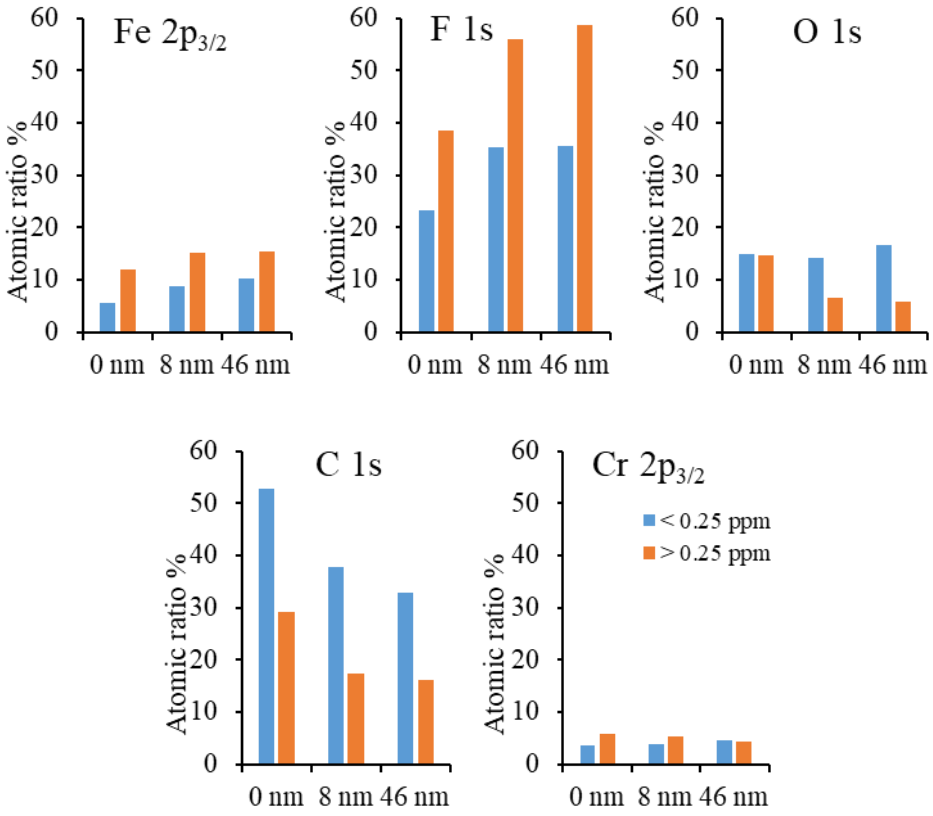

Fig. 6. 5. Correlation between atomic ratios of transfer films formed atop disk surfaces and moisture content in high pressure contact

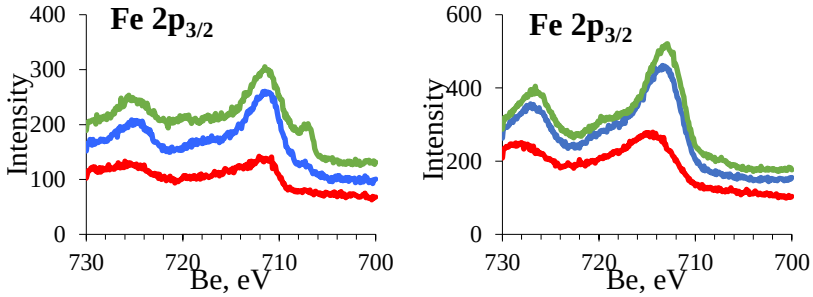

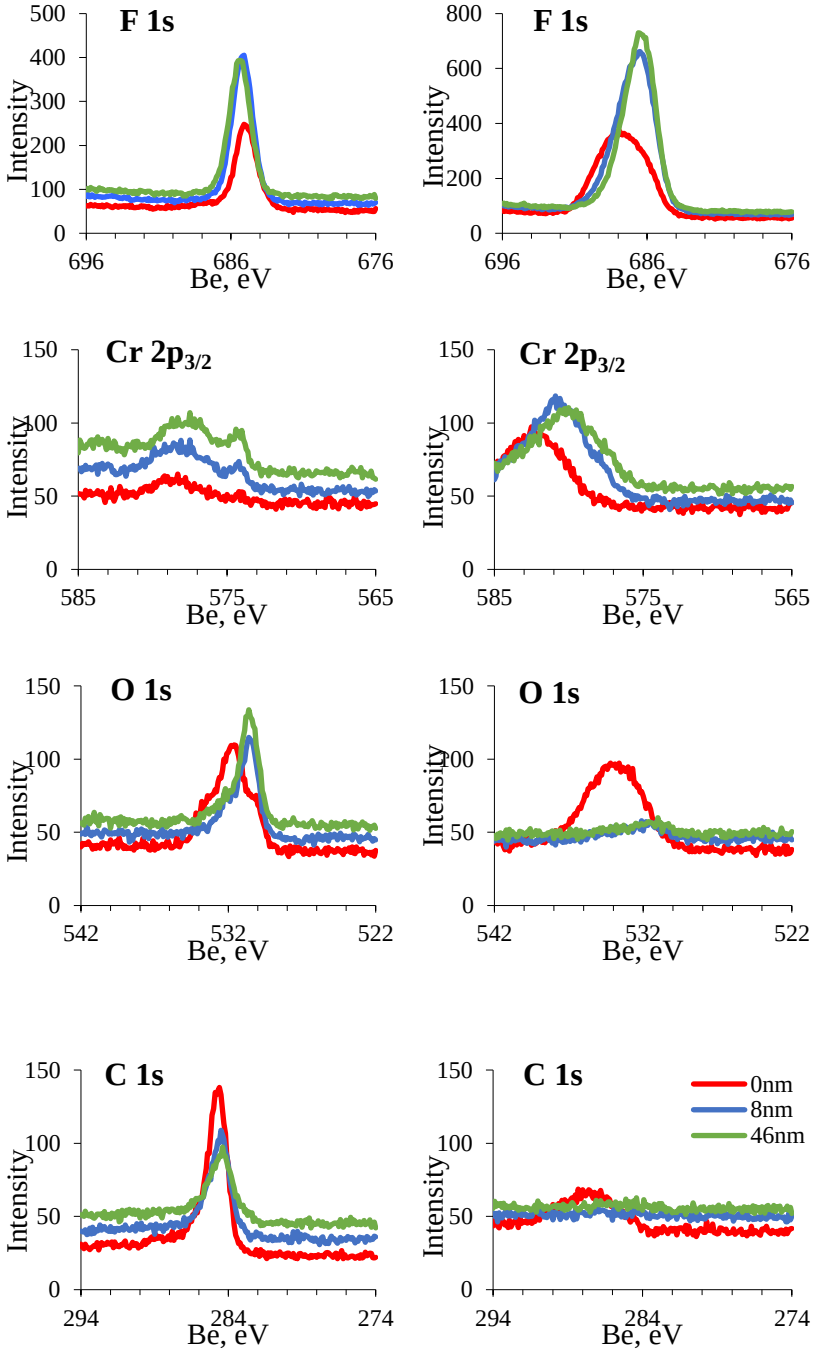

Fig. 6. 6. XPS spectra at 5 element regions from disk surfaces with different initial moisture content in high pressure contact (left: at initial moisture content less than 0.25 ppm; right: at initial moisture content larger than 0.25 ppm)

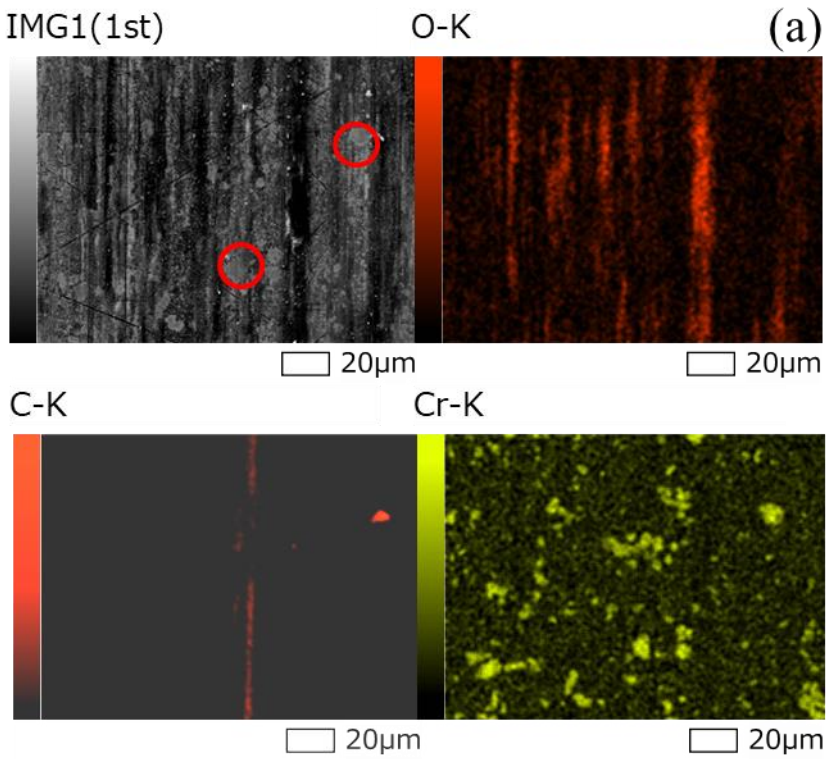
IMG1(1st)
O-K
(a)
20μm
20μm
C-K
Cr-K
20μm
20μm

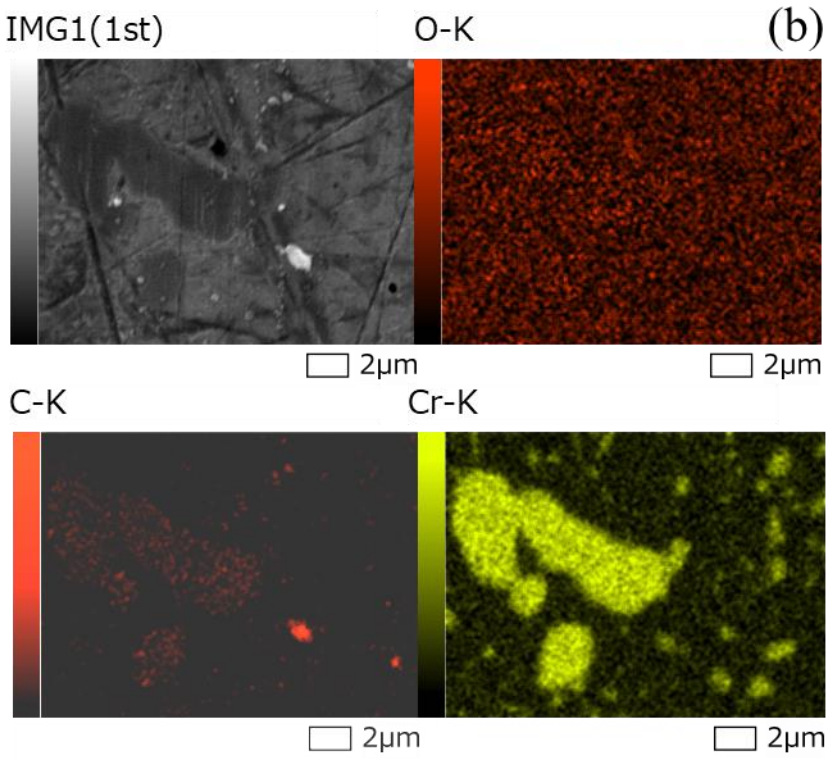
IMG1(1st)
O-K
(b)
2μm
2μm
C-K
Cr-K
2μm
2μm

Fig. 6. 7. SEM-EDX images of transfer films atop stainless steel specimens ((a) discontinued parts of brown patches with initial moisture content less than 0.25 ppm, (b) discontinued parts of purple patches with initial moisture content over 0.25 ppm.)

6.2.4 Tribofilm formation and their role on friction and wear mechanisms

All the results of the present experiments indicate that the initial moisture content in hydrogen under high contact pressure is significant for the formation of carbon-based films, friction, and wear. Varieties in the chemical compositions of formed transfer films were thought to give rise to the characteristic friction and wear behaviors of the PAN-based CF-filled PTFE composites.

6.2.4.1. Tribofilm formation at moisture content less than 0.25 ppm

When sliding at a moisture content level lower than 0.25 ppm, carbon-based tribofilm and transfer film formed atop the worn surfaces of sliding couple. It is considered that the fracture and transfer of PTFE and CFs debris within the interfaces in high pressure contact resulted in these carbon films. The strong carbon-carbon interactions within these films were thought eliminated by hydrogen termination, as suggested by Erdemir [124]. Transfer wear processes was suggested as the dominant wear mechanism and sliding between these carbon-based films resulted in the lowest friction and most stable wear behavior.

The presence of pure metals at the depth of 46 nm of the transfer film (Fig. 6. 6. left) is thought partly due to the removal of passive layers which consisted of metal oxides or metal hydroxides [36] on the surfaces of disk specimens and has been demonstrated to decrease significantly in such environments [37], and partly due to the reduction reaction between metal oxides and hydrogen. These pure transition metals are considered to catalyze the formation of the carbon-based transfer film, as reported in previous studies [39,40], in which the iron particles function as a carbon nanotube reactor. Moreover, metal

fluorides and part of the C-C bonds found in the transfer films are also regarded as the reaction products from the tribochemcial reaction between PTFE and metal oxides which has been demonstrated by Onodera et al. [34,35].

6.2.4.2. Contact temperature during sliding

Temperature was measured 5 mm away from the contact surface during the whole sliding test. The surface temperature is over 120 ℃ at high moisture content level whilst that is lower than 50 ℃ at the moisture content less than 0.25 ppm.

The frequency of a collision of gaseous molecules against solid surface is known to be given by Hertz-Knudsen equation as follow [15],

$$F = p \cdot (2\pi \cdot m \cdot k \cdot T)^{-0.5}$$

F, p, m, k, T are the frequency of collision per second per square meter, gaseous pressure, weight of the molecule, Boltzmann's constant and temperature, respectively. In this work, the molecule is water and the critical moisture content under 1 MPa is 1 ppm and while that is about 0.25 ppm under 7 MPa. Partial pressures are calculated as 0.1 Pa and 0.025 Pa. For sliding test under 1 MPa, T is about 333 K. For sliding test under 7 MPa, T is about 393 K. Since the effect of differences in temperature is too small comparing to that of gaseous pressure, the frequency of collision is mainly dependent on moisture content in this work. The frequency of collision per second per square meter is about 3-4 times higher at high moisture content than that at low moisture content. Sliding frequency on the disk in this work is 15.9 Hz. With the increase of contact pressure, the real contact area increased at the same time, which would result in the larger frequency of contact between atoms on the sliding surface and water molecules. The increase in contact pressure was thought counteract the decrease in frequency of collision induced by lower moisture content.

Moreover, Robertson demonstrated carbon ions with lower energy will stick to the surface and remain in the lowest energy state, which means lower energy density results in more sp^2 structure and more sp^3 if the density is high [156]. Part of kinetic energies that were induced by the collision and friction force may dissipate in the transfer film and tribofilm formation.

6.2.4.3. Tribofilm formation at moisture content level higher than 0.25

ppm

For the surfaces of sliding couple which slid in a moisture content over 0.24 ppm in high pressure contact, transfer film formed on the disk surfaces contains carbon layer less than 2 nm and tribofilm on the pin surface could hardly be observed. Carbon fiber fillers that protruded from the surfaces to support load resulted in the rough surface of PTFE composites, whose area surface roughness is 2.84 μm. Moreover, the major part of the formed transfer film is metal fluorides and only on the surface of this film can PTFE debris and organic C-O groups be found. In addition, high friction heat was observed after the running-in stage of sliding, the rise in contact surface temperature in turn deteriorate the mechanical properties of PTFE composites. Direct contact between PTFE resin and metal fluorides films in company with plastic deformation and fracture of PTFE at high temperature resulted in the high friction and wear.

Since the running-in stage of the sliding test is approximately 500 m, metal fluorides layer was suggested formed immediately after the running-in stage. Real contact area as well as the contact asperities is indicated increased in high pressure contact, and the motions of water molecules absorbed in the sliding interfaces were accelerated. As demonstrated by Andersson et al. [42], water molecules can attenuate the strong covalent bond interactions between carbon atoms in carbon films, thus promoting the detachment of carbon film during the sliding. On the other hand, chromium (IV) oxides formed by oxidation reaction was thought giving rise to the formation of chromium carbide on the surfaces where metal fluorides were discontinued [136-137].

Moreover, the friction heat generated from this period of sliding may in turn foster the tribochemical reaction between PTFE and metal oxides which has been stated above. Thanks to the strongest electronegativity of fluorine molecules in metal fluorides, the tribochemically generated metal fluorides is considered to hold together with the thin carbon film formed during running-in stage on the surface of disk specimen through the delocalized π electrons by van der Waals forces. The sliding between PTFE composites and metal fluorides in turn generated large amount of friction heat, give rise to the abruptly temperature rise after the running-in stage. At high temperature, the thermal stress originated from the different coefficient of thermal expansion of the matrix and fiber during the cooling down of the thermoplastic was relaxed. Therefore, failure of

PTFE composites changed from fiber kinking to microbuckling [70]. The cycle of friction heat, PTFE plastic deformation and fracture and transfer wear process is considered the main wear mechanism of CF-filled PTFE in high pressure contact at high moisture content level in hydrogen.

6.3 Conclusion

Tribological characteristics of CF-filled PTFE were sensitive to the initial moisture content in hydrogen under high contact pressure, ultralow friction and wear coupled with the most stable behavior were observed at initial moisture content less than 0.25 ppm.
Transfer films formed on sliding counterface varied in chemical composition as the initial moisture content changes, resulting in different friction and wear behaviors. This changes of tribological behaviors are summarized as follows:
1. Thicker carbon films formed under higher contact pressure resulted in ultralow friction and wear of CF-filled PTFE in hydrogen.
2. when the initial moisture content of the sliding environment was less than 0.25 ppm, both surfaces of wear couple were covered by carbon-based tribofilms, sliding contact between those films led to the ultralow and stable friction.
3. After initial moisture content exceeded 0.25 ppm, transfer films on the surface of disk specimen contained mostly of metal fluorides whilst carbon fiber fillers protruded from the PTFE composites surface to support load, contact between these films in company with high contact temperature resulted in the increase of friction and wear.

7. Conclusions

The demand for high performance polymers such as PTFE and its composites that possesses excellent self-lubricating ability, good mechanical properties and chemically inert under extreme conditions like high contact pressure, trace moisture content are increasingly for tribological application in hydrogen.

In the introduction of this thesis, difficulties related to the use of polymer as sealing materials in the oil-free hydrogen gas compressors in hydrogen energy society have been identified. The research presented in this thesis predominantly focused on the following topics:

- effect of hydrogen gas on the formation of carbon-based tribofilm of CF-filled PTFE at room temperature and standard atmosphere.
- Effect of air contaminant like water on the carbon-based tribofilm formed in hydrogen.
- effect of trace moisture content on the tribological behavior of CF-filled PTFE in hydrogen gas.
- effect of contact pressure on the friction and wear of CF-filled PTFE in hydrogen gas.
- effect of initial moisture content on the tribofilm formation of CF-filled PTFE in hydrogen under high contact pressure
- tribofilm formation factors in hydrogen

7.1 Effects of hydrogen on the tribological performance of CF-filled PTFE

Tribological characteristics of CF-filled PTFE were affected by gaseous atmosphere, the lowest friction and wear coupled with the most stable behavior were observed in hydrogen gas. The strong carbon-carbon interactions within the carbon-based film can be eliminated by hydrogen termination. Reduction reaction between metal oxides and

hydrogen. These effects of hydrogen giving way to the transfer films formed on stainless steel surfaces varied in chemical composition as gaseous atmosphere changes, resulting in different friction and wear behaviors. The air exposure process introduced contaminants such as water and oxygen to the carbon-based tribofilm formed during the running-in stage, resulting in the discontinuous and thinner carbon films and giving rise to the increased friction and wear after the air exposure process in hydrogen environment. Transfer wear processes is the dominant wear mechanism.

7.2 Effects of trace moisture content on the tribological performance of CF-filled PTFE

Carbon films formed on sliding counterface varied in structure and amount as disk surface chemical composition changes, resulting in different friction and wear behaviors. This changes of tribological behaviors are summarized as follows:

1. when the moisture content of the sliding environment was less than 1 ppm, both surfaces of wear couple were covered by thick carbon-based tribofilms, sliding contact between those films led to the low and stable friction.
2. As moisture content increased, tribofilms became discontinued and got thinner while carbon fiber fillers protruded from the surfaces to support load, direct contact between PTFE and steel increased friction and wear.
3. After moisture content exceeded 20 ppm, worn surfaces were fully covered again by thinner but smoother carbon-based tribofilms with highly ordered graphitic structure, contact between these films resulted in the decrease of friction.

7.3 Effects of contact pressure on the tribological performance of CF-filled PTFE

Thicker carbon films formed under higher contact pressure resulted in ultralow friction and wear of CF-filled PTFE in hydrogen. Transfer films formed on sliding counterface varied in chemical composition as the initial moisture content changes, resulting in different friction and wear behaviors. Especially, when the initial moisture content of the

sliding environment was less than 0.25 ppm, both surfaces of wear couple were covered by carbon-based tribofilms, sliding contact between those films led to the ultralow and stable friction. The moisture content and contact pressure counteracts with each other to affect the carbon film formation of CF-filled PTFE in hydrogen gas environment.

7.4 Tribofilm formation factors

One of the main focuses of this work was to understand the relationship between operating conditions, gaseous environment and the formation of tribofilm and transfer film. These factors are usually seen in the tribochemical wear mechanism stated in Section 2 as well. All the specimens of sliding couple in this thesis showed the formation of transfer film. The chemical compositions of these transfer films were analyzed using Raman, XPS, FTIR and SEM-EDX. The differences in load, moisture content and gaseous atmosphere indeed affected the formation of transfer film.

- The dominant wear mechanism in hydrogen is the transfer wear process.
- The increase in contact pressure resulted in the shortened running-in stage, contacts of asperities at a higher frequency and the acceleration of molecule dynamic between the contact interface. The latter induced the higher friction heat and more tribochemical reaction. These in turn influence the formation of transfer film.
- The moisture content, acted as the critical factor for the amount and structure of formed carbon-based film in low pressure contact. When the contact pressure increased, moisture molecule then shifted the formation of carbon-based transfer film to the metal fluorides transfer film with a small change in amount.

List of References

[1] Staffell I, Scamman D, Velazquez Abad A, Balcombe P, Dodds PE, Ekins P, et al. The role of hydrogen and fuel cells in the global energy system. Energy Environ Sci 2019;12:463–91. https://doi.org/10.1039/c8ee01157e.

[2] Sugimura J. Overview of tribology researches for high-pressure hydrogen systems. Tribol SchmierTech 2019;66:24.

[3] Tanaka K, Uchiyama Y, Toyooka S. The mechanism of wear of polytetrafluoroethylene. Wear 1973;23:153–72. https://doi.org/10.1016/0043-1648(73)90081-1.

[4] PTFE Seals in Reciprocating Compressors: Manual of Material Selection, Design, and Operating Practices. American Society of Mechanical Engineers; 1975.

[5] Briscoe BJ, Lin Heng Yao, Stolarski TA. The friction and wear of poly(tetrafluoroethylene)-poly (etheretherketone) composites: An initial appraisal of the optimum composition. Wear 1986;108:357–74. https://doi.org/10.1016/0043-1648(86)90013-X.

[6] Sawae Y, Morita T, Takeda K, Onitsuka S, Kaneuti J, Yamaguchi T, et al. Friction and wear of PTFE composites with different filler in high purity hydrogen gas. Tribol Int 2021;157:106884. https://doi.org/10.1016/j.triboint.2021.106884.

[7] Campbell KL, Sidebottom MA, Atkinson CC, Babuska TF, Kolanovic CA, Boulden BJ, et al. Ultralow Wear PTFE-Based Polymer Composites—The Role of Water and Tribochemistry. Macromolecules 2019;52:5268–77. https://doi.org/10.1021/acs.macromol.9b00316.

[8] Krick BA, Ewin JJ, Blackman GS, Junk CP, Gregory Sawyer W. Environmental dependence of ultra-low wear behavior of polytetrafluoroethylene (PTFE) and alumina composites suggests tribochemical mechanisms. Tribol Int 2012;51:42–6. https://doi.org/10.1016/j.triboint.2012.02.015.

[9] Harris KL, Pitenis AA, Sawyer WG, Krick BA, Blackman GS, Kasprzak DJ, et al. PTFE Tribology and the Role of Mechanochemistry in the Development of Protective Surface Films. Macromolecules 2015;48:3739–45. https://doi.org/10.1021/acs.macromol.5b00452.

[10] Haidar DR, Alam KI, Burris DL. Tribological insensitivity of an ultralow-wear poly(etheretherketone)–polytetrafluoroethylene polymer blend to changes in environmental moisture. J Phys Chem C Nanomater Interfaces 2018;122:5518–24. https://doi.org/10.1021/acs.jpcc.7b12487.

[11] Lancaster JK. A review of the influence of environmental humidity and water on friction, lubrication and wear. Tribol Int 1990;23:371–89. https://doi.org/10.1016/0301-679X(90)90053-R.

[12] Schubert R. The Influence of a Gas Atmosphere and Its Moisture on Sliding Wear in PTFE Compositions. J Lubr Technol 1971;93:216–23. https://doi.org/10.1115/1.3451544.

[13] Fuchsluger JH, Taber RD. The Effect of Atmospheric Environment on the Wear Properties of Filled TFE Materials. J Lubr Technol 1971;93:423–9. https://doi.org/10.1115/1.3451611.

[14] McNicol A, Dowson D, Davies M. The effect of humidity and electrical fields upon the wear of high density polyethylene and polytetrafluoroethylene. Wear 1995;181–183:603–12. https://doi.org/10.1016/0043-1648(95)90176-0.

[15] Fukuda K, Sugimura J. Influences of Trace Water in a Hydrogen Environment on the Tribological Properties of Pure Iron. Tribology Online 2013;8:22–7. https://doi.org/10.2474/trol.8.22.

[16] Sadezky A, Muckenhuber H, Grothe H, Niessner R, Pöschl U. Raman microspectroscopy of soot and related carbonaceous materials: Spectral analysis and structural information. Carbon N Y 2005;43:1731–42. https://doi.org/10.1016/j.carbon.2005.02.018.

[17] Kaniyoor A, Ramaprabhu S. A Raman spectroscopic investigation of graphite oxide derived graphene. AIP Adv 2012;2:032183. https://doi.org/10.1063/1.4756995.

[18] Qian X, Wang X, Zhong J, Zhi J, Heng F, Zhang Y, et al. Effect of fiber microstructure studied by Raman spectroscopy upon the mechanical properties of carbon fibers. J Raman Spectrosc 2019;50:665–73. https://doi.org/10.1002/jrs.5569.

[19] Fayed SM, Chen D, Li S, Zhou Y, Wang H. Effect of Bias Voltage on Characteristics of Multilayer Si-DLC Film Coated on AA6061 Aluminum Alloy. J Mater Eng Perform 2021;30:743–59. https://doi.org/10.1007/s11665-020-05397-2.

[20] Bonelli B, Civalleri B, Fubini B, Ugliengo P, Areán CO, Garrone E. Experimental and Quantum Chemical Studies on the Adsorption of Carbon Dioxide on Alkali-Metal-Exchanged ZSM-5 Zeolites. J Phys Chem B 2000;104:10978–88. https://doi.org/10.1021/jp000555g.

[21] Obreja AC, Cristea D, Gavrila R, Schiopu V, Dinescu A, Danila M, et al. Isocyanate functionalized graphene/P3HT based nanocomposites. Appl Surf Sci 2013;276:458–67. https://doi.org/10.1016/j.apsusc.2013.03.117.

[22] Baykal A, Senel M, Unal B, Karaoğlu E, Sözeri H, Toprak MS. Acid Functionalized Multiwall Carbon Nanotube/Magnetite (MWCNT)-COOH/Fe3O4 Hybrid: Synthesis, Characterization and Conductivity Evaluation. J Inorg Organomet Polym Mater 2013;23:726–35. https://doi.org/10.1007/s10904-013-9839-4.

[23] Wang R, Xu G, He Y. Structure and properties of polytetrafluoroethylene (PTFE) fibers. E-Polymers 2017;17:215–20. https://doi.org/10.1515/epoly-2016-0059.

[24] Krick BA, Pitenis AA, Harris KL, Junk CP, Sawyer WG, Brown SC, et al. Ultralow wear fluoropolymer composites: Nanoscale functionality from microscale fillers. Tribol Int 2016;95:245–55. https://doi.org/10.1016/j.triboint.2015.10.002.

[25] Ţucureanu V, Matei A, Avram AM. FTIR Spectroscopy for Carbon Family Study. Crit Rev Anal Chem 2016;46:502–20. https://doi.org/10.1080/10408347.2016.1157013.

[26] Briggs D, Beamson G. High resolution XPS of organic polymers: The scienta ESCA300 database. Chichester, England: John Wiley & Sons; 1992.

[27] Díaz J, Paolicelli G, Ferrer S, Comin F. Separation of the sp3 and sp2 components in the C1s photoemission spectra of amorphous carbon films. Phys Rev B Condens Matter 1996;54:8064–9. https://doi.org/10.1103/physrevb.54.8064.

[28] Scientific TF. Table of Elements, X-ray photoelectron spectroscopy of atomic elements n.d. https://www.thermofisher.com/jp/ja/home/materials-science/learning-center/periodic-table.html.

[29] Palchan I, Crespin M, Estrade-Szwarckopf H, Rousseau B. Graphite fluorides: An XPS study of a new type of C-F bonding. Chem Phys Lett 1989;157:321–7. https://doi.org/10.1016/0009-2614(89)87255-0.

[30] John FM, William FS, Peter ES, Kenneth DB. Handbook of X-ray photoelectron

spectroscopy. Perkin-Elmer Corporation Physical n.d.

[31] Heuer JK, Stubbins JF. An XPS characterization of FeCO3 films from CO2 corrosion. Corros Sci 1999;41:1231–43. https://doi.org/10.1016/S0010-938X(98)00180-2.

[32] Kasrai M, Urch DS. Electronic structure of iron(II) and (III) fluorides using X-ray emission and X-ray photoelectron spectroscopies. J Chem Soc 1979;75:1522–31. https://doi.org/10.1039/F29797501522.

[33] Murata Y, Minami R, Takada S, Aoyanagi K, Tojo T, Inada R, et al. A fundamental study on carbon composites of FeF3·0.33H2O as open-framework cathode materials for calcium-ion batteries, Author(s); 2017. https://doi.org/10.1063/1.4974787.

[34] Onodera T, Kawasaki K, Nakakawaji T, Higuchi Y, Ozawa N, Kurihara K, et al. Chemical Reaction Mechanism of Polytetrafluoroethylene on Aluminum Surface under Friction Condition. J Phys Chem C 2014;118:5390–6. https://doi.org/10.1021/jp412461q.

[35] Onodera T, Kawasaki K, Nakakawaji T, Higuchi Y, Ozawa N, Kurihara K, et al. Effect of tribochemical reaction on transfer-film formation by poly(tetrafluoroethylene). J Phys Chem C Nanomater Interfaces 2014;118:11820–6. https://doi.org/10.1021/jp503331e.

[36] Shimizu S, Asai H, Shohei RYU, Shinichi ITO, Muto M. Native Passive Films Formed on 18Cr Stainless Steel Surfaces—A Factor of Corrosion Resistance and In-Situ Structural Change—. Surface Science 2017;38:559–64.

[37] Nakashima K, Yamaguchi A, Kurono Y, Sawae Y, Murakami T, Sugimura J. Effect of high-pressure hydrogen exposure on wear of polytetrafluoroethylene sliding against stainless steel. Proc Inst Mech Eng Pt J: J Eng Tribol 2010;224:285–92. https://doi.org/10.1243/13506501JET642.

[38] Heimann RB, Evsyukov SE, Kavan L. Carbyne and Carbynoid Structures. Springer Science & Business Media; 2012.

[39] Conroy D, Moisala A, Cardoso S, Windle A, Davidson J. Carbon nanotube reactor: Ferrocene decomposition, iron particle growth, nanotube aggregation and scale-up. Chem Eng Sci 2010;65:2965–77. https://doi.org/10.1016/j.ces.2010.01.019.

[40] Joselevich E, Dai H, Liu J, Hata K, H. Windle A. Carbon Nanotube Synthesis and Organization. In: Jorio A, Dresselhaus G, Dresselhaus MS, editors. Carbon

Nanotubes: Advanced Topics in the Synthesis, Structure, Properties and Applications, Berlin, Heidelberg: Springer Berlin Heidelberg; 2008, p. 101–65. https://doi.org/10.1007/978-3-540-72865-8_4.

[41] Kurahashi Y, Tanaka H, Terayama M, Sugimura J. Effects of Environmental Gas and Trace Water on the Friction of DLC Sliding with Metals. Micromachines (Basel) 2017;8. https://doi.org/10.3390/mi8070217.

[42] Andersson J, Erck RA, Erdemir A. Frictional behavior of diamondlike carbon films in vacuum and under varying water vapor pressure. Surf Coat Technol 2003;163–164:535–40. https://doi.org/10.1016/S0257-8972(02)00617-5.

[43] Kalantar J, Drzal LT. The bonding mechanism of aramid fibres to epoxy matrices. J Mater Sci 1990;25:4186–93. https://doi.org/10.1007/bf00581071.

[44] Khruschov MM. Principles of abrasive wear. Wear 1974;28:69–88. https://doi.org/10.1016/0043-1648(74)90102-1.

[45] Lancaster JK. Lubricated wear of polymers. In: Dowson D, editor. Mixed lubrication and lubricated wear, The University of Leeds; 1985, p. 213–23.

[46] Tanaka K. Friction and Wear of Semicrystalline Polymers Sliding Against Steel Under Water Lubrication. J Lubr Technol 1980;102:526–33. https://doi.org/10.1115/1.3251590.

[47] S. Zakaria, and B. J. Briscoe, “Why rubber explodes”, Chemtech, Vol.20, Aug, pp. 492–495 (1990).

[48] A. Stevenson, and G. Morgan, “Fracture of Elastomers by Gas Decompression”, Rubber Chemistry and Technology, Vol. 68, pp. 197 –211 (1995).

[49] B. J. Briscoe, T. Savvas, and C. T. Kelly, “Explosive Decompression Failure of Rubbers: A Review of the Origins of Pneumatic Stress Induced Rupture in Elastomers”, Rubber Chemistry and Technology, Vol. 67, pp. 384 – 416 (1994).

[50] Zapffe C. Discussion of metal arc welding of steels by S. A. Herres. Transactions, American Society for Metals1947;39:191±2.

[51] Kazinczy Fd. A theory of hydrogen embrittlement. Journal of the Iron and Steel Institute 1954;177:85±92.

[52] Petch NJ. Delayed fracture of metals under static load. Nature 1952;169:842±3.

[53] Petch NJ. Lowering of the fracture stress due to surface adsorption. Phil Mag

1956;1:331±5.

[54] Morlet JG, Johnson HH, Troiano AR. A new concept of hydrogen embrittlement in steel. Journal of the Iron and Steel Institute 1958;189:37±41.

[55] Troiano AR. The role of hydrogen and other interstitials in the mechanical behavior of metals. Trans ASM1960;52:54±80

[56] I.M. Robertson, The effect of hydrogen on dislocation dynamics, Engineering Fracture Mechanics 64 (1999) 649±673

[57] B.J. Briscoe, The tribology of composite materials: a preface, Chapter 1 in: K. Friedrich, editor. Advances in composite tribology, 1993 Elsevier Science Publishers B. V.

[58] B.J. Briscoe, Acta Metall. 24(5) (1990) 839.

[59] J.K. Lancaster, ed., Speciality Bearings, Special Issue, Tribol. Int. 15(5) (1982).

[60] J.K. Lancaster, in: Tribology in the 80's, NASA Conference Publication 2300 (NASA, Cleveland, OH, 1984).

[61] J.K. Lancaster, Tribol. Int. 23 (1990) 371.

[62] G. Zhang and A. K. Schlarb. Correlation of the tribological behaviors with the mechanical properties of poly-ether-ether-ketones (PEEKs) with different molecular weights and their fiber filled composites. Wear, 266(1-2):337–344, 2009.

[63] W. M. Garrison, Khruschov's rule and the abrasive wear resistance of multiphase solids, Wear, 32 (1982) 213-220.

[64] H. Voss, K. Friedrich, On the wear behavior of short-fiber-reinforced PEEK composites, Wear, 116 (1987) 1-18.

[65] John. C. Anderson, The wear and friction of commercial polymers and composites, Chapter 10 in: K. Friedrich editor, Friction and wear of polymer composites, 1986 Elsevier Science Publishers B. V.

[66] D. Dowson, J.R. Atkinson and K. Brown, in L.H. Lee (Ed.), Advances in Polymer Friction and Wear, Vol. 5B, Plenum Press, London, 1974, p. 533.

[67] J.K. Lancaster, Tribol. Int., 12 (1979) 65.

[68] J. Hanchi, N.S. Eiss, Tribological behavior of polyether-etherketone, a thermotropic liquid crystalline polymer and in situ composites based on their blends under dry sliding conditions at elevated temperatures, Wear 200 (1996) 105-121.

[69] P. Samyn, G. Schoukens, Experimental extrapolation model for friction and wear of polymers on different testing scales, Int. J. Mech. Sci. 50 (2008) 1390-1403.

[70] A. Gebhard, F. Haupert, A.K. Schlarb, Development of nanostructured slide coatings for automotive components, Chapter 18 in: K. Friedrich and A.K. Schlarb editor, Tribology of polymeric nanocomposites, 2013 Elsevier B. V.

[71] L.A. Pilato, M.J. Michno, Advanced Composite Materials, Spinger, 1994 ISBN: 0-387-57563-4.

[72] Y. Zheng, R. Ning, Glass fiber-reinforced polymer composites of high compressive strength, Journal of Reinforced Plastics and Composites 23 (16) (2004) 1729–1740.

[73] B. Wunderich, Macromolecular physics, Volume I crystal structure, morphology, defects, Academic Press New York and London 1973.

[74] S. Murahashi, T. Tanaka, M. Kamachi, T. Norisue, Polymer chemistry, 5th edition, Kyoritsu Shuppan 2007.

[75] B.J. Briscoe, S.K. Sinha, Tribological applications of polymers and their composites-past, present and future prospects, Chapter 1 in: K. Friedrich and A.K. Schlarb editor, Tribology of polymeric nanocomposites, 2013 Elsevier B. V.

[76] Y. Sawae, J. Sugimura, Tribology in gaseous hydrogen, J. Vac. Soc. Jpn, Vol. 53, No. 4, 2010.

[77] Nakashima K, Yamaguchi A, Kurono Y, Sawae Y, Murakami T, Sugimura J. Effect of high-pressure hydrogen exposure on wear of polytetrafluoroethylene sliding against stainless steel. Proc Inst Mech Eng Part J J Eng Tribol 2010;224:285–92. https://doi.org/10.1243/13506501JET642.

[78] Nosaka M, Kikuchi M, Oike M, Kawai N. Tribo-characteristics of cryogenic hybrid ceramic ball bearings for rocket turbopumps: bearing wear and transfer film©. Tribol Trans 1999;42:106–15. https://doi.org/10.1080/10402009908982197.

[79] Nosaka M, Kikuchi M, Kawai N, Kikuyama H. Effects of iron fluoride layer on durability of cryogenic high-speed ball bearings for rocket turbopumps. Tribol Trans 2000;43:163–74. https://doi.org/10.1080/10402000008982326.

[80] Morita T, Sato F, Sawae Y, Sugimura J. Effects of metal counter surfaces on friction and wear of polymeric seal materials in hydrogen. BHR Gr. - 21st Int. Conf. Fluid Seal. 2011:167–78.

[81] Sawae Y, Fukuda K, Miyakoshi E, Doi S, Watanabe H, Nakashima K, et al. Tribological characterization of polymeric sealing materials in high pressure hydrogen gas. Am. Soc. Mech. Eng. Tribol. Div. TRIB 2010:251–3. https://doi.org/10.1115/IJTC2010-41238.

[82] Sawae Y, Miyakoshi E, Doi S, Watanabe H, Kurono Y, Sugimura J. Friction and wear of bronze filled PTFE and graphite filled PTFE in 40 MPA hydrogen gas. Am. Soc. Mech. Eng. Tribol. Div. TRIB 2011:249–51. https://doi.org/10.1115/IJTC2011-61215.

[83] B.J. Briscoe and P. J. Tweedale, in: Proc. 6th Int. Conf. on Composite Materials and 2nd European Conf. on Composite Materials, 5/282 Imperial College, London, eds F.L. Matthews, N. Buskell, J.M. Hodgkinson and J. Morton (Elsevier, London, 1987) p. 187

[84] G. W. Stachowiak and A. W. Batchelor. Adhesion and Adhesive Wear. In Engineering Tribology (Third Edition), chapter 12, pages 553–572. Butterworth-Heinemann, Burlington, 2006.

[85] M. John, P.L. Menezes, Self-lubricating materials for extreme condition applications, Materials 2021, 14, 5588.

[86] H. Torres, M. R. Ripoll, B. Prakash, Tribological behavior of self-lubricating materials at high temperatures, Int. Mater. Rev. 2017, 63, 309–340. doi: 10.1080/09506608.2017.1410944.

[87] M.L. Parucker, A.N. Klein, C. Binder, W. Ristow, R. Binder, Development of self-lubricating composite materials of nickel with molybdenum disulfide, graphite and hexagonal boron nitride processed by powder metallurgy: preliminary study. Mater Res. 2014; 17:180–185

[88] C. Baker, R. Chromik, K. Wahl, J. Hu, A. Voevodin, Preparation of chameleon coatings for space and ambient environments. Thin Solid Films 2007, 515, 6737–6743.

[89] C.M. Pooley and D. Tabor, Proc. R. Soc. London Ser. A, 329 (1972) 251.

[90] S. Zhang, J. Zhou, B. Guo, H. Zhou, Y. Pu, J. Chen, Friction and wear behavior of laser cladding Ni/hBN self-lubricating composite coating. Mater Sci Eng A. 2008;491: 47–54

[91] Z.A. Zailani, N.M. Zaibi, R. Hamidon, A. Harun, M.S. Bahari, S. Zakaria, Improvement on the surface quality in machining of aluminum alloy involving boron nitride nanoparticles. In Intelligent Manufacturing and Mechatronics; M.S. Bahari, A. Harun, Z. Abidin, R. Hamidon, S. Zakaria, Eds, Springer: Singapore, 2021; pp. 351–363.

[92] S. Hernandez, J. Hardell, C. Courbon, H. Winkelmann, B. Prakash, High temperature friction and wear mechanism map for tool steel and boron steel tribopair. Tribol. Mater. Surf. Interfaces 2014, 8, 74–84.

[93] T.U. Siddiqui, S.K. Singh, Design, fabrication and characterization of a self-lubricated textured tool in dry machining. Mater. Today Proc. 2020, 41, 863–869.

[94] S. Zhu, J. Cheng, Z. Qiao, J. Yang, High temperature solid-lubricating materials: A review. Tribol. Int. 2018, 133, 206–223.

[95] K.J. Wahl, L.E. Seitzman, R.N. Bolster, I.L. Singer, M.B. Peterson, Ion-beam deposited Cu-Mo coatings as high temperature solid lubricants. Surf Coat Technol. 1997; 89:245–251

[96] C. Dunckle, M. Aggleton, J. Glassman, P. Taborek, Friction of molybdenum disulfide–titanium films under cryogenic vacuum conditions. Tribol. Int. 2011, 44, 1819–1826.

[97] E.E. Nunez, R. Gheisari, A.A. Polycarpou, Tribology review of blended bulk polymers and their coatings for high-load bearing applications. Tribol. Int. 2018, 129, 92–111.

[98] D.L. Burris, Investigation of the tribological behavior of polytetrafluoroethylene at cryogenic temperatures. Tribol. Trans. 2008, 51, 92–100.

[99] E. Rothuizen, W. Merida, M. rokni, M.W. Ibsen, Optimization of hydrogen vehicle refueling via dynamic simulation, Int J Hydrogen Energy 2013, 38, 4221-31.

[100] K. Tanaka, Effects of various fillers on friction and wear of PTFE-based composites, Chapter 5 in: K. Friedrich editor, Friction and wear of polymer composites, 1986 Elsevier Science Publishers B. V.

[101] K. Friedrich, Z. Zhang, P. Klein, Wear of polymer composites, Edited by P. Sydenham and R. Thorn in: G.W. Stachowiak (Ed.), Wear-Materials, Mechanisms and Practice, as Part of Handbook of Measuring System Design, John Wiley & Sons,

2005, pp. 269–290.

[102] Z. Zhang, K. Friedrich, Tribological characteristics of micro- and nanoparticle filled polymer composites, in: K. Friedrich, S. Fakirov, Z. Zhang (Eds.), Polymer Composite— from Nano- to Macro-scale, Springer, 2005, pp. 169–185.

[103] J. Karger-Kocsis, Z. Zhang, Structure–property relationships in nanoparticles/semicrystalline thermoplastic composites, in: J.F. Balta Calleja, G. Michler (Eds.), Mechanical Properties of Polymers Based on Nanostructure and Morphology, CRC Press, New York, 2005, pp. 547–596.

[104] Z. Yang, B. Dong, Y. Huang, L. Liu, F.Y. Yan, H.L. Li, Enhanced wear resistance and micro-hardness of polystyrene nanocomposites by carbon nanotubes, Materials Chemistry and Physics 94 (2005) 109–113.

[105] Q. Jacobs, W. Xu, B. Schädel, W. Wu, Wear behaviour of carbon nanotube reinforced epoxy resin composites, Tribology Letters 23 (2006) 65–75.

[106] S. Bahadur, The development of transfer layers and their role in polymer tribology, Wear 245 (2000) 92–99.

[107] C. Donnet, A. Erdemir, Historical developments and new trends in tribological and solid lubricant coatings, Surface and Coatings Technology 180–181 (2001) 76–84.

[108] D.G. Teer, New solid lubricant coatings, Wear 251 (2001) 1068–1074.

[109] M.B. Peterson and W.O. Winer (Eds.), Wear Control Handbook, American Society of Mechanical Engineers, New York, 1980, pp. 1143-1303

[110] N.P. Suh and H.C. Sin, Wear, 69 (1981) 91.

[111] J.K. Lancaster, J. Phys. D, 1 (1968) 549.

[112] K. Tanaka, Y. Uchiyama, S. Ueda and T. Shimizu, in T. Sakurai (Ed.), Proc. JSLE-ASLE Int. Lubrication Conf., Tokyo, June 9-11, 1975, Elsevier, Amsterdam, 1976, pp. 110-118.

[113] K. Tanaka, J. Lubr., 99 (1977) 408

[114] K. Tanaka and S. Kawakami, Wear, 79 (1982) 221.

[115] K. V. Shooter and D. Tabor. The Frictional Properties of Plastics. Proceedings of the Physical Society. Section B, 65(9):661, 1952.

[116] F. P. Bowden and D. Tabor. The friction and lubrication of solids: Part I. Oxford University Press, 1954

[117] J.T. Burwell, Wear, 1 (1959) 119.

[118] O.R. Lang, Wear, 43 (1977) 25

[119] J.F. Archard, in M.B. Peterson and W.O. Winer (Eds.), Wear Control Handbook, American Society of Mechanical Engineers, New York, 1980, pp. 35-80

[120] Q. Chen, T. Morita, Y. Sawae, K. Fukuda, J. Sugimura, Effects of trace moisture content on tribofilm formation, friction and wear of CF-filled PTFE in hydrogen. Tribology International 188 (2023) 108905.

[121] A. Jean-Fulcrand, M. A. Masen, T. Bremner, J. S. S. Wong, High temperature tribological properties of polybenzimidazole (PBI). Polymer, 128 (2017), pp. 159-618.

[122] C. Donnet, J. Fontaine, A. Grill, T. Le Mogne, The Role of Hydrogen on the Friction Mechanism of Diamond-Like Carbon Films. Tribol. Lett. 2000, 9, 137–142.

[123] J. Fontaine, M. Belin, T. Le Mogne, A. Grill, How to Restore Superlow Friction of DLC: The Healing Effect of Hydrogen Gas. Tribol. Int. 2004, 37, 869–877.

[124] A. Erdemir, O.L. Eryilmaz, S.H. Kim, Effect of tribochemistry on lubricity of DLC films in hydrogen. Surf. Coat. Technol. 2014, 257, 241–246.

[125] J.K. Lancaster, Composites for aerospace dry bearing applications, Chapter 11 in K. Friedrich editor, Friction and wear of polymer composites, 1986 Elsevier Science Publishers B. V.

[126] B.J. Briscoe, Acta Metall. 24(5) (1990) 839.

[127] J. Ye, Lubricants, 2016, 4(1), 4.

[128] J. Ye, J Phys Chem C, 2020, 124, 6188.

[129] C.M. Pooley, D. Tabor, Proc. R. Soc. London Ser. A, 329 (1972) 251.

[130] K. Tanaka, T. Miyata, Wear, 41 (1977) 383.

[131] K.R. Mkinson, D. Tabor, Proc. R. Soc. London Ser. A., 281 (1964) 49.

[132] J. Ye, Tribol Lett 2015, 59, 50.

[133] J. Ye, Tribol Lett 2017; 66: 12.

[134] W.A. Glaeser, J.W. Kissel, D.K. Snediker, Proc. Conf. Polym. Sci. Technol., April 1-4, 1974, Los Angeles, CA, pp. 651-662.

[135] Y. Chen, D. An, S. Sun, J. Gao, L. Qian, Reduction and Removal of Chromium VI in Waterby Powdered Activated Carbon, Materials 2018,11, 269.

[136] M. Mahajan, S. Rajpoot, O.P. Pandey, In-situ synthesis of chromium carbide (Cr3C2) nanopowders by chemical-reduction route, Int. Journal of Refractory Metals and Hard Materials 50 (2015) 113–119.

[137] C. Wei, J. Yen, Effect of film thickness and interlayer on the adhesion strength of diamond like carbon films on different substrates, Diamond & Related Materials 16 (2007) 1325–1330.

[138] R. Kirchheim, Hydrogen solubility and diffusivity in defective and amorphous metals, Progress in Materials Science Vol. 32, pp. 261-325, 1988.

[139] W.H. Johnson, "On some remarkable changes produced in iron and steel by the action of hydrogen and acids", Proceedings of the Royal Society of London, Vol.23, No.156-163, pp.168-179 (1874).

[140] J. Yamabe, S. Nishimura, Influence of fillers on hydrogen penetration properties and blister fracture of rubber composites for O-ring exposed to high-pressure hydrogen gas, international journal of hydrogen energy 34 (2009) 1977–1989.

[141] J. Yamabe, M. Nakao, H. Fujiwara, S. Nishimura, Blister fracture of rubbers for O-ring exposed to high pressure hydrogen gas, In: Hydrogen conference, Jackson Lake Lodge, USA; 2008.

[142] J. Yamabe, M. Nakao, H. Fujiwara, S. Nishimura, Influence of fillers on hydrogen penetration properties and blister fracture of EPDM composites exposed to 10 MPa hydrogen gas. Transactions of the Japan Society of Mechanical Engineers 2008; 74: 971–81.

[143] A.N. Gent, D.A. Tompkins, Nucleation and growth of gas bubbles in elastomers. Journal of Applied Physics 1969;40: 2520–5.

[144] A.N. Gent, P.B. Lindley, Internal rupture of bonded rubber cylinders in tension. Proceedings of the Royal Society 1958; A249:195–205.

[145] M. Dadfarnia, A. Nagao, S. Wang, M.L. Martin, B.P. Somerday, P. Sofronis, Recent advances on hydrogen embrittlement of structural materials, Int J Fract (2015) 196:223–243.

[146] R. Kirchheim, Revisiting hydrogen embrittlement models and hydrogen-induced homogeneous nucleation of dislocations, Scripta Materialia 62 (2010) 67–70.

[147] M.C. Tiegel, M.L. Martin, A.K. Lehmberg, M. Deutges, C. Borchers, R. Kirchheim,

Crack and blister initiation and growth in purified iron due to hydrogen loading, Acta Materialia 115 (2016) 24-34.

[148] R. Kirchheim, B. Somerday, P. Sofronis, Chemomechanical effects on the separation of interfaces occurring during fracture with emphasis on the hydrogen-iron and hydrogen-nickel system, Acta Materialia 99 (2015) 87–98.

[149] P. Sofronis, R.M. Mcmeeking, Numerical analysis of hydrogen transport near a blunting crack tip, J. Mech. Phys. Solids Vol. 37. No. 3. pp. 317-350. 1989.

[150] M.N Gardos, Self-lubricating composites for extreme environmental conditions, Chapter 12 in: K. Friedrich editor, Friction and wear of polymer composites, 1986 Elsevier Science Publishers B. V.

[151] E.N. Brown, D.M. Dattelbaum, The role of crystalline phase on fracture and microstructure evolution of polytetrafluoroethylene (PTFE), Polymer 46 (2005) 3056-3068.

[152] E.S. Clark, The crystal structure of polytetrafluoroethylene, forms I and IV, J. Macromolecular Sci, Part B: Phys, 45: 201-213, 2006.

[153] E.S. Clark, The molecular conformations of polytetrafluoroethylene: forms II and IV, Polymer 40 (1999) 4659-4665.

[154] T. Takahagi, A. Ishitani, X-ray photoelectron spectroscopy study of an ion sputtering process of fluoro polymers using monte carlo simulation, Macromolecules 1987, 20, 407-413.

[155] T. Yamamoto, Master thesis, Kyushu university, 2022.

[156] J. Robertson, Diamond-like amorphous carbon, Materials Sci and Engineering R 37 (2002) 129-281.

[157] R. Umei, R. Taninoguchi, K. Sakaki, T. Morita, Y. Sawae, J. Sugimura, Effect of trace moisture content on low friction mechanism of carbon fiber filled PTFE, Proceedings of Asia Int Conf on Tri 2018, pp. 259-260, Sept 2018.

[158] R. Taninoguchi, Master thesis, Kyushu university, 2019.

[159] K. Sakaki, Master thesis, Kyushu university, 2020.